CHALMERS
UNIVERSITY OF TECHNOLOGY

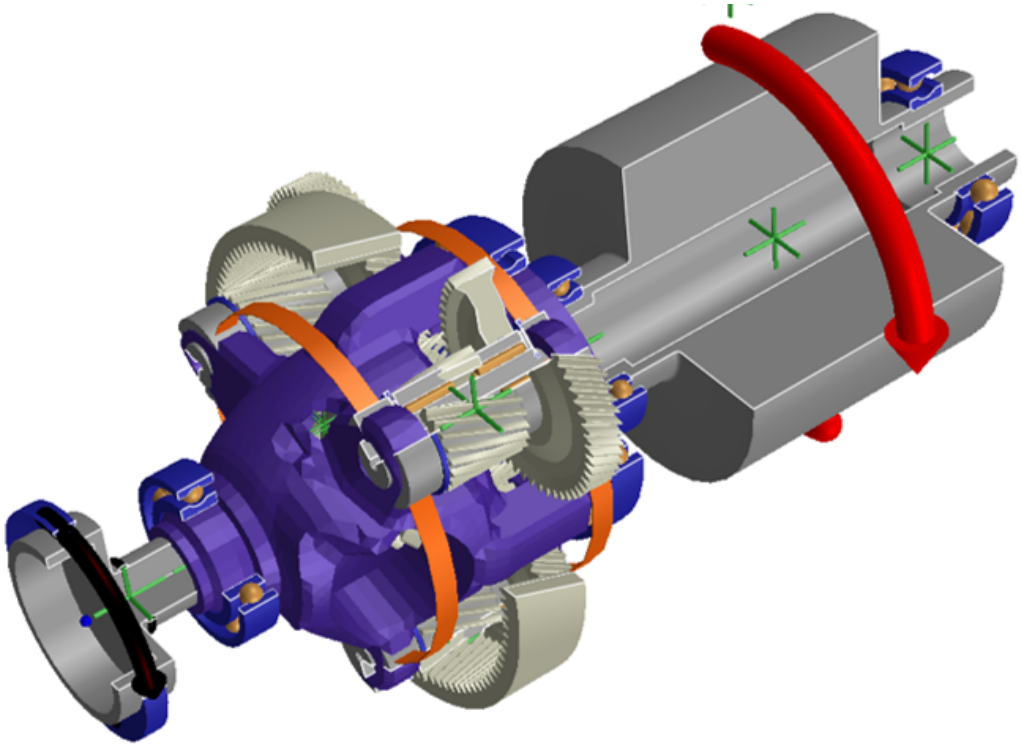

Electric Transmission System Efficiency Simulation

Planetary transmission mechanical efficiency prediction through CAE simulation

Master's thesis in Automotive Engineering

Aniket Baddur

Prabhanjan Madhusudan Pandurangi

Department of Mechanics and Maritime Sciences
CHALMERS UNIVERSITY OF TECHNOLOGY
Gothenburg, Sweden 2020

Master's thesis 2020:64

Electric Transmission System Efficiency Simulation

Planetary transmission mechanical efficiency prediction through CAE simulation

Aniket Baddur
Prabhanjan Madhusudan Pandurangi

CHALMERS
UNIVERSITY OF TECHNOLOGY

Department of Mechanics and Maritime Sciences
Division of Combustion and Propulsion Systems
Chalmers University of Technology
Gothenburg, Sweden 2020

Electric Transmission System Efficiency Simulation
Planetary transmission mechanical efficiency prediction through CAE simulation
Aniket Baddur, Prabhanjan Madhusudan Pandurangi

Supervisors: Martin Hedström and Christian Lönnqvist, Electric Drive department, Volvo Car Corporation
Examiner: Sven B.Andersson, Professor, Chalmers University of Technology

Master's Thesis 2020:64
Department of Mechanics and Maritime Sciences
Division of Combustion and Propulsion Systems
Chalmers University of Technology
SE-412 96 Gothenburg
Telephone +46 31 772 1000

Typeset in LaTeX
Printed by Chalmers University of Technology
Gothenburg, Sweden 2020

Abstract

Accurate prediction of the range of battery electric vehicles is a major challenge for the OEMs. In order to do so, the power loss which occurs in the vehicle driveline in the driving cycle should be predicted. The transmission system is one of the major contributors to these losses. The investigation presented in this report uses power loss models for the individual machine elements (i.e.: bearings, gears, seals and thrust washers) that contribute to the powerloss of the system to effectively predict the transmission efficiency. The evaluation and validation of the power loss models of the individual components is done by setting up analytical models on MATLAB with reference to the literature and comparing with the results from sub-models designed in ROMAX. The most suitable models with the closest correlation to the experimental test results are selected for analysis of the system model. The efficiency of the system model is compared with the results from the test bench. The transmission system is also simulated in the WLTP cycle to analyse the operating points on the efficiency map.

Keywords: Planetary transmission, power loss model, efficiency, ROMAX, bearing loss, gear mesh loss, gear drag loss, seal loss, test bench

Acknowledgements

We would like to express great appreciation to our Examiner Sven B Andersson who supported us and also obliged to evaluate our work.

We are particularly grateful for the assistance given by Christian Lönnqvist and Martin Hedström at the Volvo Car Corporation, Gothenburg. We sincerely appreciate them for the opportunity to conduct the research work and their expertise that served as a valuable guidance during the research. We are grateful to our colleagues at Volvo Cars for providing us with necessary data when needed. We also like to acknowledge the support staff at ROMAX who provided valuable inputs for the use of the CAE tool.

We would like to acknowledge the Mechanics and Maritime Science department at the Chalmers Institute Of Technology, Gothenburg for providing us the opportunity to write the thesis.

Finally, we want to express gratitude to our family and friends for the constant support and encouragement.

Aniket Baddur, Prabhanjan Madhusudan Pandurangi, Gothenburg, June 2020

Contents

List of Figures

List of Tables

1
Introduction

1.1 Aim

- Describe the benefits and limitations of numerical (static) calculation models for efficiency predictions on electric transmission systems.
- To carryout transmission efficiency prediction simulations using power loss models for individual components in the transmission such as gears, bearings, seals, etc.
- To compare the correlation of system efficiency between simulation and the test bench results.
- To simulate the transmission in the WLTP driving cycle.

1.2 Objectives

- Study and understand the analytical power loss models on component level (bearings, gears, seals).
- Understand the prediction accuracy of an electric transmission power loss model (static) for its typical operating conditions (speed and load), by comparing numerical calculation results to measurement results.
- Describe the analytical formulation and prediction limitations of component level power loss models for their typical operating conditions.
- Analyze the accuracy of analytical churning loss models.

1.3 Limitations

- Efficiency calculations will be based on static analysis results.
- Computational Fluid Dynamics for prediction of speed dependent churning losses will provide more accurate results. It is outside the scope of this thesis work.

- The FVA345 coefficients for the lubricant are unavailable. Conduction an FVA rig test will provide more accurate results for the gear losses.

1.4 Transmission model

A transmission is used in a power train to effectively apply the power from the source (IC engine or motor) in vehicle. In this thesis, a stepped planet type of planetary transmission is studied. In this type of transmission, the planetary shaft houses two planet gears manufactured as a single unit which rotate at equal angular velocities. The output from the motor shaft is directly coupled to the sun gear through a spline. This is the input for the transmission. The sun gear meshes with the larger gear in the stepped planetary assembly. This transmission consists of three planet gear assemblies that rotate about the sun gear and each planet assembly rotates about its own planet shaft axis. The planet gear assemblies are mounted on to a planet carrier via the planet shaft. The carrier also houses the differential.

The ring gear is mounted on to the transmission housing and remains stationary at all times. The smaller gear rotates along with the the larger gear the stepped planetary assembly and meshes with the ring gear. Hence, the power output occurs though the planet carrier.

The powertrain consists of two such planetary transmissions that are driven by either side of the shaft of the electric motor (EM). The transmission system modelled in ROMAX is shown in Figure 1.1. FAG61822-Y is labelled as big bearing, while FAG6009 is labelled as the small bearing. The model also includes two seals: Driveshaft seal and rotor shaft seal (not visible in Figure 1.1).

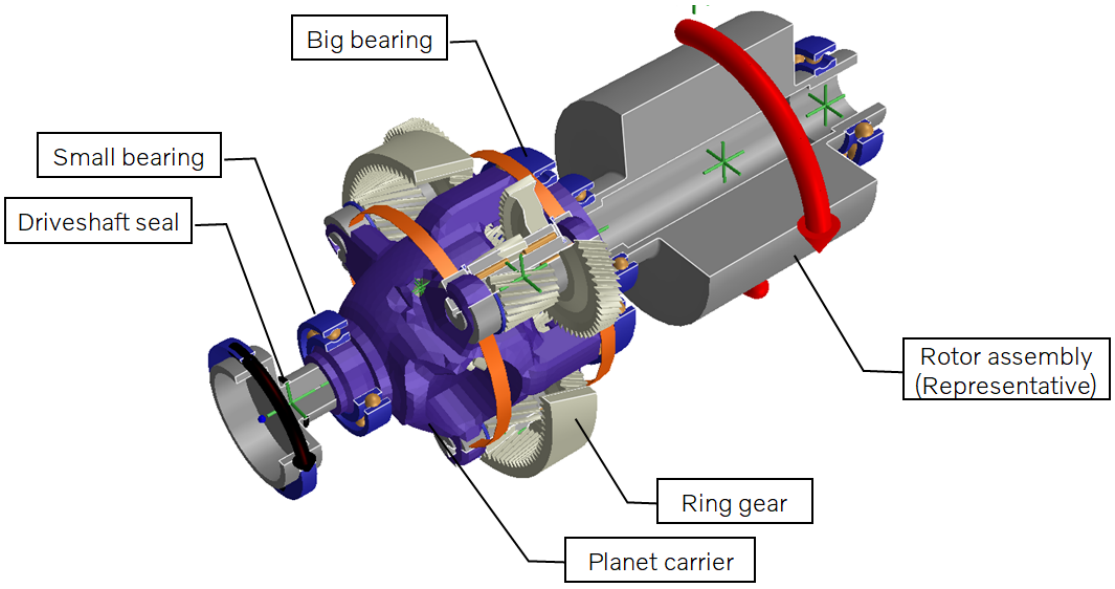

Figure 1.1: Transmission system modelled on ROMAX

The layout of the transmission is shown in Figure 1.2.

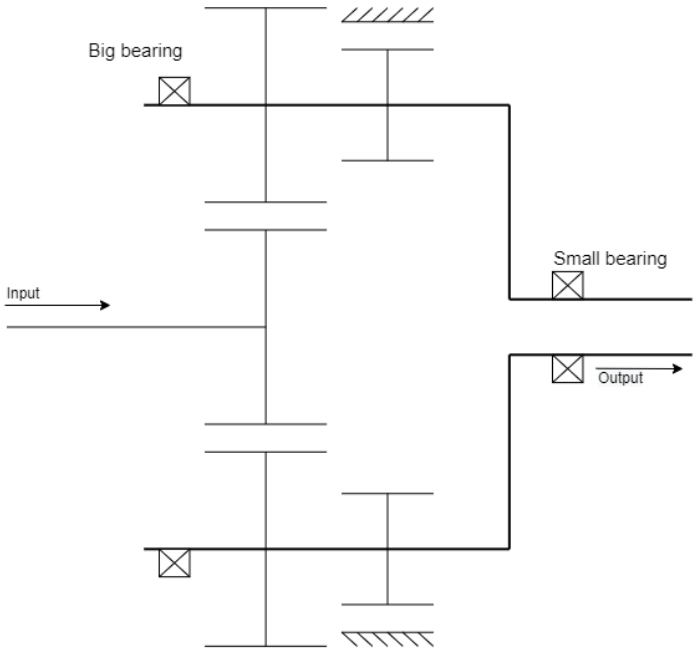

Figure 1.2: Layout of the transmission

1.5 Test Bench

The transmission was mounted to a fixture that was isolated from the structure of the test rig by rubber bushings. The fixture consisted of two laser cut flanges where

the transmission and E-motor was attached to respective outside of each flange. Between the two flanges there was space to fit a torque sensor to accurately measure the torque and speed between the E-motor and transmission input shaft. The setup is shown in Figure 1.3.

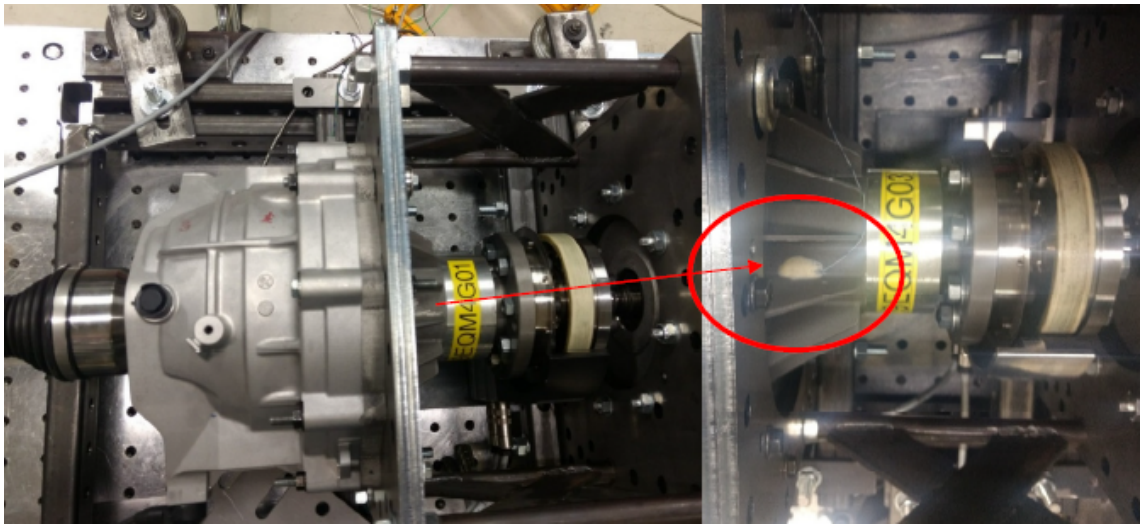

Figure 1.3: Test bench

2

Theory

The power losses in a transmission can be split into load-dependent and load-independent (spin) losses. The load-dependent power losses are from the gears and bearings when the torque is transferred through them [25]. The load-independent power losses occur due to the rotation of the shafts, which causes the gears and bearings to be immersed in the lubricant. The load-independent power losses occur even when there is no torque being transmitted. Both types of losses are comparable in magnitude under high-load and low-operating speed conditions and the load-independent losses generally dominate the overall power losses at higher operating speeds. Figure 2.1 shows the types of losses in both load-dependent and load-independent power losses.

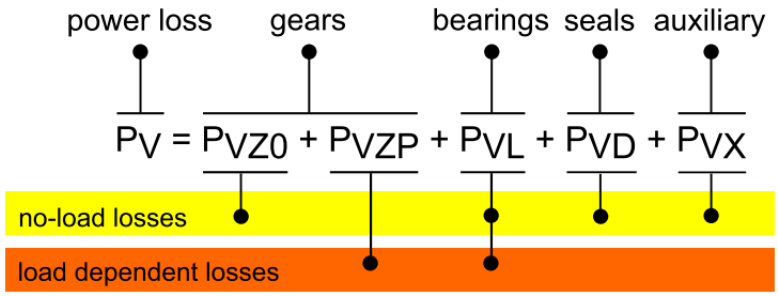

Figure 2.1: Power loss contributions[11].

According to Höhn et al.[18], load dependent losses are usually dominant in case of nominal power transmission. For part load and high speed operating points, the total power loss in a gearbox is dominated by load independent losses. In order to optimize the gearbox over a whole operating range, both the load dependent and load independent losses have to be addressed.

Spin power losses in a transmission system can be categorised into churning losses if the rotating components of the system are immersed in an oil bath and windage losses if the lubrication method is jet-type and the surrounding medium is air or a fine mist of oil and air. In case of low and medium speed gears, power losses mainly originate from tooth friction and lubricant churning whereas, at high operating speeds windage losses are prominent. The study of spin power losses is challenging

as the environment inside the transmission can be described as a pseudo-single phase mixture of oil and vapour and it also includes the gears rotating in mesh. [23] [7]

2.1 Bearing losses

The bearing losses are categorised into load independent and load dependent losses. The load independent losses occur with rotation of components even without the transmission of torque. They are mainly related to the operating conditions, design of the gearbox, viscosity and density of the lubricant. Load dependent losses are related to the transmitted torque, coefficient of friction and sliding velocity between the moving components determined by the design [10]. Among many friction loss models, the SKF and Palmgren model are the most used.

2.1.1 ISO 14179-1 model

According to International Organisation for Standardisation[19], the method used to determine load dependent losses for bearings is based on [31]. ISO 14179 - 1 [19] and ISO 14179 - 2 [20] have the same analytical model for all types of bearings. This model is applicable for both deep groove ball bearings and needle bearings.

The power loss for an individual bearing is determined by using Equation 2.1.

$$P_{Bi} = \frac{(M_1 + M_2).n}{9549} \tag{2.1}$$

where,
P_{Bi} = Power loss for an individual bearing [kW]
M_1 = Bearing load dependent torque [Nm]. It is defined in Equation 2.2.
M_2 = Cylindrical roller bearing axial load dependent moment [Nm]
n = Bearing rotational speed [rpm]

$$M_1 = \frac{f_1.(P_1)^a.(d_m)^b}{1000} \tag{2.2}$$

where,
f_1 = Friction coefficient. It is defined in Equation 2.3
P_1 = Bearing dynamic load [N]. It is defined in Equation 2.5
d_m = Bearing mean diameter [mm] = 0,5 (d + D)
d = Bearing bore diameter [mm]
D = Bearing outside diameter [mm]
From Table 3 in [19], the values of exponents 'a' and 'b' for all types of bearings except for spherical roller bearings are 1.

From Table 2 in [19], the expressions for f_1 and P_1 for deep groove ball bearings can be defined as Equations 2.3 and 2.5 respectively.

$$f_1 = (0,0006....0,0009) * (P_0/C_0)^{0,55} \tag{2.3}$$

$$P_0 = (0,5.F_a) + (0,6.F_r) \tag{2.4}$$

$$P_1 = (3.F_a) - (0,1.F_r) \tag{2.5}$$

where,
P_0 = Equivalent static bearing load [N]. It is defined in Equation 2.4.
C_0 = Basic static load rating [N]. It is found in manufacturer's bearing tables.
F_a = Axial component of dynamic bearing load [N]
F_r = Radial component of dynamic bearing load [N]

In Equation 2.3 for f_1, the small values are for the light series bearings, whereas the large values are for the heavy series bearings. In Equation 2.5 for P_1, if $P_1 < F_r$, then $P_1 = F_r$ should be considered. In Equation 2.4 for P_0, if $P_0 < F_r$, then $P_0 = F_r$ should be used.

In case of cylindrical roller bearings, the axial load dependent moment is given by Equation 2.6.

$$M_2 = \frac{f_2.F_a.d_m}{1000} \tag{2.6}$$

where,
f_2 = Factor depending on bearing design and lubrication. It is taken as 0,003 for single-row full complement bearings with oil lubrication. The values stated for f_2 assume that the viscosity ratio is $K \geqslant 1,5$.
F_a = Axial bearing load [Nm]

2.1.2 Palmgren model

According to Palmgren [28], the total friction torque of the roller bearing under moderate load and speed conditions is given by the sum of the load friction torque (M_1) and viscous friction torque (M_v). The terms M_1 and M_v are based on empirical formula, so the effect of rolling element-cage pocket sliding is included. It is determined by using Equation 2.7.

$$M = M_1 + M_v \tag{2.7}$$

2.1.2.1 Torque due to Applied load

According to Palmgren [28], Equation 2.8 gives the expression for the load friction torque in a roller ball bearing.

$$M_1 = f_1.F_\beta.d_m \tag{2.8}$$

where,
d_m = Bearing pitch diameter [mm]
f_1 = Factor depending on the bearing design and relative bearing load. It is expressed in Equation 2.9.

$$f_1 = z.\left(\frac{F_s}{C_s}\right)^y \tag{2.9}$$

where,
F_s = Static equivalent load [N] given by Equation 2.10
C_s = Basic static load rating given by Equation 2.11. It is given in the manufacturer's catalog.
The values of 'z' and 'y' are defined in Table 10.1 in the book by Harris A. et al.[15].

For bearings with radial loads, the static equivalent load (F_s) can be determined as,

$$F_s = X_s.F_r + Y_s.F_a \tag{2.10}$$

where,
F_s = Static equivalent load [N]
F_r = Radial load [N]
F_a = Axial load [N]
The values of 'X_s' and 'Y_s' are taken from Table 9.3 in the book by Harris A. et al.[15].

The basic static load rating (C_s) can be expressed as,

$$C_s = 0,2.i.Z.Q_{max}.cos\alpha \tag{2.11}$$

where,
C_s = Basic static load rating
i = Number of rows of rolling elements
Z = Number of bearing elements
Q_{max} = Maximum loaded rolling element load given by Equation 2.12
α = Contact angle [°]

The maximum loaded rolling element load (Q_{max}) may be approximated as,

$$Q_{max} = \frac{5.F_r}{i.Z.cos\alpha} \tag{2.12}$$

In case of deep-groove ball bearings with a nominal contact angle on 0°, Equation 2.13 can be used to determine F_β.

$$F_\beta = 3.F_a - 0,1.F_r \tag{2.13}$$

2.1.2.2 Torque due to lubricant viscous friction

Palmgren [28] established that the torque due to lubricant viscous friction is caused due to orbiting rolling elements as they plough through the lubricant which occupies the free space within the bearing boundaries. Equations 2.14 and 2.15 are only valid for lubricants which have a specific gravity of approximately 0,9. For lubricants with different densities, Palmgren [28].

$$M_v = 10^{-7}.f_0.(\nu_o.n)^{2/3}.{d_m}^3 \qquad if\ \nu_o.n \geqslant 2000 \tag{2.14}$$

$$M_v = 160 * 10^{-7}.f_0.{d_m}^3 \qquad if\ \nu_o.n < 2000. \tag{2.15}$$

where,
ν_0 = Lubricant kinematic viscosity [cSt or mm^2/s]
n = Bearing rotational speed [rpm]
f_0 = Factor depending on the type of bearing and method of lubrication.

2.1.3 SKF Model

The SKF power loss model is based on experimental fitting by using the recommended values for the coefficients given in the SKF catalogue [31]. The load independent losses consist of friction losses in the seals and friction torque due to churning losses, windage and drag. Load dependent friction is divided into rolling and sliding friction torque. The change in friction in a bearing as a function of speed is divided into four regimes as shown in Figure 2.2.

1. **Boundary layer lubrication,** where the surface asperities carry the load and hence the friction is high.

2. **Mixed lubrication condition,** where a part of the load is carrier by the surface asperities and the oil film separating the sliding layers also carry a part of the load. Hence, the friction decreases.

3. **Full film lubrication condition,** where the lubricant layer carries the load with increased viscous losses and so the friction increases.

4. **Full film lubrication with thermal and starvation effects,** where the inlet shear heating and kinematic replenishment reduction factors compensate partially for the viscous forces, and the friction remains constant during change in speed.

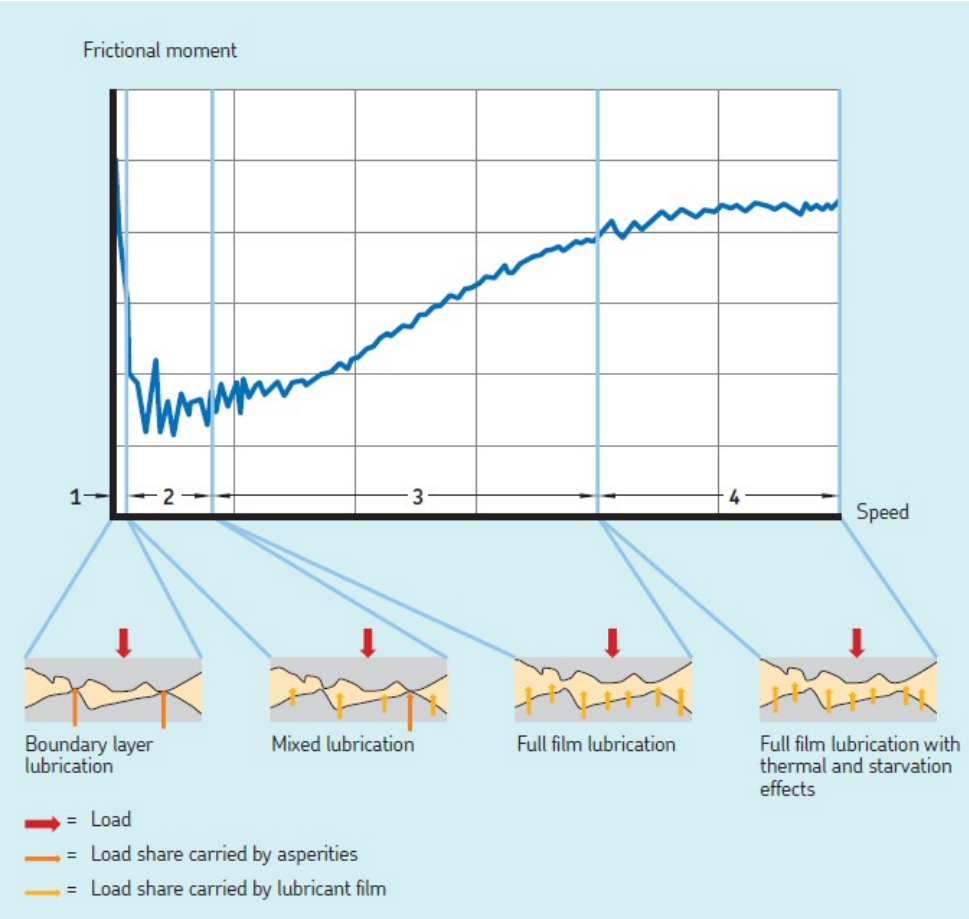

Figure 2.2: Frictional bearing moment as a function of speed or viscosity[31].

SKF provides the friction loss models for oil and grease lubrication. But in this study, the model for the conditions relevant to the electric transmission under examination is presented in the sections below.

The SKF model for calculating the frictional moment is give by Equation 2.16. M_{seal} will not be considered in this analysis.

$$M = M_{rr} + M_{sl} + M_{seal} + M_{drag} \tag{2.16}$$

where,
M = Total frictional moment [Nmm]
M_{rr} = Rolling frictional moment [Nmm]
M_{sl} = Sliding frictional moment [Nmm]
M_{seal} = Frictional moment of seals [Nmm]
M_{drag} = Frictional moment of drag losses, churning, splashing etc. [Nmm]

2.1.3.1 Rolling friction torque

The rolling frictional torque, the effects of high-speed starvation and inlet shear heating are taken into account. It is given by the Equation 2.17.

$$M_{rr} = \phi_{ish}.\phi_{rs}.G_{rr}(\nu.n)^{0,6} \tag{2.17}$$

where,
M_{rr} = Rolling friction torque [Nmm]
ϕ_{ish} = Inlet shear heating reduction factor
ϕ_{rs} = Kinematic replenishment/starvation reduction factor
n = Rotational speed [rpm]
ν = Actual operating viscosity of the oil or the base oil of the grease $[mm^2/s]$
G_{rr} = Rolling frictional variable, depending on:

- Bearing type.
- Bearing mean diameter d_m [mm] = 0,5 (d + D).
- Radial load F_r [N].
- Axial load F_a [N].

d = Bearing bore diameter [mm]
D = Bearing outside diameter [mm]

From [31], the rolling frictional Variable (G_{rr}) for deep groove ball bearings is defined as:

$$G_{rr} = R_1.(d_m)^{1,96}.(F_r)^{0,54}, \ \ when\ F_a = 0 \tag{2.18}$$

$$G_{rr} = R_1.(d_m)^{1,96}.\left(F_r + \frac{R_2.F_a}{sin\ \alpha_F}\right)^{0,54}, \ \ when\ F_a > 0 \tag{2.19}$$

$$\alpha_F = 24,6.(F_a/C_0)^{0,24}[^\circ] \tag{2.20}$$

where,
C_0 = Basic static load rating [N]. It is found in manufacturer's bearing tables.
R_1 and R_2 are geometric constants for rolling frictional moments.

Inlet shear heating reduction factor:
A thin layer of lubricant is sufficient to form the hydrodynamic film, the excess fluid is displaced by the moving contact surfaces. This causes a reverse flow of lubricant and a shearing effect leading to localised heating. This heat reduces the viscosity at the contact area and has an influence on the power loss in the bearing. The coefficient of inlet shear heating reduction factor (ϕ_{ish}) is calculated using the Equation 2.21.

$$\phi_{ish} = \frac{1}{1 + (1,84 * 10^{-9}.(n.d_m)^{1,28}.\nu^{0,64})} \tag{2.21}$$

where,
ϕ_{ish} = Inlet shear heating reduction factor. It is taken from Figure 2 in the SKF catalogue [31]

n = Rotational speed [rpm]
d_m = Bearing mean diameter [mm]
ν = Actual operating viscosity of the oil or the base oil of the grease $[mm^2/s]$

Kinematic replenishment/starvation reduction factor:
The raceways are constantly being displaced of the lubricant when rolling. With high speed and viscosity applications, the time for the lubricant to fill these raceways are insufficient. This influences the hydrodynamic film and the rolling friction by reducing the film thickness. The Kinematic replenishment/starvation reduction factor is shown in Equation 2.22.

$$\phi_{rs} = \frac{1}{e^{\left[K_{rs}.\nu.n.(d+D).\sqrt{\frac{K_Z}{2(D-d)}}\right]}} \tag{2.22}$$

where,
ϕ_{rs} = Kinematic replenishment/starvation reduction factor
e = base of natural logarithm ≈ 2,718
K_{rs} = Replenishment/starvation constant
$= 3 * 10^{-8}$ low level oil bath and oil jet lubrication
$=6 * 10^{-8}$ grease and oil-air lubrication
K_Z = Bearing type related geometric constant
ν = Actual operating viscosity of the oil or the base oil of the grease $[mm^2/s]$
d = Bearing bore diameter [mm]
D = Bearing outside diameter [mm]
n = Rotational speed [rpm]

2.1.3.2 Sliding frictional moment

The sliding frictional torque (M_{sl}) is given by the Equation 2.23.

$$M_{sl} = G_{sl}.\mu_{sl} \tag{2.23}$$

where,
M_{sl} = Sliding frictional moment [Nmm]
μ_{sl} = Sliding friction coefficient
G_{sl} = Sliding frictional variable, depending on:

- Bearing type.
- Bearing mean diameter (d_m) [mm] = 0,5 (d + D).
- Radial load (F_r) [N].
- Axial load (F_a) [N].

From [31], the sliding frictional Variable (G_{sl}) for deep groove ball bearings is defined as:

$$G_{sl} = S_1.(d_m)^{-0,26}.(F_r)^{5/3}, \ \ when\ F_a = 0 \tag{2.24}$$

$$G_{sl} = S_1.(d_m)^{-0,145}.\left(F_r^5 + \frac{S_2.(d_m)^{1,5}.(F_a)^4}{sin\ \alpha_F}\right)^{1/3} \quad when\ F_a > 0 \tag{2.25}$$

where,
α_F = It is defined in Equation 2.20.
S_1 and S_2 are geometric constants for Sliding frictional moments.

Effect of lubrication on sliding friction:
The effect of sliding friction for hydrodynamic and full film lubrication is given by Equation 2.26.

$$\mu_{sl} = \phi_{bl}.\mu_{bl} + (1 - \phi_{bl}).\mu_{EHL} \tag{2.26}$$

$$\phi_{bl} = \frac{1}{e^{2,6*10^{-8}.(n.v)^{1,4}}d_m} \tag{2.27}$$

where,
μ_{sl} = Sliding friction coefficient
ϕ_{bl} = Weighting factor for the sliding friction coefficient. It is defined is Equation 2.27.
e = Base of natural logarithm ≈ 2,718
n = Rotational speed [rpm]
d_m = Bearing mean diameter [mm] = 0,5 (d + D).
μ_{bl} = Constant depending on movement:
= 0,12 for n ≠ 0
= 0,15 for n = 0 (starting torque calculation)
μ_{EHL} = Sliding friction coefficient in full-film conditions.

The value for μ_{EHL} is decided depending on the type of bearing and lubrication:

- 0,02 for cylindrical roller bearings
- 0,002 for tapered roller bearings

Other bearings:

- 0,05 for lubrication with mineral oils
- 0,04 for lubrication with synthetic oils
- 0,1 for lubrication with transmission fluids

2.1.3.3 Friction drag losses

When the bearings are partially or completely submerged in a lubricant by oil bath method of lubrication, there will be drag losses when the bearing starts rotating. These losses will contribute to the total frictional moment. The drag losses are influenced by bearing speed, lubricant viscosity, lubricant level, size and geometry

of the oil reservoir. The SKF model [31] takes all the above parameters into account except for size and geometry of the oil reservoir and gives the following model. The size and geometry of the oil reservoir is not considered as the reservoir is quite large. Hence, these effects are negligible.

The frictional moment of drag losses for ball bearings can be approximated by using Equation 2.28.

$$M_{drag} = 0,4.V_M.K_{ball}.d_m^5.n^2 + 1,093 * 10^{-7}.n^2.d_m^3.(\frac{n.d_m^2.f_t}{\nu})^{-1,379}.R_s \tag{2.28}$$

The frictional moment of drag losses for roller bearings can be approximated by using Equation 2.29.

$$M_{drag} = 4.V_M.K_{roll}.C_w.B.d_m^4.n^2 + 1,093 * 10^{-7}.n^2.d_m^3.(\frac{n.d_m^2.f_t}{\nu})^{-1,379}.R_s \tag{2.29}$$

The rolling element related constants can be defined as Equations 2.30 and 2.31.

$$K_{ball} = \frac{i_{rw}.K_Z.(d+D)}{D-d} * 10^{-12} \tag{2.30}$$

$$K_{roll} = \frac{K_L.K_Z.(d+D)}{D-d} * 10^{-12} \tag{2.31}$$

The variables used in expressions Equations 2.28 and 2.29 are defined as follows:

$$C_w = (2,789 * 10^{-10}.l_D^3) - (2,786 * 10^{-4}.l_D^2) + 0,0195.l_D + 0,6439 \tag{2.32}$$

$$l_D = 5.\frac{K_L.B}{d_m} \tag{2.33}$$

$$f_t = \begin{cases} sin(0,5t), & \text{when } 0 \leqslant t \leqslant \pi \\ 1, & \text{when } \pi \leqslant t \leqslant 2\pi \end{cases}$$

$$R_s = 0,36.d_m^2.(t - sint).f_A \tag{2.34}$$

$$t = 2.cos^{-1}\left(\frac{0,6d_m - H}{0,6d_m}\right), \ when\ H \geq 1,2d_m, use\ H = 1,2d_m \tag{2.35}$$

$$f_A = 0,05 * \left(\frac{K_Z.(D+d)}{D-d}\right) \tag{2.36}$$

where,
M_{drag} = Frictional moment of drag losses [Nmm]
V_M = Drag loss factor
B = Bearing width [mm]

- for tapered roller bearings - width (T)
- for thrust bearings - height (H)

d_m = Bearing mean diameter [mm] = 0,5(d+D)
d = Bearing bore diameter [mm]
D = Bearing outside diameter [mm]
ν = Actual operating viscosity of the lubricant $[mm^2/s]$
n = Rotational speed [rpm]
H = Oil level [mm]
i_{rw} = Number of ball rows
K_Z = Bearing type related geometric constant
K_L = Roller bearing type related geometric constant

2.1.4 Palmgren Model - Needle Bearings

According to J.Liu et al. [21], the total frictional torque for the bearings is determined by adding the load independent and load dependent friction torques which is given by the Equation 2.37. This model includes the influence of applied load, bearing speed, friction and lubricant viscosity.

$$M = M_0 + M_1 \tag{2.37}$$

where,
M = Total frictional torque [Nm]
M_0 = Load independent frictional torque [Nm]
M_1 = Load dependent frictional torque [Nm]

2.1.4.1 Load independent frictional torque

The load independent frictional torque (M_0) depends on the lubricant viscosity, bearing speed and bearing geometry. The values of f_0 as defined in [15] are 1.5 for oil fog lubrication, 2.5 for grease lubrication and 6 for oil spray lubrication.

$$M_0 = 10^{-7}.f_0.(\nu.n)^{2/3}.(d_m)^3, \;\; when\,(\nu.n) \geqslant 2000 \tag{2.38}$$

$$M_0 = 160 * 10^{-7}.f_0.(d_m)^3, \;\; when\,(\nu.n) < 2000 \tag{2.39}$$

where,
f_0 = Coefficient determined by the bearing type and lubricant conditions.
ν = Lubricant kinematic viscosity [cSt]
n = Bearing speed [rpm]
d_m = Bearing pitch diameter [mm]

2.1.4.2 Load dependent frictional torque

The load dependent frictional torque (M_1) defined in Equation 2.40 depends on the applied load and bearing geometry.

$$M_1 = f_1.P.d_m \tag{2.40}$$

where,
f_1 = Coefficient determined by the bearing load and design geometries. It is defined in Equation 2.41.
P = Applied load [N]

$$f_1 = \zeta . \left(\frac{F_s}{C_s}\right)^{\tau} \tag{2.41}$$

where,
$\zeta \, and \, \tau$ = Dimensionless parameters
F_s = Static equivalent load [N]
C_s = Load rating

2.1.5 SKF Model - Needle Bearings

According to SKF [31], the total frictional torque (M) for the needle bearings can be divided into rolling friction torque (M_{rf}), slipping friction torque (M_{sf}), seal friction torque (M_{ef}) and viscous friction torque (M_{vf}). The SKF model cannot be applied to Needle roller bearings in ROMAX, as there is no option to estimate the friction loss factors.

$$M = \psi_1 . \psi_2 . M_{rf} + M_{sf} + M_{ef} + M_{vf} \tag{2.42}$$

where,
ψ_1 = Small oil backfill reduction coefficient. It is defined in Equation 2.43.
ψ_2 = Shear heat reduction coefficient caused by lubricant oil. It is defined in Equation 2.44.

$$\psi_1 = \frac{1}{e^{K_{rs} . \nu . n . (D+d) . \sqrt{\frac{K_t}{2.(D-d)}}}} \tag{2.43}$$

where,
K_{rs} = Small oil backfill coefficient. It's value is $3 * 10^{-8}$ for oil-bath and gas-oil lubrication conditions, and $6 * 10^{-8}$ for grease and oil spray lubricant conditions.
ν = Lubricant kinematic viscosity [cSt]
n = Bearing speed [rpm]
D = Bearing outer diameter [mm]
d = Bearing inner diameter [mm]
K_t = Geometric constant coefficient determined by the bearing geometries.

$$\psi_2 = \frac{1}{1 + (1,84 * 10^{-9} . (n . d_m)^{1,28} . \nu^{0,64})} \tag{2.44}$$

where,
d_m = Bearing pitch diameter [mm]

2.1.5.1 Rolling friction torque

The rolling friction torque (M_{rf}) defined in Equation 2.45 depends on the bearing geometry, applied load, bearing speed and lubricant viscosity.

$$M_{rf} = G_{rf}.(\nu.n)^{0,6} \tag{2.45}$$

where,
G_{rf} = Coefficient determined by the bearing geometries and applied loads. It is defined in Equation 2.46.

$$G_{rf} = R_1.(d_m^{2,41}).(P^{0,31}) \tag{2.46}$$

where,
R_1 = Constant coefficient
P = Applied load [N]

2.1.5.2 Slipping friction torque

The slipping friction torque (M_{sf}) defined in Equation 2.47 depends on slipping friction coefficient, bearing geometry and applied load.

$$M_{sf} = \mu_{sf}.G_{sf} \tag{2.47}$$

where,
μ_{sf} = Slipping friction coefficient, whose value is 0,02 for synthetic oil lubrication condition and 0,05 for a mineral oil lubrication condition.
G_{sf} = Slipping friction parameter depending on the bearing type. It is defined in Equation 2.48.

$$G_{sf} = S_2.d_m.P \tag{2.48}$$

where,
S_2 = Constant parameter

2.1.5.3 Seal friction torque

The seal friction torque (M_{ef}) defined in Equation 2.49 depends on bearing and seal types. If there is only one seal in the system, the seal friction torque will be equal to $0,5M_{ef}$.

$$M_{ef} = K_{s1}.d_s^{\beta} + K_{s2} \tag{2.49}$$

where,
K_{s1} = Constant coefficient depending on bearing type
K_{s2} = Constant coefficient depending on bearing and seal types
d_s = Diameter of the contact area between the bearing raceway and seal [mm]
β = Constant exponent depending on the bearing and seal types

2.1.5.4 Viscous friction torque

The viscous friction torque (M_{vf}) defined in Equation 2.50 depends on bearing geometry, bearing speed and lubricating oil depth.

$$M_{vf} = 10.V_m.K_{roll}.B.d_m^4.n^2 \tag{2.50}$$

where,
V_m = Drag loss parameter
K_{roll} = Constant drag loss coefficient. It is defined in Equation 2.51.
B = Inner raceway width of the bearing [mm]

$$K_{roll} = \frac{10^{-12}.K_L.K_t.(D+d)}{D-d} \tag{2.51}$$

where,
K_L = Constant geometric coefficient depending on the bearing type

2.2 Gear mesh losses

According to Kahraman et al.[32], when both the pinion and the gear are meshing under torque, there will be drag torque losses. The load dependent part of the gear mesh losses is generated as a result of lubricated contacts, which generates friction and sliding between the meshed gear teeth. Gear mesh losses typically depend on speed, torque, geometry, lubricant and temperature. The following analytical models will be used to determine the load dependent losses in gear meshes.

2.2.1 ISO 14179-1 model

In [19], the International Organisation for Standardisation (ISO) expresses mesh efficiency as a function of sliding ratios and mesh coefficient of friction [5] [9]. The gear tooth mesh losses can be determined by Equation 2.52. The Mesh mechanical advantage (Equation 2.53) and mesh coefficient of friction (Equation 2.56) should be evaluated before solving for mesh power loss.

$$P_{Mi} = \frac{f_m.T_1.n_1.cos^2\beta_w}{9549.M} \tag{2.52}$$

where,
P_{Mi} = Mesh power loss [kW]
f_m = Mesh coefficient of friction
T_1 = Pinion Torque [Nm]
n_1 = Pinion rotational speed [rpm]
β_w = Operating Helix angle [°]
M = Mesh mechanical advantage

The mesh mechanical advantage (M) can be determined by Equation 2.53. In case of external gears, the sliding ratio at the start of approach (H_s) is determined by

Equation 2.54 and the sliding ratio at the end of recess (H_t) is determined by Equation 2.55.

$$M = \frac{2cos\alpha_w.(H_s + H_t)}{H_s^2 + H_t^2} \tag{2.53}$$

where,
α_w = Transverse operating pressure angles [°]
H_s = Sliding ratio at the start of approach
H_t = Sliding ratio at the end of recess

$$H_s = (u+1)\left[\left(\frac{r_{o2}^2}{r_{w2}^2} - cos^2\alpha_w\right)^{0,5} - sin\alpha_w\right] \tag{2.54}$$

$$H_t = \left(\frac{u+1}{u}\right)\left[\left(\frac{r_{o1}^2}{r_{w1}^2} - cos^2\alpha_w\right)^{0,5} - sin\alpha_w\right] \tag{2.55}$$

where,
u = Gear ratio = z_2/z_1
z_1 = Number of pinion teeth
z_2 = Number of gear teeth
r_{o2} = Gear outside radius [mm]
r_{w2} = Gear operating pitch radius [mm]
r_{o1} = Pinion outside radius [mm]
r_{w1} = Pinion operating pitch radius [mm]

The mesh coefficient of friction can be expressed by Equation 2.56. This expression should only be used if the pitch line velocity is between 2 m/s and 25 m/s and the load intensity (K) varies between 1,4 N/mm^2 and 14 N/mm^2. If any one of the these variables is outside the limits, the value of f_m should be determined by experience according to ISO. The exponents j, g and h modify the viscosity (ν), load intensity (K) and tangential pitch line velocity (V) respectively.

$$f_m = \frac{\nu^j.K^g}{C_1.V^h} \tag{2.56}$$

where,
ν = Kinematic oil viscosity at operating sump temperature [mm^2/s]
K = Load intensity [N/mm^2]
C_1 = Constant = 3,239
V = Tangential pitch line velocity [m/s]
j = 0,223
g = 0,40
h = 0,70
Load intensity (K) can be expressed by Equation 2.57. It is mainly dependent on the gear geometry.

$$K = \frac{1000.T_1.(z_1 + z_2)}{2.b_w.r_{w1}^2.z_2} \tag{2.57}$$

where,
b_w = Face width in contact [mm]

2.2.2 ISO 14179-2/FVA 345 method

The FVA 345 method used the FZG back-to-back gear test rig (Figure 2.3) to determine the efficiency of a gear pair influenced by the lubricant behaviour. The setup is a modified FZG test rig which consists of two standard FZG gear pairs of 14 mm face width. The two gears pairs in the test and slave gearbox are coupled to each other by shafts. The input power is measured directly by applying the principle of power circulation where the power loss is the input power in the power circle. A torque meter is used between the power circle and motor to measure the loss. The frictional loss due to the lubricant behaviour is influenced by load, speed and temperature [26].

The friction coefficient depends on the lubrication regime as shown in figure 2.4.

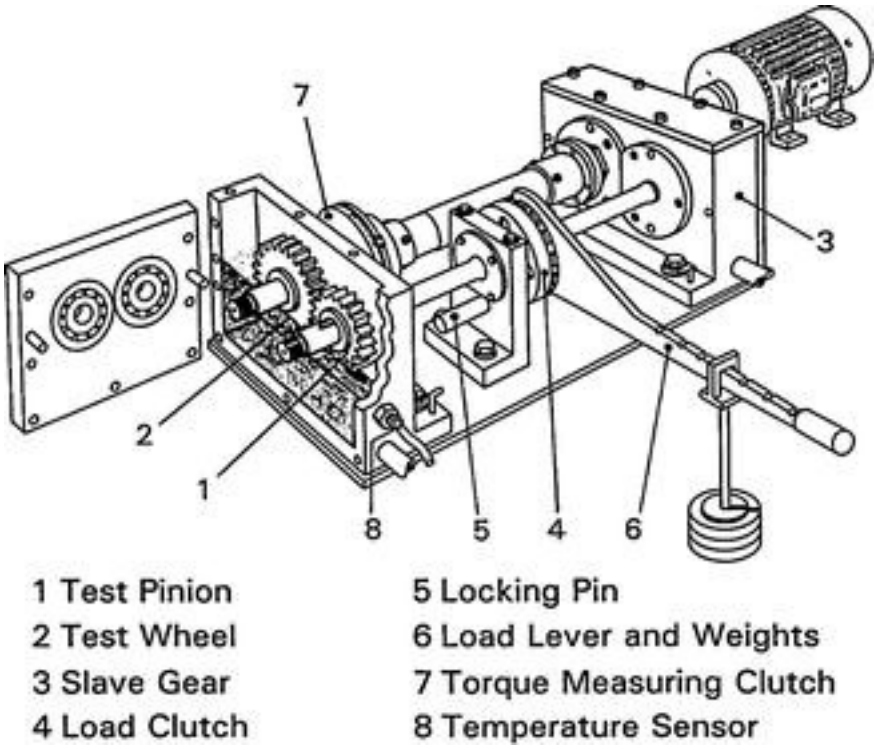

Figure 2.3: FZG efficiency test rig. [13]

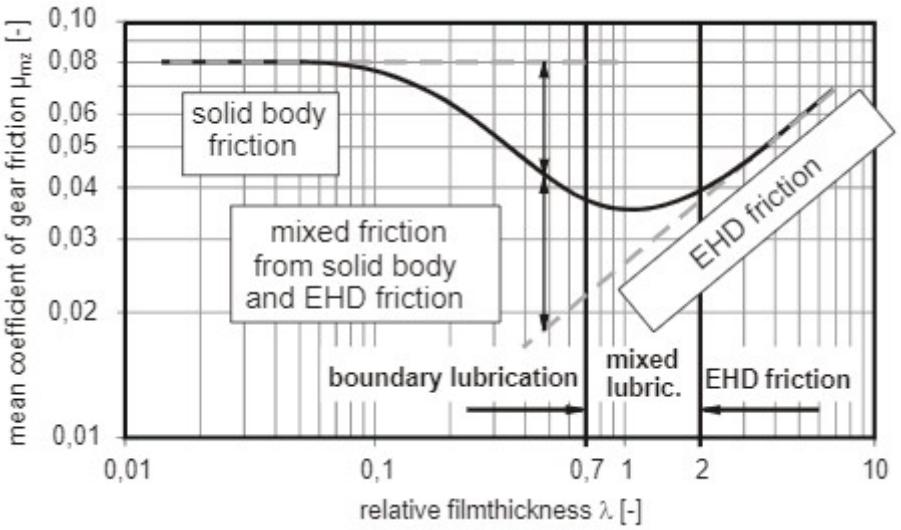

Figure 2.4: Lubrication Regime - Friction Coefficient vs Relative Film Thickness

The test methods consists of lubrication regimes that are calculated using the relative film thickness (λ) according to Dowson/Higginson. According to this model, the regimes are categorised as - boundary, mixed, elastohydrodynamic (EHL) lubrication. If $\lambda > 2$, a full separation exists in the contact with full film lubrication. The mixed lubrication regime occurs in metal-to-metal contact where $0,7 < \lambda < 2$. A sequence of four tests are performed:

1. **Run-in:** The new surfaces are smoothed to obtain a uniform tooth surface with least asperities.

2. **Control test:** It is used to identify the changes in equipment and measuring over a long usage period.

3. **Reference test:** Performed to compare the results between different labs and measure data for lubricant loss factors. A standard reference mineral oil FVA3A with 4% Anglamol 99 is used.

4. **Candidate test:** This test is performed with the candidate lubricant. A detailed test procedure with the different test duration and load cases have been described by Michaelis, Bernd-Robert and Andreas [26].

The lubricant loss factors are derived from the power loss ratio of the candidate to the reference lubricant at the given operating conditions which enable the comparison of different lubricant behaviour in mixed, boundary and poor conditions of EHL. The lubricant loss factors in FVA345 method are evaluated as a function of temperature due to the strong dependence of the lubricant on the temperature. The loss factors are:

- No load loss factor (X_{L0}): Compares the measured no load losses of candidate to the reference mineral oil with varying temperature.

- Load loss factor (X_{LL}): Compares the load influenced loss of the candidate to the reference mineral oil with varying temperature at pure sliding contact conditions. This factor is majorly influenced by EHL.

- Boundary loss factor (X_{LG}): Compares the load influenced loss of the candidate to the reference mineral oil with varying temperature at boundary contact conditions.

The contact condition to determine these load loss factors is decided based on the sliding velocities (v_s) and the relative film thickness (λ).

The comparison is made between the lubricant under examination and the reference FVA3A lubricant (MIN100). Base oil type influence EHL and mixed lubrication conditions while the effects of additives is critical for boundary lubrication conditions. Load, no-load and boundary lubrication loss factors are calculated depending on the lubrication regime and their behaviour with change in temperature is observed.

The steady state temperature is influenced by the equilibrium between the energy input and the energy output in terms of heat dissipated. For example, properties of the lubricant (especially viscosity) plays a major role in the dissipated heat and thus the steady state temperature. This is expressed in terms of the difference between the mean temperature of the test and main gearbox and the ambient temperature to reduce the effect of ambient temperature to the measurement of the power loss. The measurement of coefficient of friction in the gear mesh is influenced by the lubrication regime.

The total loss consists of losses from the bearings, gears and seals. The load dependent gear loss is given by the Equation 2.58. This is the general equation governing the powerloss for the FZG setup.

$$P_{VZP} = P_V - P_{VZ0} - P_{VL0} - P_{VLP} - P_{VD}. \tag{2.58}$$

where,
P_v = Total power loss [kW]
P_{VZ0} = Load independent gear losses [kW]
P_{VZP} = Load dependent gear losses [kW]
P_{VL0} = Load independent bearing losses [kW]
P_{VLP} = Load dependent bearing losses [kW]

The term P_{VLP} is given by the SKF bearing model described in Section 2.1.3. It can be modified to suit synthetic oil by including the load loss factor as shown in Equation 2.59.

$$P_{VLP} = f_1.d_m.F_N.\frac{2\pi.n}{60}.X_{LL} \tag{2.59}$$

where,
d_m = Mean diameter of the bearing [mm]
X_{LL} = Load loss factor

The transmitted power is measured and used in the final powerloss equation 2.60.

The determination of the friction coefficient μmz is further described below.

$$P_{VZP} = \mu_{mz}.P_A.H_V \tag{2.60}$$

where,
P_{VZP} = Load dependent gear power loss [kW]
μ_{mz} = Mean friction coefficient along the path of contact
P_A = Transmitted total input power [kW]
H_V = Ohlendorf's sliding loss factor described in Equations 2.68 and 2.69.

The contact friction μ_{mz} (Equation 2.60) is divided into solid body friction (μ_F) and EHD friction (μ_{EHD}).

$$\mu_{mz} = (1 - \xi)\ \mu_f + \xi.\mu_{EHD} \qquad for\ \mu_f \geqslant \mu_{EHD} \tag{2.61}$$

$$\mu_{mz} = \mu_{EHD} \qquad for\ \mu_f < \mu_{EHD} \tag{2.62}$$

The fraction of EHD friction (ξ) is calculated as a function of the relative film thickness (λ) shown in Equations 2.63, 2.64 and 2.65. The value of ξ versus λ can be seen from the Figure 2.5.

$$\xi = 1 - \left(1 - \frac{\lambda}{2}\right)^2 \qquad for\ \lambda < 2 \tag{2.63}$$

$$\xi = 1 \qquad for\ \lambda \geq 2 \tag{2.64}$$

$$\lambda = \frac{h_0}{0,5\,(Ra_1 + Ra_2)} \tag{2.65}$$

where,
h_0 = Measured film thickness
Ra_1 and Ra_2 are the surface roughness of the wheel and pinion respectively.

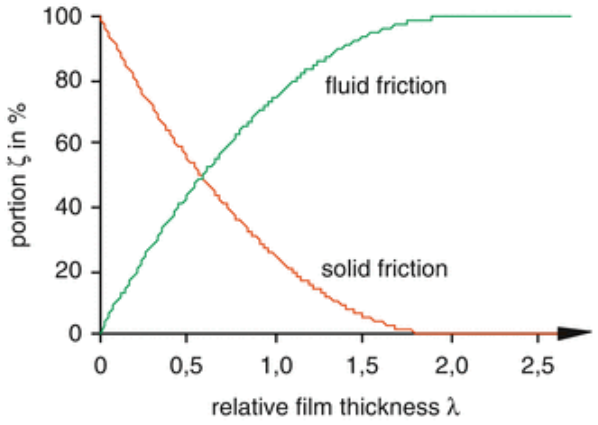

Figure 2.5: Fluid and solid friction in EHD contact. [26]

In the reference test, the value of solid body friction is calculated using Equation 2.66 and the mean friction coefficient (μ_z) is set equal to EHD friction coefficient

(μ_{EHD}). The reference conditions for calculating the friction coefficients are mentioned in [26]. Subsequently, the EHD friction is calculated using equation 2.67. The lubricant dependent and reference values in equations 2.67 and 2.66 are obtained by performing the FZG rig test.

$$\mu_f = \mu_{FR}.\left(\frac{p_h}{p_R}\right)^{\alpha_f}.\left(\frac{v_\Sigma}{v_{RF}}\right)^{\beta_f} \tag{2.66}$$

where,
μ_f = Solid body friction coefficient.
μ_{FR} = Solid body friction coefficient from reference test.
p_h = Contact pressure $[N/mm^2]$.
p_r = Contact pressure from reference test $[N/mm^2]$.
v_Σ = Sum velocity $[m/s]$.
v_RF = Reference value of speed from solid friction.
α_F = Pressure exponent for solid friction test.
β_F = Speed exponent for solid friction test.

$$\mu_{EHD} = \mu_{EHD,R}.\left(\frac{p_h}{p_R}\right)^{\alpha_{EHD}}.\left(\frac{v_\Sigma}{v_{EHD,R}}\right)^{\beta_{EHD}}.\left(\frac{\eta_\Sigma}{\eta_R}\right)^{\gamma_{EHD}} \tag{2.67}$$

where,
μ_{EHD} = Fluid friction coefficient.
$\mu_{EHD,R}$ = Fluid friction coefficient from reference test.
p_h = Contact pressure $[N/mm^2]$.
p_r = Contact pressure from reference test $[N/mm^2]$.
v_Σ = Sum velocity $[m/s]$.
$v_{EHD,R}$ = Reference value of speed from fluid friction.
α_{EHD} = Pressure exponent for fluid friction test.
β_{EHD} = Speed exponent for fluid friction test.
γ_{EHD} = Viscosity exponent for fluid friction test.

Ohlendorf [27] [18] proposed a loss factor H_V (Equation 2.68) which depends on geometrical data of the gear. This factor is only applicable for external gear mesh.

$$H_V^{Ohl} = \frac{\pi.(u+1)}{z_1.u.cos(\beta_b)}.\left(1 - \epsilon_\alpha + \epsilon_1^2 + \epsilon_2^2\right) \tag{2.68}$$

where,
H_V = Gear loss factor
z_1 = Number of teeth on the Pinion
u = Gear ratio (z_2/z_1)
β_b = Helix angle at base cylinder [°]
ϵ_α = Profile contact ratio
$\epsilon_{1,2}$ = Tip contact ratio, pinion and gear

In case of internal gear mesh, the Ohlendorf factor shown in Equation 2.69 should be used. The only difference between Equations 2.68 and 2.69 is the gear ratio (u)

term in the denominator.

$$H_V^{Ohl} = \frac{\pi.(u+1)}{z_1.cos(\beta_b)}.\left(1 - \epsilon_\alpha + \epsilon_1^2 + \epsilon_2^2\right) \tag{2.69}$$

A good way to estimate the gear contact friction without conducting the FVA efficiency test is given by equation 2.70 [17] [12].

$$\mu_z = 0,048.\left(\frac{F_{bt}/b}{v_{\Sigma c}.\rho_{redC}}\right).{\eta_{oil}}^{-0.05}.Ra^{0.5}.X_L \tag{2.70}$$

where,
μ_z = Mean gear mesh friction coefficient
F_{bt} = Normal tooth load [N]
$v_{\Sigma c}$ = Sum velocity at pitch point [m/s]
ρ_{redC} = Reduced radius of curvature at pitch point [mm]
${\eta_{oil}}^{-0.05}$ = Dynamic lubricant viscosity [mPas]
$Ra^{0.5}$ = Mean roughness of pinion and gear
X_L = Factor based on lubricant type (=0,9 for hydrocrack oil)

In conclusion, it is possible to compare the efficiency of a gear mesh with different lubricates by calculating the coefficient of friction under the solid and EHD contact regime and the load loss factors are used to derive the influence of temperature to provide more detailed comparison between the lubricants.

2.2.3 Micro-Geometry model with Variable friction coefficient

In this model, the total friction loss can now be expressed as,

$$P_{VZP} = P_a.\mu_{mz}.H_V \tag{2.71}$$

where,
P_{VZP} = Load gear losses [kW]
P_a = Transmitted power [kW]
μ_{mz} = Mean coefficient of gear friction
H_V = Gear loss factor

The transmitted power (P_a) can be evaluated by using Equation 2.72.

$$P_a = \frac{2.\pi.n.T}{60} \tag{2.72}$$

where,
n = Gear rotational speed [rpm]
T = Torque on the gear [Nm]

In order to determine mean coefficient of gear friction (μ_{mz}), friction coefficient is plotted over the surface of the gear tooth in Romax. This gives the range over which friction coefficient varies along the gear mesh, using which the mean coefficient of gear friction is evaluated. The gear loss factor by Ohlendorf given by Equations 2.68 and 2.69 is determined in the same way as described in Section 2.2.2.

2.2.4 Anderson model

Anderson and Loewenthal [4] gives a analytical model to estimate the power losses in spur gears, which was later used by Heingartner et al. [16] to estimate the power losses in helical gears. This was done by modifying the expression for instantaneous coefficient of friction to consider the helical gear contact length. The total gear contact friction loss given by Equation 2.73 can be determined by adding the individual power losses from Equations 2.74 and 2.78.

$$P_{VZP} = P_S + P_R \tag{2.73}$$

2.2.4.1 Sliding Friction loss

According to Heingartner et al.[16], the instantaneous sliding friction loss is a function of the instantaneous sliding velocity and sliding force. The sliding force in turn is a function of the instantaneous normal tooth load and instantaneous friction coefficient. Power consumption increases as a result of the effect of the sliding friction and its magnitude depends on the point of contact.

The instantaneous sliding power loss (P_S) is given by Equation 2.74.

$$P_S = V_S.F_S \tag{2.74}$$

where,
P_S = Sliding power loss [W]
F_S = Sliding force [N]
V_S = Sliding velocity $[mm/s]$

Sliding force can be defined as the frictional force which is generated as a result of mechanical contact between mating gears. It is determined by using Equation 2.75.

$$F_S = \mu.w \tag{2.75}$$

where,
μ = Friction coefficient
w = Normal gear contact load [N]

The expression for the instantaneous coefficient of friction for spur gears given by Anderson [3, 4] was employed by Heingartner et al.[16] to give the expression for friction coefficient, which is given by Equation 2.76.

$$\mu = 0,0127.log\left(\frac{C_1.w}{b.\mu_0.V_S.V_T^2}\right) \tag{2.76}$$

where,
C_1 = Constant = 29,66
b = Face width [mm]
μ_0 = Ambient viscosity at ambient temperature $[mm^2/s]$
L_C = Contact line length [mm]
V_T = Rolling velocity $[mm/s]$

In order to determine the expression for the friction coefficient for helical gears, contact length has to be taken into consideration. The authors of [29] detailed the contact length on helical gears and substituted into Equation 2.76. The friction coefficient for helical gears can now be given by Equation 2.77. The friction coefficient used here is not dependent on the surface temperature of the gear, which is incorrect.

$$\mu = 0,0127.log\left(\frac{C_1.w}{L_C.\mu_0.V_S.V_T^2}\right) \tag{2.77}$$

2.2.4.2 Rolling Friction loss

Heingartner et al.[16] stated that the rolling friction loss depends on the rolling velocity and the instantaneous lubricant film thickness. As the gear teeth come into mesh, this engagement draws the lubricant into the contact zone and forms an elastohydrodynamic lubricant film. Rolling friction losses depend on the angular velocity of the gears, pressure angle, lubricant film thickness and the point of contact along its contact path. The lubricant properties like the thermal behaviour, its shear values, gear material and the normal tooth load have a major impact on the lubricant film.

The rolling power loss (P_R) is given by Equation 2.78.

$$P_R(x) = 10^{-3}.V_T(x).F_R(x) \tag{2.78}$$

where,
P_R = Rolling power loss [W]
V_T = Rolling velocity $[mm/s]$
F_R = Rolling friction force [N]

Anderson et al.[4] gave the expression for determining the instantaneous rolling friction loss for spur gears, which was used by Heingartner et al.[16] to modify the expression for helical gears, as the contact line length in helical gears is not synonymous with face width. The instantaneous rolling friction loss in helical gears (F_R) is given by Equation 2.79.

$$F_R(x) = C_2.h(x).\phi_t(x).L_C \tag{2.79}$$

where,
F_R = Rolling friction force [N]
C_2 = Constant = $9 * 10^7$
h = Isothermal central film thickness [mm]
ϕ_t = Thermal reduction factor
L_C = Contact line length [mm]

2.3 Gear drag/Churning loss

Churning losses are speed dependent losses which occur when the gears are being dragged in the lubricant. These type of losses are influenced by the viscosity of the

lubricant, oil level and the rotational speed. Churning losses are one of the major contributors to the overall power loss in a transmission system. All the rotating components dipped into the lubricant will contribute to the churning losses and deeper the components are submerged the higher the losses. They can be reduced by using a lubricant with lower viscosity or by reducing the oil level in the system. But, that would result in bad lubrication of gears and higher operating temperatures.[6].

2.3.1 ISO 14179-1 model

The International Organisation for Standardisation (ISO) [19] developed a model for estimating the gear windage and churning power loss. The Equations 2.80, 2.81 and 2.82 are derived from Section 12.5.2 of Dudley [9] and modified to take into account the oil viscosity, gear dip factor (f_g), arrangement constant (A_g) and gear outer diameter (D).

The gear dip factor (f_g) is dependent on the immersion depth of the gear into the oil. The factor will be equal to 0 if the gear does not dip into the oil. If the gear is partly immersed in the oil, the factor will linearly interpolate between 0 and 1. If the gear is fully immersed in the oil, the factor will be 1. According to ISO [19], the value of the arrangement constant (A_g) is 0,2.

This model consists of three categories as explained below in Equations 2.80, 2.81 and 2.82.

1. **Smooth outside diameter**: This is applied when the component has a smooth outside diameter.
   e.g. outside diameter of a shaft.

$$P_{SOD} = \frac{7,37.f_g.\nu.n^3.D^{4,7}.L}{A_g.10^{26}} \tag{2.80}$$

2. **Side of the gear**: This is used to determine the losses of the smooth sides of the disc. Equation 2.81 includes both the sides of the gear.
   e.g. faces of a gear

$$P_{side} = \frac{1,474.f_g.\nu.n^3.D^{5,7}}{A_g.10^{26}} \tag{2.81}$$

3. **Tooth surfaces**: This is used to determine the losses from the gear tooth surfaces. e.g. outside diameter of a gear or pinion.

$$P_{tooth} = \frac{7,37.f_g.\nu.n^3.D^{4,7}.b.\frac{R_f}{\sqrt{tan\beta}}}{A_g.10^{26}} \tag{2.82}$$

The power loss equation for tooth surfaces (Equation 2.82) includes a term called roughness factor (R_f). Equation 2.83 gives an approximation of the values from

Dudley [9].

$$R_f = 7,93 - \frac{4,648}{m_t} \tag{2.83}$$

where,
f_g = Gear dip coefficient
ν = Oil kinematic viscosity $[mm^2/s]$
n = Rotational speed [rpm]
D = Gear outer diameter [mm]
L = Length of shaft[mm]
A_g = Arrangement constant
R_f = Roughness factor
b = gear face width [mm]
β = Helix angle [°]
m_t = Gear transverse module

The total churning power loss in each gear given by Equation 2.84 which can be determined by adding the individual power losses from Equations 2.80, 2.81 and 2.82.

$$P_{churning} = P_{SOD} + P_{side} + P_{tooth} \tag{2.84}$$

2.3.2 ISO 14179-2 model

According to the International Organisation for Standardisation[20], the load independent gear losses depend on the formulations derived by Mauz [24]. The load independent gear losses are determined by multiplying the total hydraulic loss torque with the angular velocity of the gear. The total load independent gear losses are calculated by taking the sum of the power losses in each stage (Equation 2.85).

$$P_{VZ0} = \sum_{i=1}^{stage} T_{Hi}.\left(\frac{\pi.n_i}{30}\right) \tag{2.85}$$

where,
P_{VZ0} = Load independent gear losses or Gear drag losses [W]
T_H = Total hydraulic loss torque [Nm]
n = Gear speed [rpm]

In case of Splash lubrication, the total hydraulic loss torque in a gear stage can be determined by Equation 2.86.

$$T_H = C_{SP}.C_1.e^{C_2\left(\frac{v_t}{v_{t0}}\right)} \tag{2.86}$$

where,
C_{SP} = Splash oil factor
v_t = Tangential speed [m/s]

v_{t0} = Reference Tangential speed [m/s]

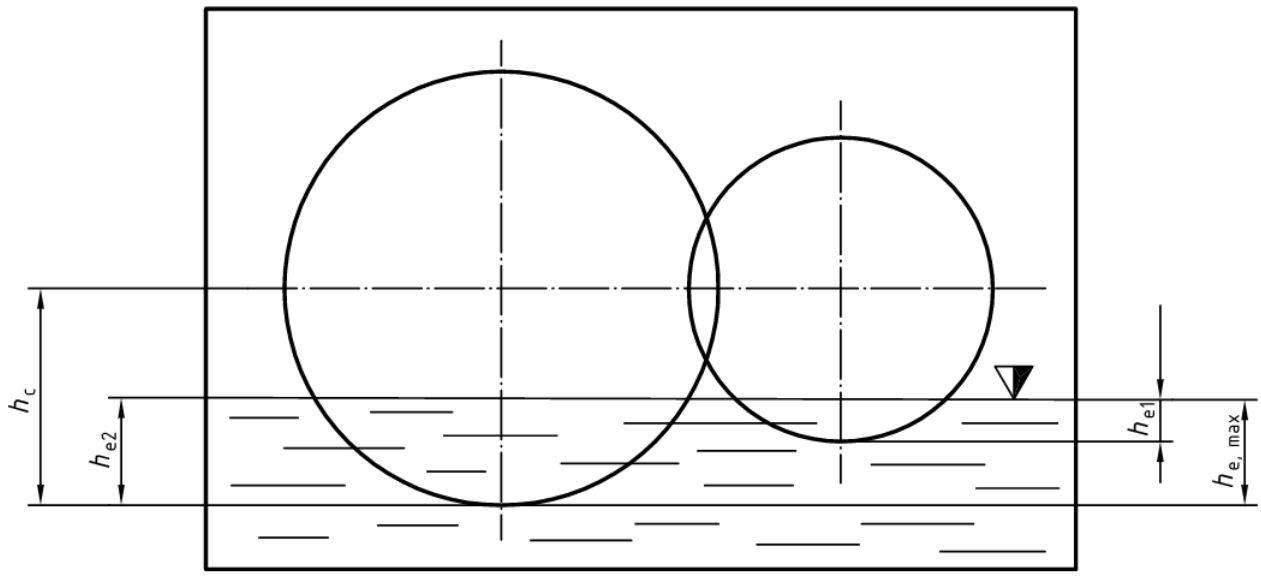

Figure 2.6: Splash oil factor[20]

The splash oil factor (C_{SP}) can be evaluated by using Equation 2.87. The effect of splash oil supply is taken into account by considering the immersion depth to determine the factor (Figure 2.6). The factors C_1 and C_2 which are used to define the effect of tooth width and immersion depth are defined in Equation 2.88 and Equation 2.89 respectively. The effect of viscosity was not measurable at low immersion depth, where as conflicting results were observed at high immersion depth. The gear drag losses increased with increasing viscosity in some cases, whereas in other cases the losses decreased. Hence, viscosity is not considered in any of the equations.

$$C_{SP} = \left(\frac{4.h_{e,max}}{3.h_c}\right)^{1,5} . \left(\frac{2.h_c}{l_h}\right) \tag{2.87}$$

$$C_1 = 0,063\left(\frac{h_{e1} + h_{e2}}{h_{e0}}\right) + 0,0128\left(\frac{b}{b_0}\right)^3 \tag{2.88}$$

$$C_1 = \left(\frac{h_{e1} + h_{e2}}{80.h_{e0}}\right) + 0,2 \tag{2.89}$$

where,
$h_{e,max}$ = Maximum Tip circle immersion depth with oil level stationary [mm]
h_c = Height of point of contact above the lowest point of the immersing gear [mm]
$h_{e1,e2}$ = Tip circle immersion depth with oil level stationary [mm]
h_{e0} = Reference value of immersion depth [mm]
b = Tooth width [mm]

b_0 = Reference value of tooth width [mm]
l_h = Hydraulic length [mm] (Figure 2.7).

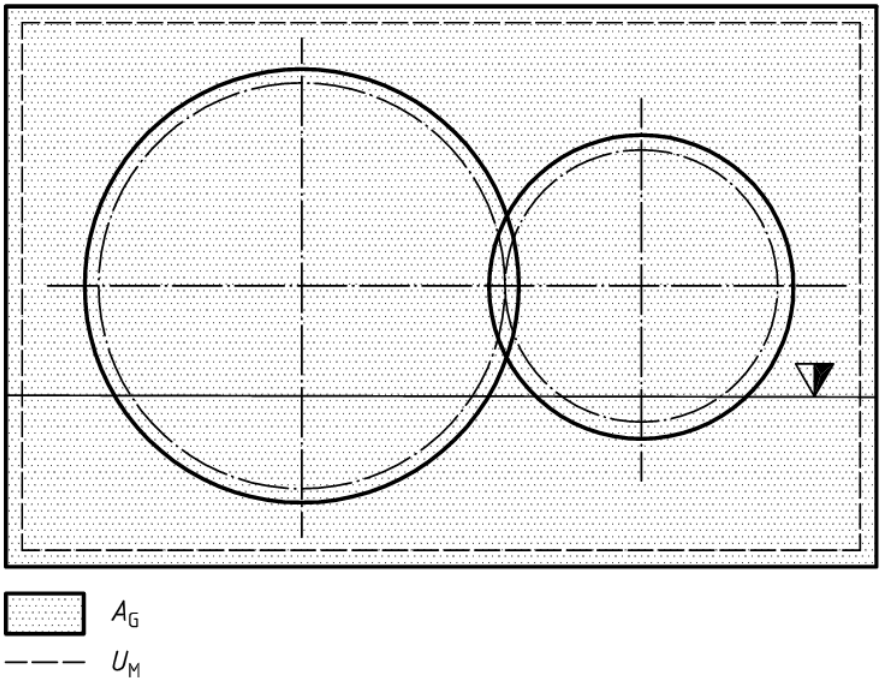

Figure 2.7: Hydraulic length (l_h)[20]

Hydraulic length (l_h) is defined in Equation 2.90. It is evaluated by taking the ratio of enclosure area to the enclosure circumference (Figure 2.7).

$$l_h = \frac{4.A_G}{U_M} \tag{2.90}$$

where,
A_G = Enclosure area [mm^2]
U_M = Enclosure Circumference [mm]

2.3.3 Terekhov model

According to A.S. Terekhov [33], the hydraulic losses in a gearbox immersed in lubricant will have two components which contribute to the power loss i.e. the energy loss during the interaction between the rotating gears and the oil bath (or the disc losses) and the energy loss due to the displacement of oil in the roots of the gear teeth at the start of the engagement process.

According to Figure 2 in [33], the disc losses (M_D) are mainly dependent on the rotational frequency of the gears, immersion depth and viscosity of the lubricant. The losses increase as the volume of lubricant poured over the gears increases, even as the immersion depth is constant. There is also a critical value for the volume of

the lubricant after which there is no effect on the disc losses. In this model, it is assumed that the gear module has no effect on the losses, because the tooth spaces get filled with the lubricant and the gear rotates like a smooth disc when the teeth are passing through the oil bath.

The losses due to lubricant expulsion (M_{oe}) depend on the rotational speed of the gears and viscosity of the lubricant. The losses are independent of any ratio between the frictional and viscous forces. The losses also increase with an increase in the diameter and width of the gear and with the reduction of its module.

From Figure 3 in [33], as the rotational speed of the gears increases, the losses for different lubricant viscosities initially increase and then start decreasing. As the lubricant viscosity increases, the peak in the curve shifts to the higher speed region. This is caused because at low speeds (or low lubricant viscosities) the tooth spaces are completely filled with lubricant and the losses increase as the speed increases. As the speed keeps on increasing, the lubricant is thrown out from the gears by the centrifugal forces and the losses decrease.

In this model, two zones of fluid flow are formed in the neighbourhood of the rotating disc. The lubricant is poured onto the disc and rotates with it like a belt in the first zone. The flow of the lubricant is approximately laminar in this zone. At some critical value of the Reynolds number, the fluid flow becomes turbulent (Re=2250). The effect of (V_g/V_o) is not constant in the first zone. At low speeds (high viscosities), the impact of (V_g/V_o) is even lower. This ratio only affects the losses upto a specified limit. The first zone is divided into two sub-zones 1_1 and 1_2. The boundary between these two sub-zones is defined by the ratio of the Reynolds and Froude numbers. Sub-zone 1_1 is defined by $Re^{-0,6}.Fr^{-0.25} > 8,7 * 10^{-3}$.

The general function for the moment of the disc losses in a gear (M_D) is of the form.

$$M_D = f(R, b, h, \omega, g, \rho, \nu, V_o) \tag{2.91}$$

where,
R = Outer radius of the gear $[m]$
b = Breadth of the pinion $[m]$
h = Immersion depth of gear into the lubricant $[m]$
ω = Angular velocity of the pinion $[r/s]$
g = Acceleration due to gravity $[m^2/s]$
ρ = Density of the lubricant $[kg/m^3]$
μ = Kinematic viscosity of lubricant $[m^2/s]$
V_o = Volume of the lubricant poured into the gear $[m^3]$

The disc losses in a gear (M_D)can be determined by using Equation 2.92.

$$M_D = C_M.\rho.\omega^2.R^4.b \tag{2.92}$$

The general function for the moment factor for the disc losses in a gear (C_M) is as

shown below.

$$C_M = f(Re, Fr, \frac{h}{R}, \frac{b}{R}, \frac{V_g}{V_o}) \tag{2.93}$$

where,
Re = Reynolds number = $(\omega.R^2)/\nu$
Fr = Froude number = $(\omega^2.R)/g$
V_g = Immersed volume of the gear $[m^3]$
(h/R) = Ratio of the immersion depth of the gear to its radius
(b/R) = Ratio of the breadth of the gear to its radius
(V_g/V_o) = Ratio of the immersed volume of the gear to the volume of lubricant poured over it.

Equation 2.94, 2.95 and 2.96 are used to determine the moment of the disc losses of each gear for zones 1_1, 1_2 and 2 respectively. These equations are only applicable to the following ranges of variation in the general parameters.

- Re = 10 - 36000;
- Fr = 1,6 - 1400;
- (h/R) = 0,025 - 1,0;
- (b/R) = 0,006 - 1,0;
- (V_g/V_o) = 0,1 - 0,25;
- $(\Sigma V_g/V_o)$ = 0,02 - 0,5;

$$C_M = 4,57 * Re^{-0,6} * Fr^{-0,25} * \left(\frac{h}{R}\right)^{1,5} * \left(\frac{b}{R}\right)^{-0,4} * \left(\frac{V_g}{V_o}\right)^{-0,3} * \left(\frac{\Sigma V_g}{V_o}\right)^{-0,2} \tag{2.94}$$

$$C_M = 2,63 * Re^{-0,6} * Fr^{-0,25} * \left(\frac{h}{R}\right)^{1,5} * \left(\frac{b}{R}\right)^{-0,17} * \left(\frac{V_g}{V_o}\right)^{-0,53} * \left(\frac{\Sigma V_g}{V_o}\right)^{-0,2} \tag{2.95}$$

$$C_M = 0,376 * Re^{-0,3} * Fr^{-0,25} * \left(\frac{h}{R}\right)^{1,5} * \left(\frac{b}{R}\right)^{-0,124} * \left(\frac{V_g}{V_o}\right)^{-0,376} * \left(\frac{\Sigma V_g}{V_o}\right)^{-0,2} \tag{2.96}$$

The general function for the moment of the losses due to lubricant expulsion (M_{oe}) is of the form.

$$M_{oe} = f(R_0, b, l, \omega, \rho, g, \nu) \tag{2.97}$$

where,
Re = Reynolds number = $(\omega.R_0.l)/\nu$
Fr = Froude number = $(\omega^2.R_0^2)/(gl)$
R_0 = Radius of the pitch circle [m]
l = Tooth depth [m]

The losses due to lubricant expulsion (M_{oe}) can be determined by using Equation 2.98.

$$M_{oe} = C_M.\rho.\omega^2.R_0^3.b.l \tag{2.98}$$

The general function for the losses due to the expulsion of lubricant (C_M) is mentioned below.

$$C_M = f(Re, Fr, \frac{b}{l_0}, \frac{l}{l_0}) \tag{2.99}$$

where,
l_0 = Scale factor for length. It is introduced for dimensional compensation.

The losses due to lubricant expulsion vary in both the first and second zones (Figure 3 in [33]), which are described by the Equations 2.100 and 2.101 respectively. These equations are only applicable to the following ranges of variation in the general parameters.

- Re = 7 - 2100;
- Fr = 22 - 3112;
- (l/l_0) = 0,45 - 1,8;
- (b/l_0) = 1 - 6;

$$C_M = 616,6 * Re^{-0,65} * Fr^{-0,46} * \left(\frac{l}{l_0}\right)^{-1,66} * \left(\frac{b}{l_0}\right)^{-0,46} \tag{2.100}$$

$$C_M = 5623 * Re^{-0,88} * Fr^{-0,78} * \left(\frac{l}{l_0}\right)^{-1,6} * \left(\frac{b}{l_0}\right)^{-0,36} \tag{2.101}$$

As a result of the nature of disc resistances in this direction of rotation, the moment of disc losses is described by the Equation 2.102.

$$C_M = 0,506 * Re^{-0,32} * Fr^{-0,25} * \left(\frac{h}{R}\right)^{2,1} * \left(\frac{b}{R}\right)^{-0,27} * \left(\frac{V_g}{V_o}\right)^{-0,8} * \left(\frac{\Sigma V_g}{V_o}\right)^{-0,2} \tag{2.102}$$

The moment of disc resistances are determined for each gear engagement individually. The total moment of disc resistances is determined by adding all the individual moments. These moments are then added to the moments of losses due to lubricant expulsion for each engagement.

2.4 Seal losses

Seals are used in a transmission to prevent the lubrication from escaping into the surroundings. They also avert the outside agents from entering the system. There are two types of seals - Static and Dynamic seals. Static seals are used between the housing members in a transmission and they have no impact on its efficiency, where as the Dynamic seals affect the efficiency as they are in contact with the shaft. There is loss in efficiency through friction and heat as the shaft rotates inside a stationary seal. Lubrication is applied between the shaft and seal to reduce the effect of friction. Various types of seals can be used, which lead to different amounts of power losses on the shaft. [14]

2.4.1 ISO 14179-1 model

According to the International Organisation for Standardisation[19] [1], the oil seal power losses depend on shaft size, shaft speed, oil sump temperature, oil viscosity, depth of submersion of the oil seal in the lubricant and oil seal design. The oil seal losses are determined by Equation 2.103.

$$P_{Si} = \frac{T_S.n}{9549} \tag{2.103}$$

where,
P_{Si} = Power loss for each individual oil seal [kW]
T_S = Oil seal torque [Nm]
n = Shaft speed [rpm]

The oil seal torque (T_S) depends on the material of the seal for the intended application. Either Viton or Buna N seals can be selected as the material based on the mechanical properties desired in the sealing application. The oil seal torque for Viton and Buna N seals is determined by Equation 2.104 and 2.105 respectively.

$$T_S = 3,737 * 10^{-3}.D_S \tag{2.104}$$

$$T_S = 2,429 * 10^{-3}.D_S \tag{2.105}$$

where,
D_S = Shaft diameter [mm]

2.4.2 ISO 14179-2 model

According to the International Organisation for Standardisation[20] [30], the power loss for radial shaft seals is calculated by using Equation 2.106. In case of non-contacting seals, it is assumed that they don't contribute to the power loss.

$$P_{VD} = 7,69 * 10^{-6}.D_S.n \tag{2.106}$$

where,
P_{VD} = Seal Power loss[W]
D_S = Shaft diameter [mm]
n = Shaft speed [rpm]

2.5 Windage losses

According to Heingartner [16], when the gears rotate the lubricant is flung off inside the gear housing in the form of small droplets of the lubricant. This occurs due to the centrifugal force acting on the lubricant. The small droplets of lubricant form a fine mist of oil which will be suspended inside the housing. This oil mist causes an increase in power consumption as it offers an increase in frictional resistance to the gears. As the gear teeth are engaged, the removal of the oil between the tooth surfaces causes a turbulence inside the gearbox, which also increases power consumption. Both these factors along with the losses at the side of the gears, contribute to the overall windage losses. These losses are influenced by the rotational speed of the gear, tooth module, gear diameters and the amount of oil mist present inside the gear housing. Windage losses won't be evaluated as it is out of scope of this thesis.

A mathematical model was proposed by Anderson et al. [2] to predict windage losses (Equation 2.107). This model didn't take both the tooth module and the helix angle into consideration.

$$p_i = C_1.\left(1 + (2,3).\frac{b_i}{R_i}\right).N_i^{2,8}.R_i^{4,6}.\left(0,028.\mu_i + C_2\right)^{0,2} \tag{2.107}$$

where,
p_i = Windage power loss by solid i [kW]
C_1 = 2,82 * 10^{-7} (S.I)
C_2 = 0,019 (S.I)
b_i = Face width [m]
N_i = Speed of solid i [rpm]
μ_i = viscosity [cp]
R_i = Pitch radius of solid i [m]

In a series of experimental measurements on large gears at low to medium speeds, Dawson [8] measured the deceleration of rotating gears with no power supply and formulated the expression shown in Equation 2.108.

$$P_1 = N^{2,9}.\left(0,16.D_r^{3,9} + D_r^{2,9}.F^{0,75}.m_1^{1,15}\right).10^{-20}.\Phi.\lambda \tag{2.108}$$

where,
P_1 = Windage power lsos [kW]
N = Speed [rpm]

D_r = Root diameter [mm]
F = Face width [mm]
m_1 = module [mm]
Φ = constant (for an oil-free atmosphere at ambient temperature, $\Phi = 1$)
λ = accounts for casing (λ =0,5 - 0,6 for 'fitting' casing, λ =0,6 - 0,7 for large enclosure, λ =1 with no casing)

3

Methods

The basic outline followed to evaluate and validate the power loss of the transmission model at the system level is by setting up analytical models on MATLAB with reference to literature and comparing with the results from the sub-models designed on ROMAX. Various combinations of these sub-models for the respective machine elements within the system model is also compared with the final test bench results and reasonable justification for the correlation of efficiency values are described.

3.1 Operating conditions

3.1.1 Load cases

The efficiency test was performed for the following load cases at temperature of 70 °C is under consideration. The load cases shown below in Table 3.1 will be simulated for all the sub-models and the system model.

Table 3.1: Load cases

		Load Levels[Nm]											
Output speed [RPM]	Input Speed [Nm]	-200	-100	-75	-50	-25	25	50	75	100	200	240	300
200	1715	X	X	X	X	X	X	X	X	X	X	X	X
600	5142	X	X	X	X	X	X	X	X	X	X	X	
1000	8570		X	X	X	X	X	X	X	X			
1150	9856		X	X	X	X	X	X	X	X			

3.1.2 Lubricant properties

Table 3.2: Lubricant properties

Property	
SAE Grade	75W
Relative density at 15 °C	0,847 $[g/ml]$
Appearance	Clear
Kinematic viscosity at 100 °C	4,6 mm^2/s
Kinematic viscosity at 40 °C	18 mm^2/s
Viscosity index	186
Pour point	-15 °C
Flash point, COC	190 °C

3.2 Sub-models

The sub-models of all the components are based on the transmission system model provided by Volvo car corporation. The efficiency prediction simulation using power loss models is implemented using sub-models for individual machine elements such as bearings, gears, seals etc,. All the simulations are based on static analysis results (ROMAX). The sub-models are evaluated by applying the loads and boundary conditions acting on the machine element for the respective load cases in the system model.

3.2.1 Bearing sub-models

There are two different types of bearings used in the system model - Deep groove radial ball bearings and a needle bearing. There are four methods for power loss prediction based on different models for bearing friction efficiency analysis - SKF [31], Palmgren [28], ISO 14179-1 (US) [19] and ISO 14179-2 (DE) [20]. These models have been defined in Section 2.1. Both the ISO 14179 models for bearings have the same procedure as described in their respective literature.

3.2.1.1 Deep groove radial ball bearing - FAG 61822-Y

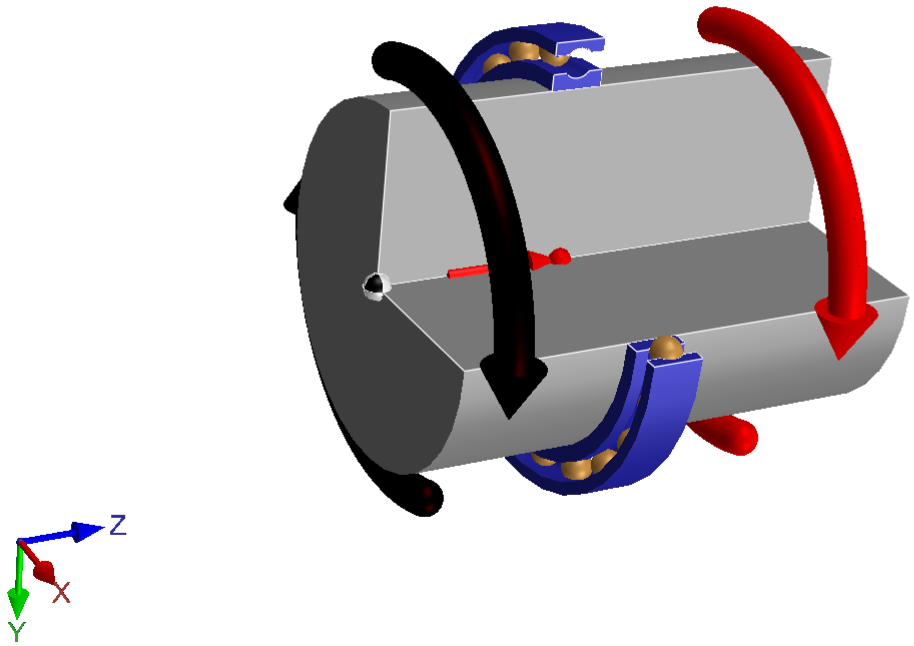

Figure 3.1: FAG 61822-Y bearing sub-model (Image taken from ROMAX software)

FAG 61822-Y bearing is the bigger of the two deep groove radial ball bearings in the transmission system model. The sub-model of FAG 61822-Y bearing used for simulation is presented in Figure 3.1. It is mounted between the planetary carrier and the housing on the rotor side of the assembly. The sub-model for this bearing is modelled by mounting the bearing on a shaft and providing the input power on one side of the shaft and the output power on the other side of it. The load cases from Table 3.1 are applied on the system model and the corresponding axial loads acting on the bearing are applied in the sub-model. Radial loads do not play a major role in the power loss of these type of bearings. The axial loads are applied as a point load on the bearing in the sub-model. The input and output power for this bearing are the same as that of planetary carrier (from system model). The bearing specifications can be found in Table 3.3.

Table 3.3: Deep groove radial ball bearing - FAG 61822-Y specifications

Type	Radial ball
Catalogue	FAG2012
Designation	61822-Y
Outer Diameter	140 mm
Bore	110 mm
Overall width	16 mm

Below is a description of how all the three analytical models were implemented in MATLAB for the deep groove ball bearing FAG 61822-Y.

3.2.1.1.1 ISO 14179-1 model: According to ISO [19], there are two major contributors to the power loss in bearings: Bearing load dependent torque (M_1) and cylindrical roller bearing axial load dependent moment (M_2) (Section 2.1.1). The losses mainly depend on bearing geometry, bearing rotational speed and load on the bearing. Although the term M_2 accounts for axial load moment in cylindrical roller bearings, it cannot be ignored for deep groove ball bearings, as doing so will result in unrealistically low power loss. The characteristic constants for the ISO 14179-1 model are shown in Table 3.4.

Table 3.4: ISO 14179-1 constants for Deep groove radial ball bearing - FAG 61822-Y and FAG 6009

Parameter	**Constant**	**Value**
Exponent	a	1
Exponent	b	1
Factor depending on bearing design and lubrication	f_2	0,003

3.2.1.1.2 Palmgren model: According to Palmgren [28], the power loss in ball bearings is mainly influenced by load friction torque (M_1) and viscous friction torque (M_v) (Section 2.1.2). This model also consists of Palmgren friction coefficient (f_1) and Palmgren churning loss factor (f_0), which are estimated in ROMAX analysis. In analytical models, both f_1 and f_0 are evaluated using their respective expressions. While f_1 depends on the bearing design and relative bearing load, f_0 depends on the bearing type and method of lubrication. The characteristic constants for the Palmgren equivalent bearing are shown in Table 3.5.

Table 3.5: Palmgren constants for Deep groove radial ball bearing - FAG 61822-Y and FAG 6009

Parameter	Constant	Value
Number of rows of rolling elements	i	1
Constant for Radial deep-groove ball bearing	z	0,0004
Constant for Radial deep-groove ball bearing	y	0,55
Constant for Radial-contact groove ball bearing	X_s	0,6
Constant for Radial-contact groove ball bearing	Y_s	0,5
Factor depending on the type of bearing and method of lubrication	f_0	2

3.2.1.1.3 SKF model According to SKF [31], the total frictional moment is the sum of rolling frictional moment (M_{rr}), sliding frictional moment (M_{sl}), frictional moment of seals (M_{seal}) and frictional moment of drag losses (M_{drag})(Section 2.1.3). M_{seal} will not be included in the analysis. In ROMAX analysis and analytical models, the SKF friction loss factors R_1, R_2, S_1 and S_2 are estimated for '618' Radial ball bearing series according to the SKF catalogue [31]. The characteristic constants for the SKF equivalent bearing are shown in Table 3.6.

Table 3.6: SKF equivalent constants for Deep groove radial ball bearing - FAG 61822-Y

Constant	Constant	Value
Replenishment/Starvation Constant	K_{rs}	$3 * 10^{-8}$
Bearing type related geometric	K_Z	3,1
constant depending on movement	mu_{bl}	0,12
sliding friction coefficient in full-film conditions mu_EHL	0,1	
Drag loss factor	V_M	0,00005
Number of ball rows	i_{rw}	1
Dynamic load rating	C_0	30500 N

3.2.1.2 Deep groove radial ball bearing - FAG 6009

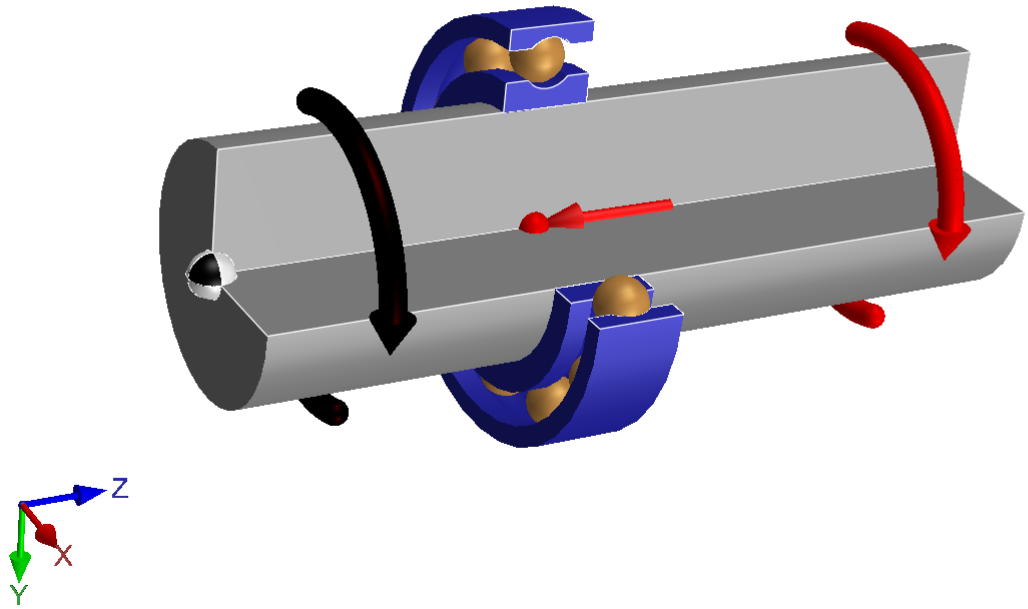

Figure 3.2: FAG 6009 bearing sub-model (Image taken from ROMAX software)

FAG 6009 bearing is the smaller of the two deep groove radial ball bearings in the transmission system model. The sub-model of FAG 6009 bearing used for simulation can be found in figure 3.2. It is mounted between the carrier and the housing on the driveshaft side of the transmission. It is modelled in a similar manner to FAG 61822-Y bearing (Section 3.2.1.1). The input and output power for this bearing are the same as that of planetary carrier. The bearing specifications can be found in Table 3.7

Table 3.7: Deep groove radial ball bearing - FAG 6009 specifications

Type	Radial ball
Catalog	FAG2012
Designation	6009
Outer Diameter	75 mm
Bore	45 mm
Overall width	16 mm

All 3 models (ISO 14179-1, Palmgren and SKF) are applied to FAG 6009 bearing in the same way as they are for FAG 61822-Y bearing (Section 3.2.1.1). The only

change is that the SKF friction loss factors R_1, R_2, S_1 and S_2 are estimated for '60' Radial ball bearing series.

The characteristic constants for the ISO 14179-1 model and Palmgren equivalent bearing are the same for both the bearings. They are shown in Table 3.4 and 3.8 respectively. The characteristic constants for the SKF equivalent bearing are shown in Table 3.8.

Table 3.8: SKF equivalent constants for Deep groove radial ball bearing - FAG 6009

Constant	Symbol	Value
Replenishment/Starvation Constant	K_{rs}	$3 * 10^{-8}$
Bearing type related geometric	K_Z	3,1
constant depending on movement	mu_{bl}	0,12
sliding friction coefficient in full-film conditions	$mu_E HL$	0,1
Drag loss factor	V_M	0
Number of ball rows	i_{rw}	1
Dynamic load rating	C_0	14400 N

3.2.1.3 Needle Bearings - INA K20x28x25

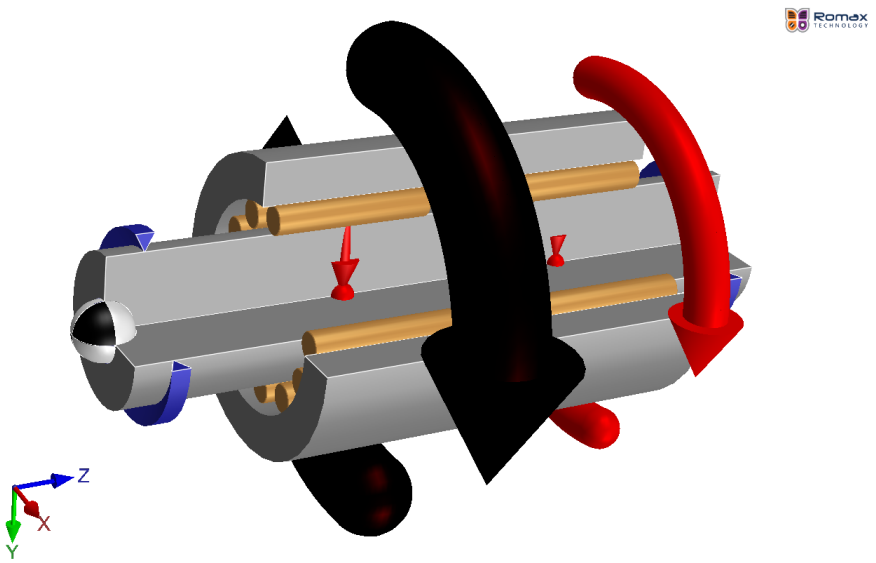

Figure 3.3: INA K20X28X25 Needle bearing sub-model (Image taken from ROMAX software)

Needle bearing is modelled between the pin shaft and sleeve in the system model. The sub-model of the Needle bearing used for simulation can be seen in Figure 3.3. There are six needle bearings in the system model with two needle bearings in each planet pin assembly. A planet pin assembly is considered as a sub-model to study

the power loss models. Out of the three planet pin assemblies, the one with the highest loads is considered in the sub-model. The loads are applied as uniformly distributed along the sleeve. The input and output power for this bearing are taken from the system model. The specifications of the needle bearing are mentioned in Table 3.9.

Table 3.9: Needle Bearing specifications

Type	Needle roller
Catalog	INA
Designation	K20X28X25
Outer Diameter	28 mm
Bore	20 mm
Overall width	25 mm

In analytical models, the power loss is initially analysed for a single planet pin assembly with 2 needle bearings. The power loss is then equated for all six needle bearings. Below is a description of how it was performed for each model.

3.2.1.3.1 ISO 14179-1 model: As described in Section 3.2.1.1.1, bearing load dependent torque (M_1) and cylindrical roller bearing axial load dependent moment (M_2) are the major contributors to the power loss in bearings. Needle bearings only have radial load acting on them. The term M_2 is not included in the analysis of needle bearings as there is no axial load involved. The characteristic constants for the ISO 14179-1 model are shown in Table 3.10.

Table 3.10: ISO 14179-1 constants for Needle bearings

Parameter	**Constant**	**Value**
Exponent	a	1
Exponent	b	1
Coefficient of Friction	f_1	0,002

3.2.1.3.2 Palmgren model: According to J.Liu et al. [21], the total frictional torque in the Palmgren model for needle bearings is made up of load independent (M_0) and load dependent friction torques (M_1) (Section 2.1.4). This model has two factors - f_0 which depends on the bearing type and lubricant conditions and f_1 which is a coefficient determined by the bearing load and design geometries. f_1 can be found in Table 10.3 in [15]. The characteristic constants for the Palmgren equivalent bearing are shown in Table 3.11.

Table 3.11: Palmgren constants for Needle bearings

Parameter	Constant	Value
Coefficient determined by the bearing type and lubricant conditions	f_0	6
Coefficient determined by the bearing load and design geometries.	f_1	0,00055

3.2.1.3.3 SKF model: The SKF model for needle bearings defined in Section 2.1.5 cannot be analysed in ROMAX, as it is not possible to estimate the SKF friction loss factors.

3.2.2 Gear mesh loss sub-model

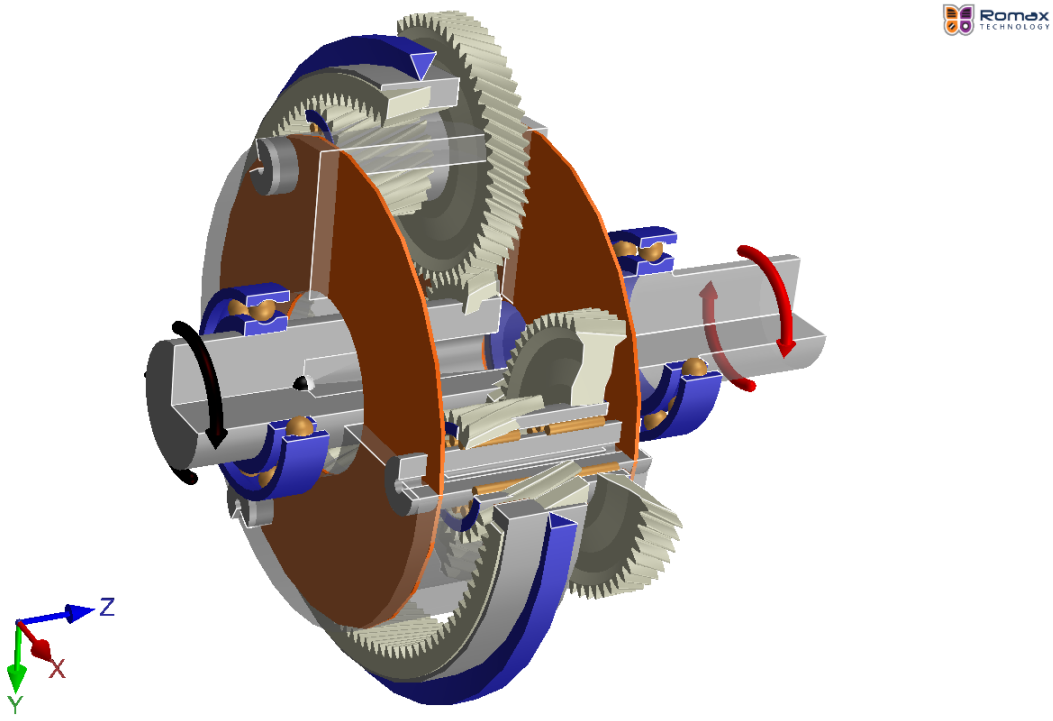

Figure 3.4: Gear mesh loss sub-model (Image taken from ROMAX software)

The gear mesh loss is modelled in ROMAX as shown in Figure 3.4. The gear geometry, lubricant and load cases are replicated from the system model. The input shaft is coupled to the sun gear and the carrier shaft is the output for the transmission. The planet gear assemblies are mounted on the two concept planetary carriers shown by the orange disks. The bearings in this sub-model are not under examination. So, their efficiency is considered to be 100%. The gear mesh power loss models compared in this study are described in Section 2.2.

3.2.2.1 ISO 14179-1 model

The operating speed and the gear properties required for the calculation of power loss using this method are obtained from the power-flow analysis result of every load case. The power loss of stage 1 and 2 of each planet gear mesh are calculated separately for every load case. The total gear mesh power loss is the sum of power loss of the sun-large planet and small planet-ring meshes. The analytical MATLAB calculation is performed for each stage at a particular speed for varying input torques where the sliding and rolling velocities would remain the same with varying torque transfer through the mesh. The constants used to determine gear mesh losse in ISO 14179-1 model are defined in Table 3.12.

Table 3.12: ISO 14179-1 constants for Gear mesh losses

Parameter	Constant	Value
Constant	C_1	3,239
Constant	j	-0,223
Constant	g	-0,40
Constant	h	-0,70

3.2.2.2 ISO 14179-2/FVA 345 method

The FVA 345 method considers the change in the lubricant properties with operating load and temperature. The same sub-model is shown in Figure 3.4. In equation 2.67, the pressure(α), speed(β) and viscosity(γ) exponents of the lubricant are the parameters that determine the mean friction coefficient for the gear mesh. Since the FVA 345 experiment is not conducted for the lubricant being used in the transmission, the exponents are approximated based on similar FVA lubricants available in ROMAX and suitable values for the exponents (in equation 2.67) are iterated to yield a mean friction coefficient estimated in Equation 2.70. The exponents thus obtained is retained though out all the load cases and the power loss correlates with the experimental results performed on the system model. This further gives confidence in the approximated exponents. The exponents for the lubricant are shown in Table 3.13.

Table 3.13: FVA345 lubricant coefficients

	EHD friction	Solid friction
Reference coefficient of friction	0,055	0,061
Load influence exponent	-0,03	0,009
Speed influence exponent	0,04	-0,15
Viscosity influence exponent	0,35	

3.2.2.3 Micro-Geometry model with Variable friction coefficient

This method is quite straight forward. It is based on the friction coefficient between the teeth due to the rolling and sliding velocity as explained in Section 2.2.3.

3.2.3 Gear drag/Churning loss sub-model

The sub-model used to analyse the gear drag/churning losses and gear mesh losses is the same (Section 3.2.2). There are three methods for gear drag loss prediction based on different models - ISO 14179-1 (US) [19], ISO 14179-2 (DE) [20] and Terekhov [33]. These models have been defined in Section 2.3. The losses are dependent on the lubricant viscosity, lubricant level and the gear rotational speed.

3.2.3.1 ISO 14179-1 model

This model consists of three categories: Smooth outside diameter, side of the gear and tooth surfaces. In this study, side of the gear and tooth surfaces will be considered. Smooth outside diameter is not taken into account as it only applies to components with smooth outside diameter. This model consists of a term called arrangement constant (A_g) which has a constant value. It also has gear dip factor (f_g) which is dependent on the immersion depth of the gear into the lubricant. f_g varies between 0 and 1. The value of f_g will be different for both stage 1 and stage 2 (Section 3.2.2) as they are at different lubricant levels. The f_g value is taken as constant in this study as ROMAX performs static analysis. But in real world application, the value of f_g will keep varying with rotation. The constants used to evaluate gear drag losses in ISO 14179-1 model are defined in Table 3.14.

Table 3.14: Constants used in ISO 14179-1 model for Gear drag losses

Parameter	**Constant**	**Value**
Arrangement constant	A_g	0,2
Gear dip factor for large planet gears	$f_{g-large}$	0,1268
Gear dip factor for small planet gears	$f_{g-small}$	0,1104

3.2.3.2 ISO 14179-2 model

This model consists of three factors: Splash oil factor (C_{SP}), C_1 and C_2. While C_{SP} depends on immersion depth, C_1 and C_2 depend on tooth width and immersion depth. According to ISO [20], viscosity is not taken into account as it gives conflicting results at different immersion depths. It also contains reference values for speed, tooth width and immersion depth. In this study, different reference values are considered for stage 1 and stage 2. The constants used to calculate gear drag losses in ISO 14179-2 model are defined in Table 3.15.

Table 3.15: Constants used in ISO 14179-2 model for Gear drag losses

Parameter	Constant	Value
Reference speed for large planet gears	$v_{t0-large}$	23
Reference tooth width for large planet gears	$b_{0-large}$	23
Reference immersion depth for large planet gears	$h_{e0-large}$	23
Reference speed for small planet gears	$v_{t0-small}$	43
Reference tooth width for small planet gears	$b_{0-small}$	43
Reference immersion depth for small planet gears	$h_{e0-small}$	43

3.2.3.3 Terekhov model

In Terekhov model [33], the gear drag losses are divided into disc losses (M_D) and losses due to lubricant expulsion (M_{oe}). While M_D depends on the immersion depth of the gear into the lubricant, M_{oe} depends on the tooth depth. M_{oe} also consists of a scale factor for length (l_0) which is introduced for dimensional compensation. As ROMAX performs static analysis, it is considered that one set of stage 1 and stage 2 planet gears are dipped into the lubricant, while the other two sets only contribute with windage losses. The constants used to calculate gear drag losses in Terekhov model are defined in Table 3.16.

Table 3.16: Constants used in Terekhov model for Gear drag losses

Parameter	Constant	Value
Scale factor for length introduced for dimensional compensation for large planet gears	$l_{0-large}$	$10 * 10^{-3}$
Scale factor for length introduced for dimensional compensation for small planet gears	$l_{0-small}$	$8 * 10^{-3}$

3.2.4 Seal sub-models

There are two different types of seals in the system model - Left driveshaft seal and rotor shaft seal. These seals will be analysed for efficiency by two types of seal drag power loss models - ISO 14179-1 (US) [19] and ISO 14179-2 (DE) [20]. The loads and torque applied don't have any impact on the seal losses, as they are only influenced by the input speed and diameter of the seal. Hence, the seal sub-models will only be simulated for the four input speed cases.

3.2.4.1 Left driveshaft seal

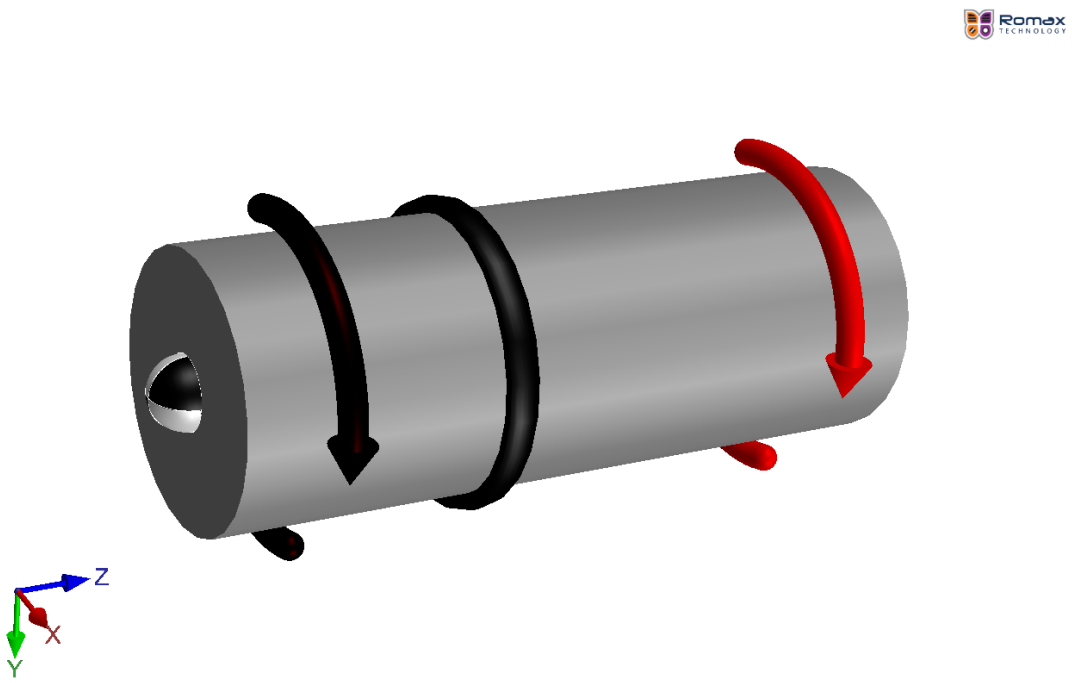

Figure 3.5: Left Driveshaft seal sub-model (Image taken from ROMAX software)

Left Driveshaft seal is mounted on the left driveshaft in the system model. The sub-model of the Left Driveshaft seal used for simulation is shown in Figure 3.5. The sub model for this seal is modelled by mounting the seal on a shaft and providing the input power on one side of the shaft and the output power on the other side of it. The seal specifications can be found in Table 3.17.

Table 3.17: Left driveshaft seal specifications

Material	Viton
Diameter	30 mm

The analytical models for seal losses (Section 2.4) which were implemented in MATLAB are described below:

3.2.4.1.1 ISO 14179-1 model: According to ISO [19], the seal power loss is mainly dependent on shaft size and shaft speed. There are two types of seal materials: Viton and Buna N. Based on the type of material used, either Equation 2.104 or Equation 2.105 is used respectively.

3.2.4.1.2 ISO 14179-2 model: Similar to the ISO 14179-1 model, ISO 14179-2 is also dependent on the shaft size and speed [20]. But, it has just one Equation 2.106 which is applicable for all types of seals. In case of non-contacting seals, it is assumed that they don't contribute to any power loss.

3.2.4.2 Rotor shaft seal

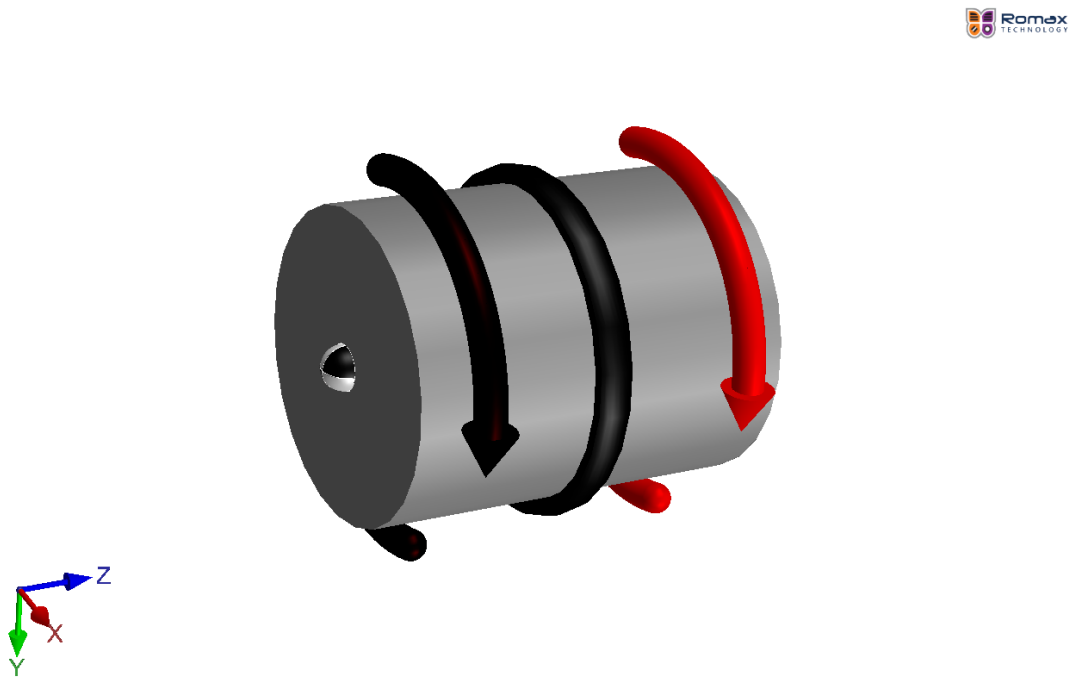

Figure 3.6: Rotor shaft seal sub-model (Image taken from ROMAX software)

Rotor shaft seal is mounted on the Rotor shaft in the system model. Figure 3.6 shows the Rotor shaft seal sub-model which is used for simulation. It is modelled in a similar manner to Left Driveshaft seal (Section 3.2.4.1). The seal specifications can be found in Table 3.18.

Table 3.18: Rotor shaft seal specifications

Material	Viton
Diameter	55 mm

Both ISO 14179-1 and ISO 14179-2 models are applied to the Rotor shaft seal in the same way as they are for Left driveshaft seal (Section 3.2.4.1).

3.2.5 Thrust Washers

The thrust washers are mounted on the pin shaft between the planet sleeve and the planet carrier. They are made up of a wear resistant material to prevent wear between the sleeve and planet carrier. They offer considerable resistance to the rotation of sleeve at solid body contact and boundary friction conditions. The clearance on either side of the thrust washers causes varying sliding velocities against the planet carrier on one side and the sleeve on the other side. For the sake of simplicity in the calculations, the sliding velocity is split equally on either side of

the washer. The sliding conditions depend on the load, speed, lubricant and the surface properties (mainly roughness) of the washer. The friction regime is defined by the Stribeck curve. This a plot of friction coefficient and sliding velocity. The calculation of the friction coefficient requires microscopic surface data such as the surface distribution of crests and troughs, mean surface height, flow rate of lubricant over the rubbing surfaces, etc. The complexity of calculating the effective friction coefficient along with lubricant flow and the force varying over the surface of the washer is out of the scope of the thesis. A more convenient method to derive the effective friction coefficient is determined by the Moes fit for central film thickness calculated using the axial force, lubricant properties and surface roughness of the sliding surfaces. This method uses a dimensionless film thickness assuming steady-state lubrication. The function in MATLAB is coded following this method [22]. The upper and lower limits of the friction coefficient are determined from the data sheet for the thrust washer used (Fibre reinforced polymer). The operating friction coefficient for each load case is then interpolated from these limits corresponding to the lubricant film thickness of the load case. A plot of the axial load vs film thickness for a sliding velocity is shown in the results section.

4

Results

The powerloss obtained in the efficiency tests and the simulations conducted with the powerloss models in the thesis are compared. Finally, the most suitable model with the closest correlation to the experimental test results are selected for analysis of the system model. The ROMAX and analytical functions coded in MATLAB for the powerloss sub-models are compared in this section.

4.1 Bearing losses

4.1.1 Deep groove radial ball bearings

The power loss in both the deep groove ball bearings on either side of the carrier show similar trends in the powerloss with changing axial loads as seen from Figures 4.1 and 4.2.

The **ISO 14179-1 and ISO 14179-2** powerloss models have the same analytical model for all types of bearings. Figures 4.1 and 4.2 show substantial difference between the ROMAX and analytical results for the ISO 14179-1 model. This is because the cylindrical roller bearing load dependent torque (M_2) is included in the analytical model. Ignoring M_2 will result in unrealistically low power loss (Section 3.2.1.1.1 and 2.1.1).

The **Palmgren model** is derived using coefficients based on lubricant, bearing type, bearing geometry and load. This makes the method less sensitive to dynamic changes in operating conditions described in Section 2.1.2.

The **SKF model** for frictional power-loss is more sensitive to loads derived from experimentally determined constants for all the bearings available in the SKF catalogue [31] pertaining to bearing geometry and type, speed, kinematic shear effects of asperity contact and the lubricant, type of lubrication, etc as described in Section 2.1.3.

From Figures 4.1 and 4.2, there is good comparison between the ROMAX and analytical results in SKF model for all the cases. SKF model best captures the influence of friction torque and axial loads. The ROMAX results for both Palmgren and ISO 14179-1 models are also similar. However, the analytical results for ISO 14179-1

model vary significantly from ROMAX results because of the above mentioned reasons. The power loss in Palmgren model is less sensitive to dynamic load changes. SKF model is selected for system level analysis.

4.1.1.1 Deep groove radial ball Bearing - FAG 61822-Y

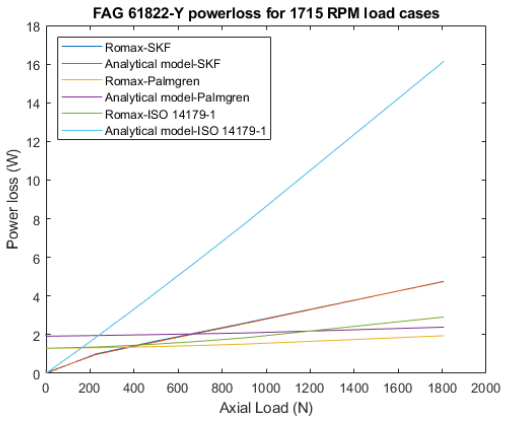

(a) Input speed 1715RPM (∼25km/h)

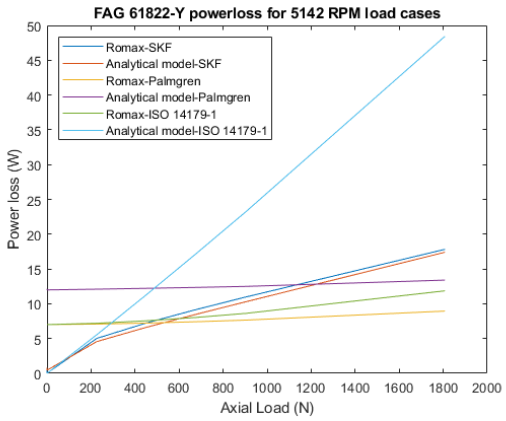

(b) Input speed 5142RPM (∼80km/h)

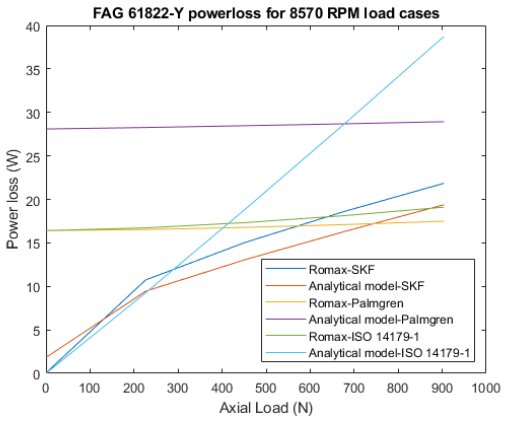

(c) Input speed 8570RPM (∼130km/h)

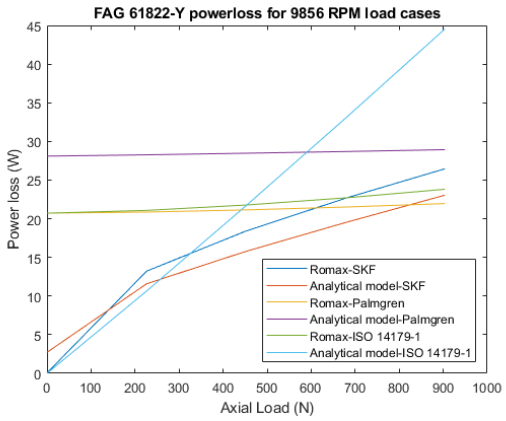

(d) Input speed 9856RPM (∼150km/h)

Figure 4.1: ROMAX and analytical model powerloss results for FAG 61822-Y bearing

4.1.1.2 Deep groove radial ball Bearing - FAG 6009

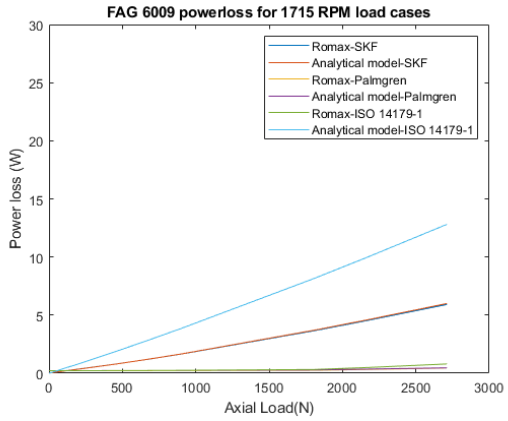

(a) Input speed 1715RPM (∼25km/h)

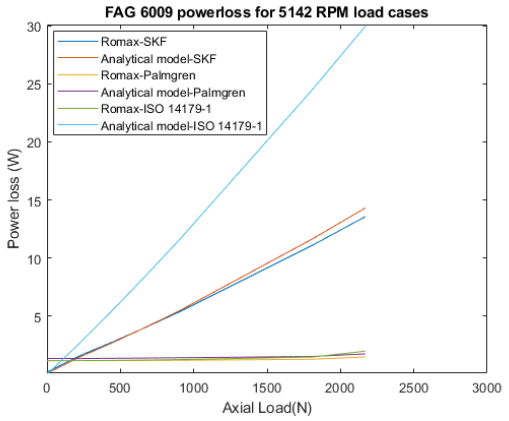

(b) Input speed 5142RPM (∼80km/h)

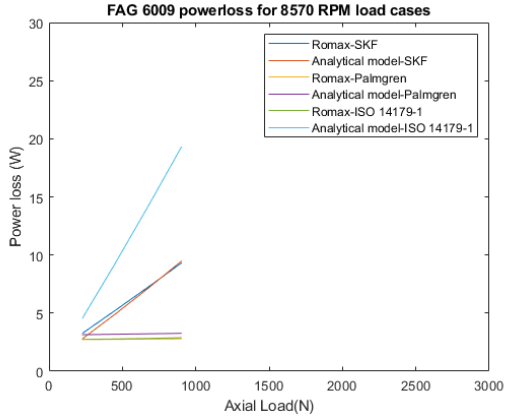

(c) Input speed 8570RPM (∼130km/h)

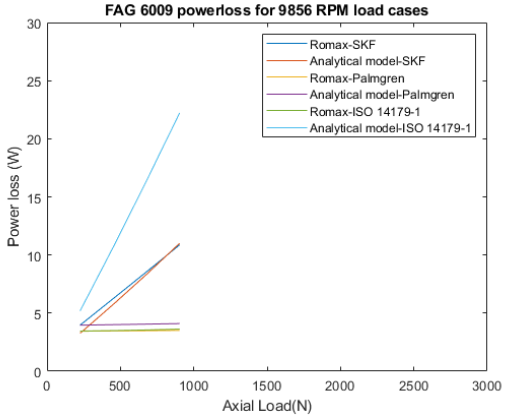

(d) Input speed 9856RPM (∼150km/h)

Figure 4.2: ROMAX and analytical model powerloss results for FAG 6009 bearing

4.1.2 Needle Bearings - INA K20x28x25

There are two types of models to analyse the losses in Needle bearings - ISO 14179-1 and Palmgren model. The SKF model (Section 2.1.5) cannot be applied to the needle bearings in ROMAX, as it is impossible to estimate the SKF friction loss factors.

The Palmgren model (Section 2.1.4) for deep groove radial ball bearings and needle bearings follow a similar trend. The losses are less sensitive to dynamic changes in operating conditions. In analysing the needle bearings, the ISO 14179-1 model (Section 2.1.1) does not face the issues faced by deep groove radial ball bearings (Section 4.1.1), as there is no axial load involved here.

The ISO 14179-1 is more sensitive to loads acting on the bearings when compared to Palmgren model. There is good comparison between the ROMAX and analytical

model results for both the models (Figure 4.3). However in ISO 14179-1 model, as the speed increases the difference between the ROMAX and analytical results increases. This occurs as the friction coefficient is considered to be constant in all the load cases for analytical models [19]. ROMAX considers the decrease in friction coefficient as the speed increases. ISO 14179-1 model is selected for system level analysis.

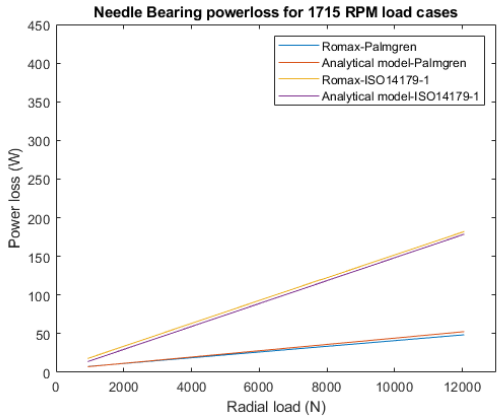

(a) Input speed 1715RPM (∼25km/h)

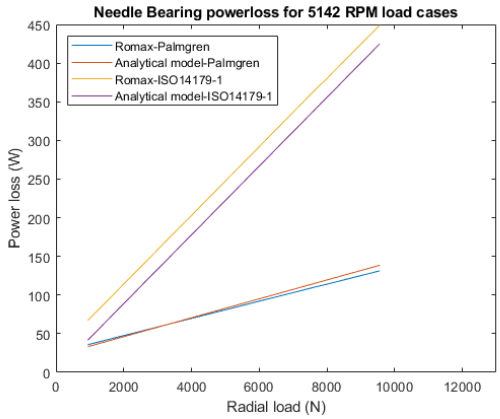

(b) Input speed 5142RPM (∼80km/h)

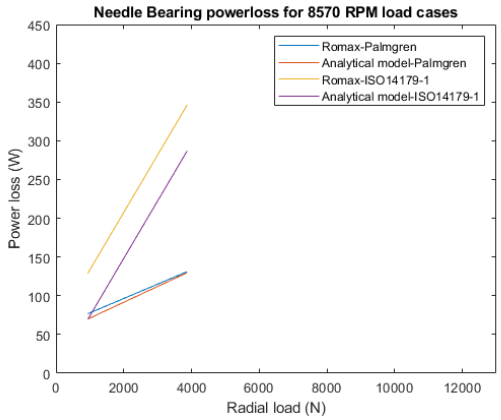

(c) Input speed 8570RPM (∼130km/h)

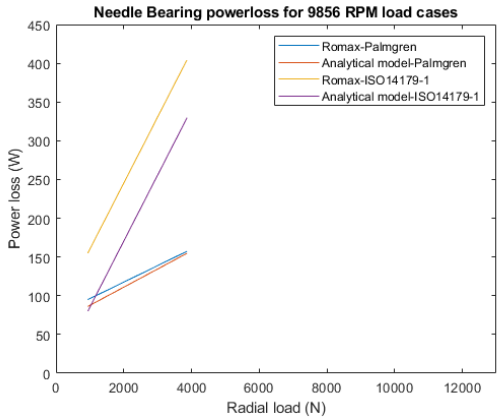

(d) Input speed 9856RPM (∼150km/h)

Figure 4.3: ROMAX and analytical model powerloss results for INA K20x28x25 bearings

4.2 Helical Gear-Mesh powerloss

The gear mesh losses according to different powerloss models for various input speed vs torque are compared in Figure 4.4. The losses are least at low load conditions and increase at higher loads for a particular speed. This occurs since the nominal tooth load increases with increase in torque leading higher load on the lubricant film. High loads on a thin lubricant film cause a higher effective coefficient of friction at the sliding portion of the gear mesh which sometimes leads to starvation of the lubricant

film causing a boundary lubrication regime. The individual plots for all the models can be found in Appendix A.1.

The ISO 14179 – 1 model takes into account sliding ratio and load intensity on the gears to measure power loss. The lubricant properties do not vary with operating conditions. It overestimates the losses at high torque values.

The ISO 14179 – 2 model and FVA 345 are identical. They give a better understanding of the influence of changes in lubricant properties through experimental coefficients for speed, viscosity and load, derived from the FVA345 test. This model is selected for system level analysis as it gives the most accurate prediction of power loss at various operating conditions.

The Micro geometry model takes into account the variable friction over the tooth profile based on roll and slide motions.

The Anderson model is purely based on a gear mesh loss factor but does not consider change in lubricant properties with load and temperature. It is also based on spur gear and modification for helical gears does not provide satisfactory results, hence it is not evaluated in this thesis.

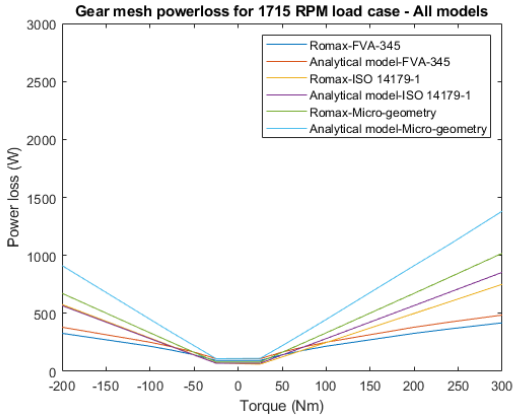

(a) Input speed 1715RPM (∼25km/h)

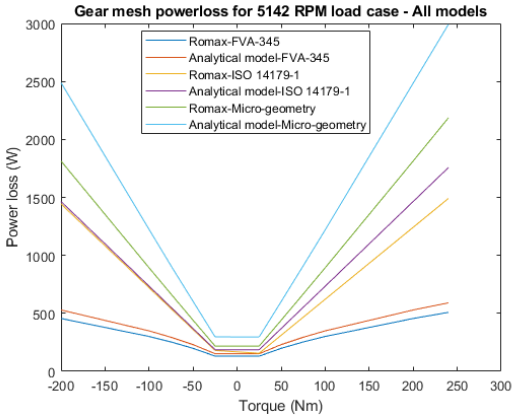

(b) Input speed 5142RPM (∼80km/h)

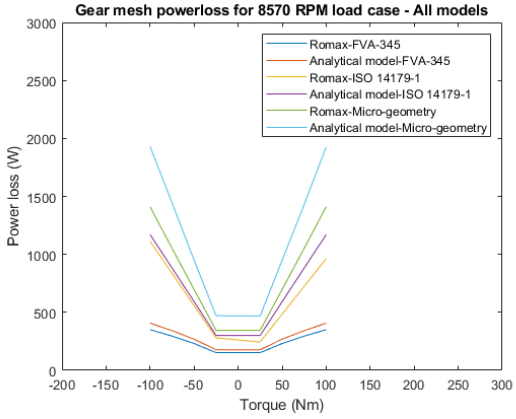

(c) Input speed 8570RPM (∼130km/h)

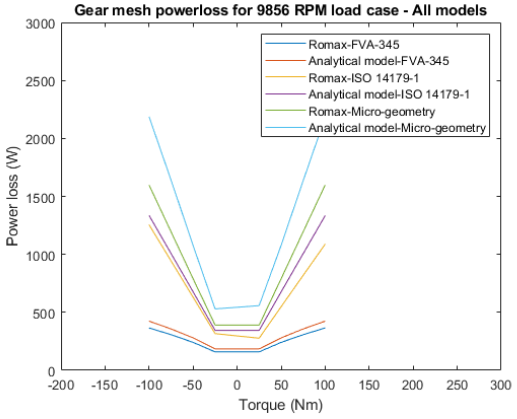

(d) Input speed 9856RPM (∼150km/h)

Figure 4.4: ROMAX and analytical model powerloss results for helical gear mesh

4.3 Churning/Gear-drag loss

There are three different models to analyse Churning/Gear drag losses - ISO 14179-1, ISO 14179-2 and Terekhov. The Gear-drag losses for different powerloss models for various input speeds can be seen in Figure 4.5. These losses are only speed dependent, which means they are not affected by the torque acting on it. The losses follow a similar pattern for all three models. They are low at lower speeds and they keep increasing as the gear rotational speed increases.

Figure 4.5d shows there is substantial difference between the three models. This is a result of the following factors being used in them - Gear dip factor (f_g) in ISO 14179-1, reference values for speed, tooth width and immersion depth in ISO 14179-2 and scale factor for length (l_0) in Terekhov model (Sections 2.3 & 3.2.3). There is good comparison between the ROMAX and analytical results of all three models. Computational fluid dynamics (CFD) is required to achieve more realistic results.

In ISO 14179-1 model, the value of gear dip factor(f_g) is considered constant for

model validation. But in real world application, the value of gear dip factor will keep varying with rotation.

In ISO 14179-2 model, lubricant viscosity is not considered in determining power loss, as including it gives contradictory results at different immersion depths [20]. This model is selected for system level analysis as it correlates the best with test bench results.

In Terekhov model, scale factor for length (l_0) is introduced for dimensional compensation. It is considered that only one set of planet gears contribute with gear drag losses, while the other two sets of planet gears contribute with windage losses, which is incorrect.

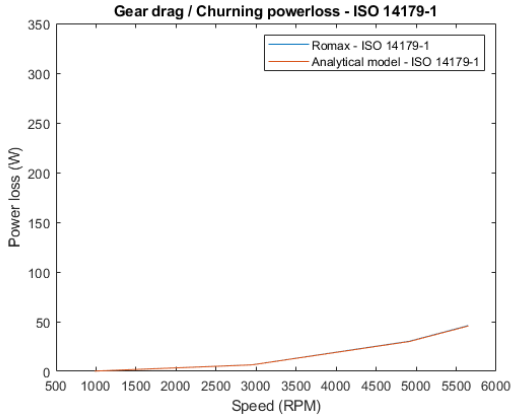

(a) ISO 14179-1 Churning powerloss model

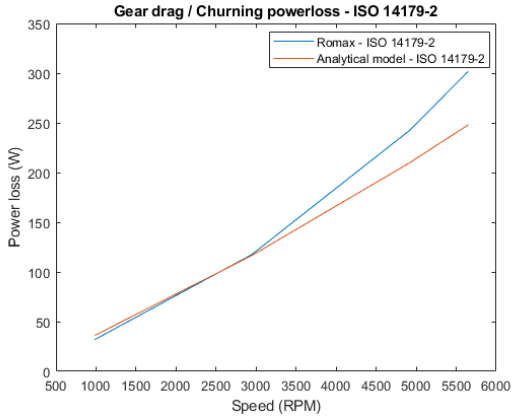

(b) ISO 14179-2 Churning powerloss model

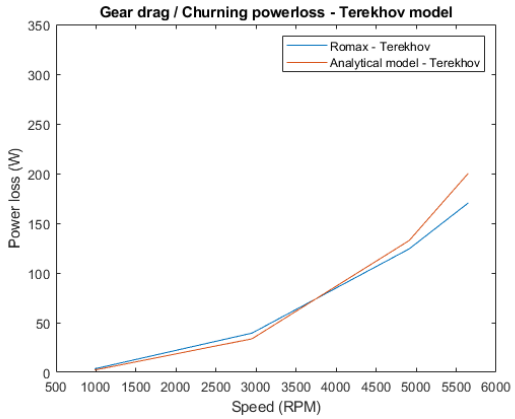

(c) Terekhov Churning powerloss model

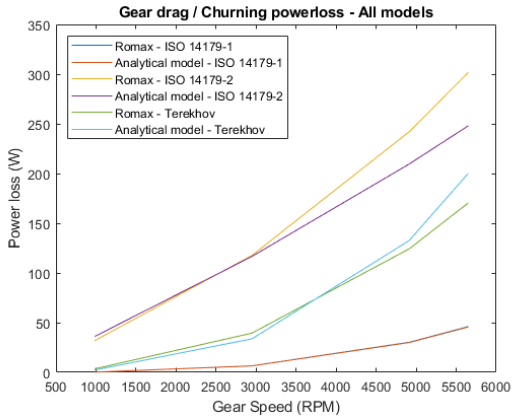

(d) Churning powerloss - All models

Figure 4.5: ROMAX and analytical model Gear drag powerloss results

4.4 Seal losses

There are two types of seals used in the system model - left driveshaft seal and the rotor shaft seal. The seal losses in both ISO 14179 - 1 and ISO 14179 - 2 powerloss

models are comparable for both the seals. This is because the models are only influenced by the input speed and diameter of the seal (Sections 2.4 & 3.2.4). Both these models are based on a power loss constant resulting from the geometry and material of the seal, resulting in a slight difference between the results. There is barely any difference between the ROMAX and analytical model results in both the models, which is the reason the curves overlap each other. ISO 14179-1 is selected for system level analysis.

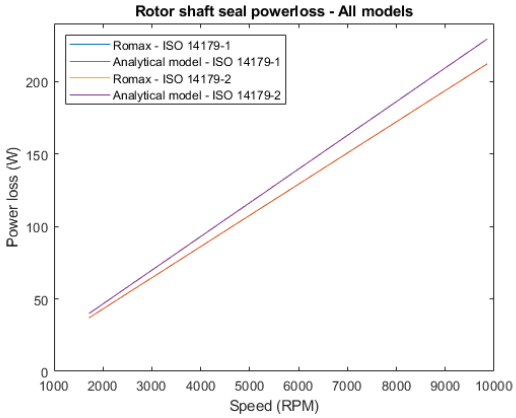

(a) Input shaft seal powerloss

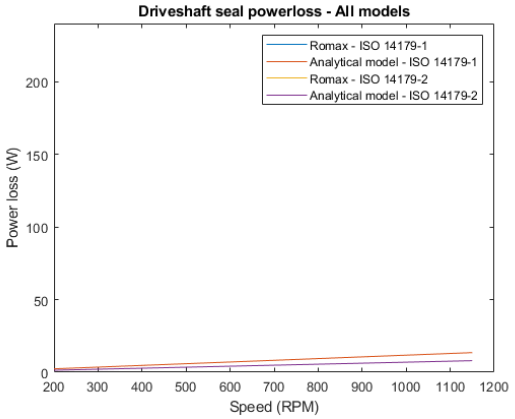

(b) Driveshaft seal powerloss

Figure 4.6: ROMAX and analytical model powerloss results for Seals

4.5 Thrust Washers

The film thickness using the Moe's-fit method is described in Section 3.2.5. The film thickness decreases with increasing axial load as shown in Figures 4.7 and 4.8.

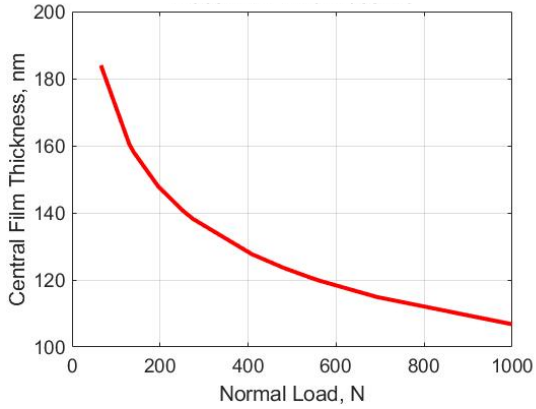

(a) Input speed 1715RPM (∼25km/h)

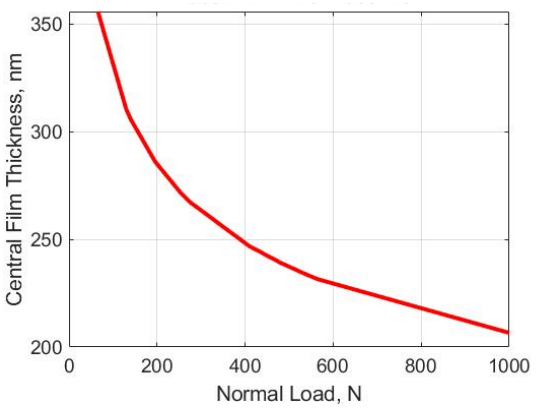

(b) Input speed 5142RPM (∼80km/h)

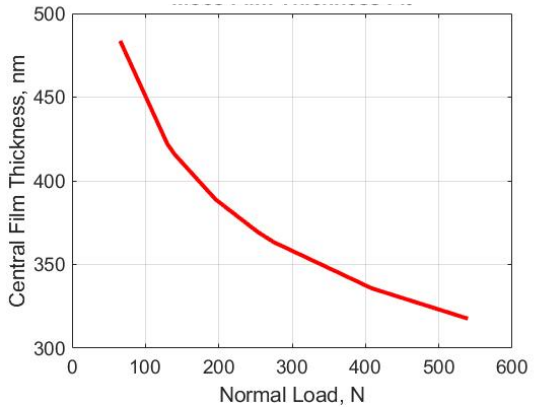

(c) Input speed 8570RPM (∼130km/h)

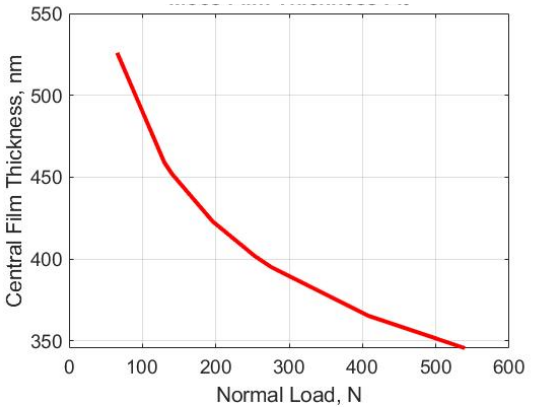

(d) Input speed 9856RPM (∼150km/h)

Figure 4.7: Axial load vs non-dimensional film thickness for left thrust washer using Moe's fit method

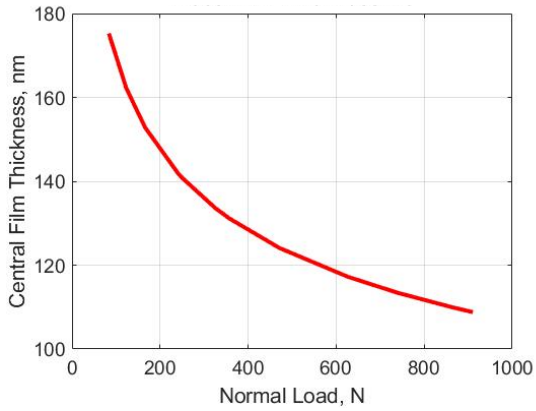

(a) Input speed 1715RPM (∼25km/h)

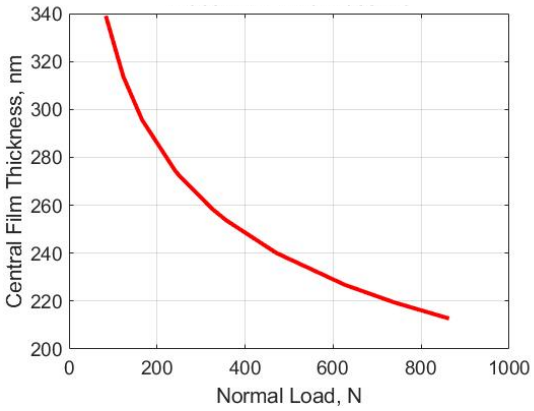

(b) Input speed 5142RPM (∼80km/h)

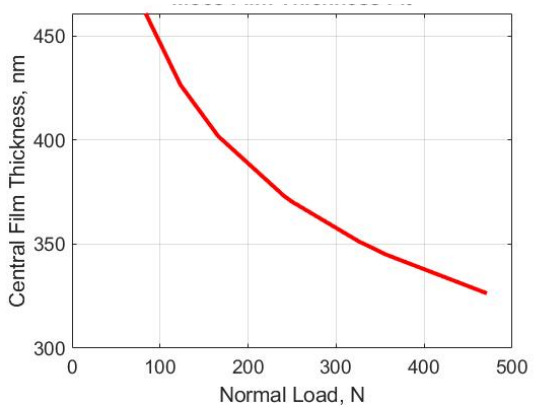

(c) Input speed 8570RPM (∼130km/h)

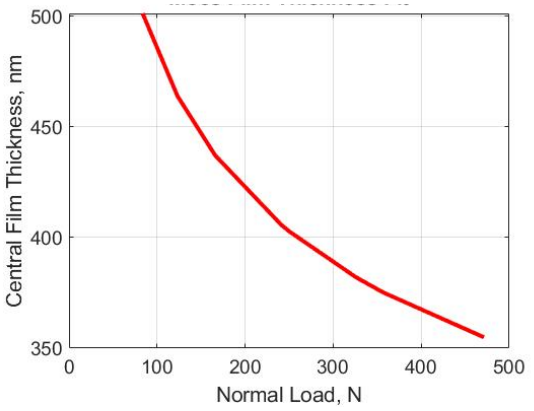

(d) Input speed 9856RPM (∼150km/h)

Figure 4.8: Axial load vs non-dimensional film thickness for right thrust washer using Moe's fit method

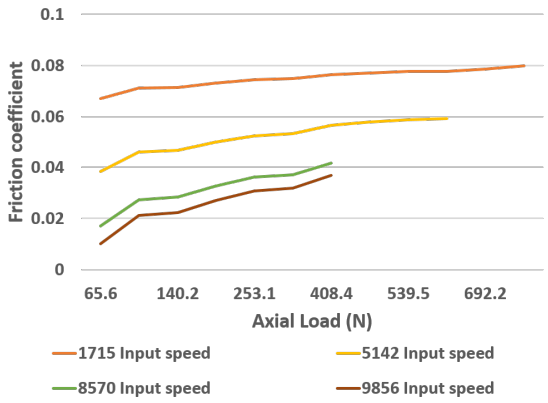

(a) Left thrust washer

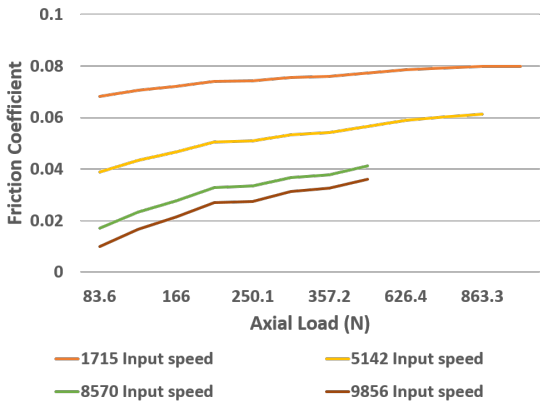

(b) Left thrust washer

Figure 4.9: Axial load vs non-dimensional film thickness for left thrust washer

Since ROMAX does not allow to use different values of friction coefficient for the

thrust pad depending on the load and speed, hence an analytical calculation of the friction coefficient has been performed. The friction coefficient calculated resulting from the film thickness are shown in Figure 4.9.

4.6 System level power loss

The results of the sub-models studied for the machine elements yield different values for power-loss. The most suitable models are selected as explained in the Sections 4.1, 4.2, 4.3, 4.4 & 4.5. The contribution of each component to the total power-loss of the system is seen in Figure 4.10. The power loss increases with increasing input torque because of higher load on the machine elements. The churning and seal losses are speed dependent. So, they remain constant with varying torque. The gear mesh losses is the major contributor for the total power-loss in the system. The thrust washer loss increases with increasing torque (Section 4.5).

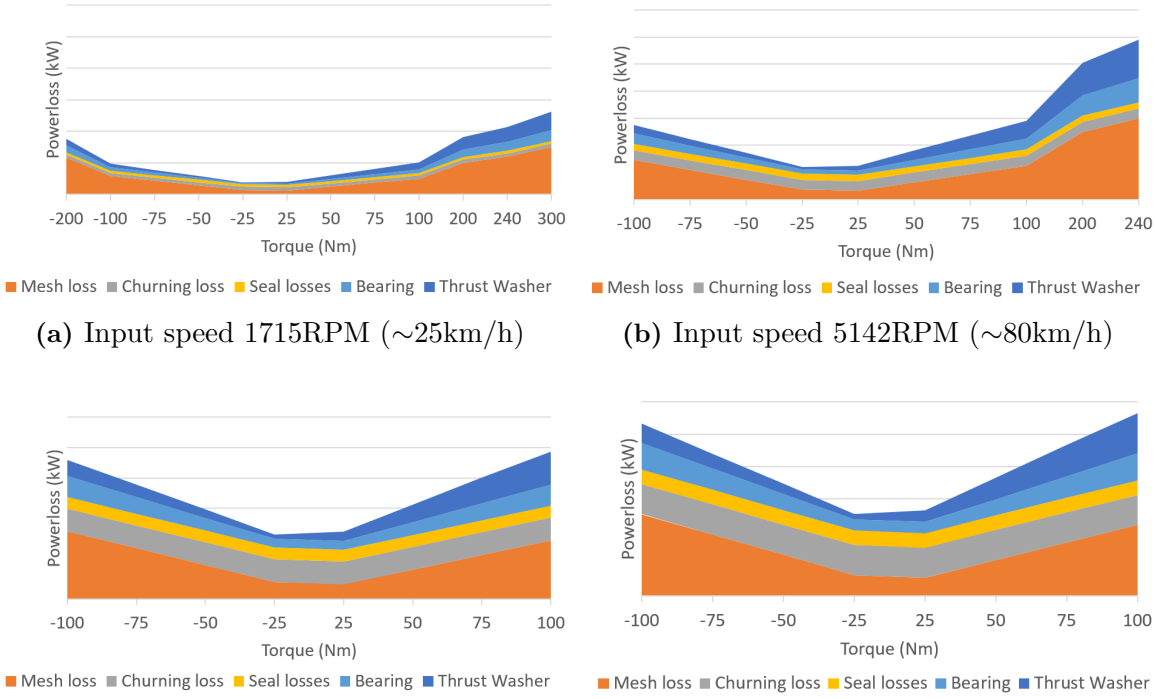

(a) Input speed 1715RPM (∼25km/h)

(b) Input speed 5142RPM (∼80km/h)

(c) Input speed 8570RPM (∼130km/h)

(d) Input speed 9856RPM (∼150km/h)

Figure 4.10: Input Torque vs Powerloss for System model

5

Conclusion

5.1 System vs Test Bench Efficiency

After analysing the power-loss from each machine element and selecting the suitable powerloss model, the transmission system efficiency is compared with the test bench efficiency results to verify (Figure 5.1). The sub-models chosen are:

1. Gear mesh power-loss: FVA345 (or ISO 14179-2).
2. Needle bearings: ISO 14179-1 (or ISO 14179-2)
3. Deep groove ball bearings: SKF.
4. Churning or gear drag: ISO 14179-2.
5. Thrust Washers: Effective friction coefficient estimation from lubricant thickness in Moe's fit method.

Since the effective friction coefficient for the sliding motion of the planet sleeve and planet carrier with the thrust washer is estimated numerically, an extreme value for friction coefficient of 0,08 has also been plotted to understand its influence on the system efficiency. The simulated results are validated since it is in close correlation with the bench test efficiency for the same load cases. The plots have been normalised not to disclose the actual system efficiency. The difference between the maximum and the minimum points in the normalised plots (Figure 5.1) looks to be large because the difference between them is approximately 8 % system efficiency.

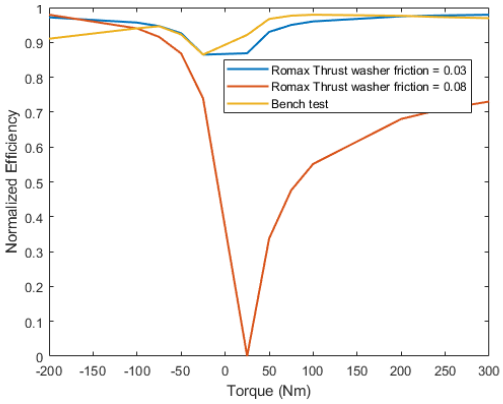

(a) Input speed 1715RPM (∼25km/h)

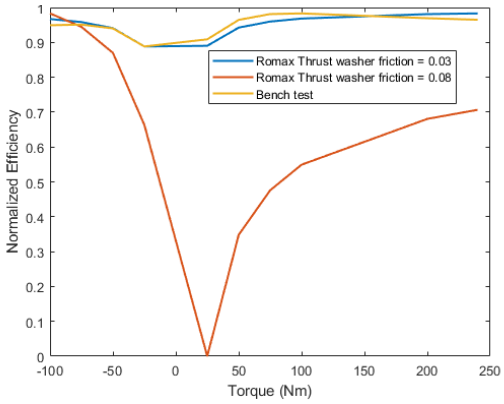

(b) Input speed 5142RPM (∼80km/h)

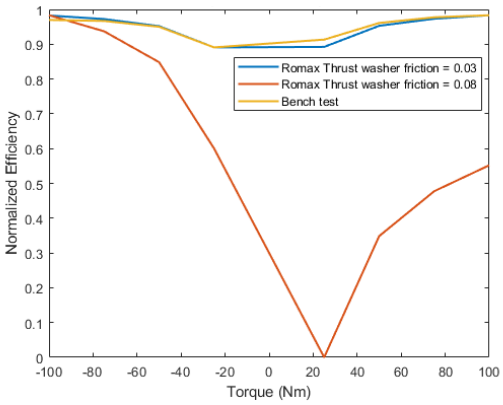

(c) Input speed 8570RPM (∼130km/h)

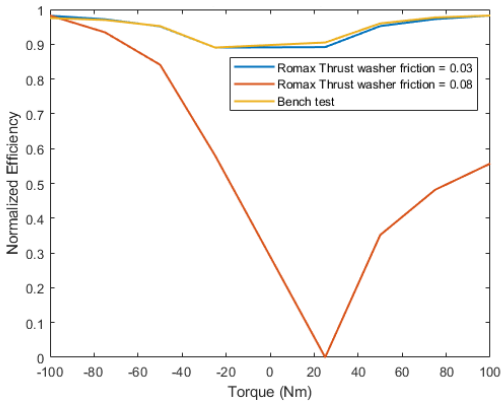

(d) Input speed 9856RPM (∼150km/h)

Figure 5.1: Input Torque vs Powerloss for System model (Normalised)

5.2 Simulation in driving cycles

5.2.1 WLTP driving cycle

The transmission is simulated in the WLTP drive cycle to show the operating points on the efficiency map. Figure 5.2 shows the plot of speed vs time for the WLTP drive cycle.

The speed and torque demand for the vehicle to follow the driving cycle is translated to the operating points of the transmission by calculations via the gear ratio. The operating points of the transmission in WLTP drive cycle are plotted by interpolating on the normalised efficiency map shown in Figure 5.3. The efficiency map shows a wide spread of operating points at both high and low speeds and torque as the WLTP drive cycle consists of both city and highway driving scenarios.

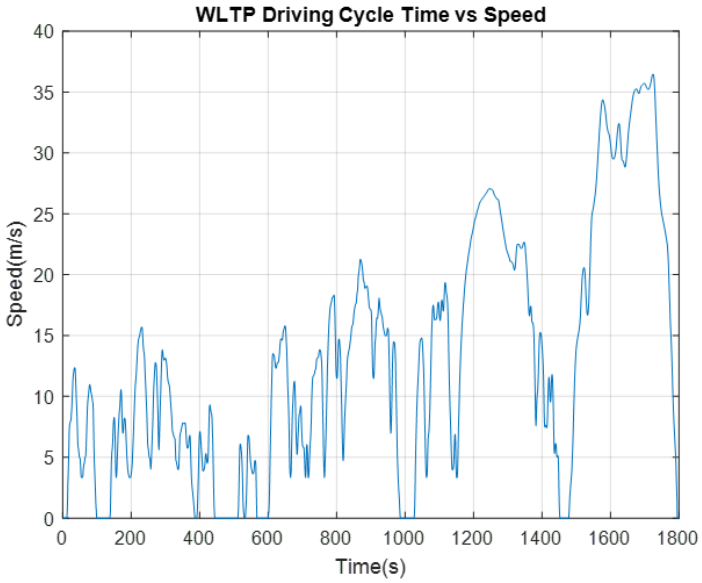

Figure 5.2: WLTP driving cycle speed vs time

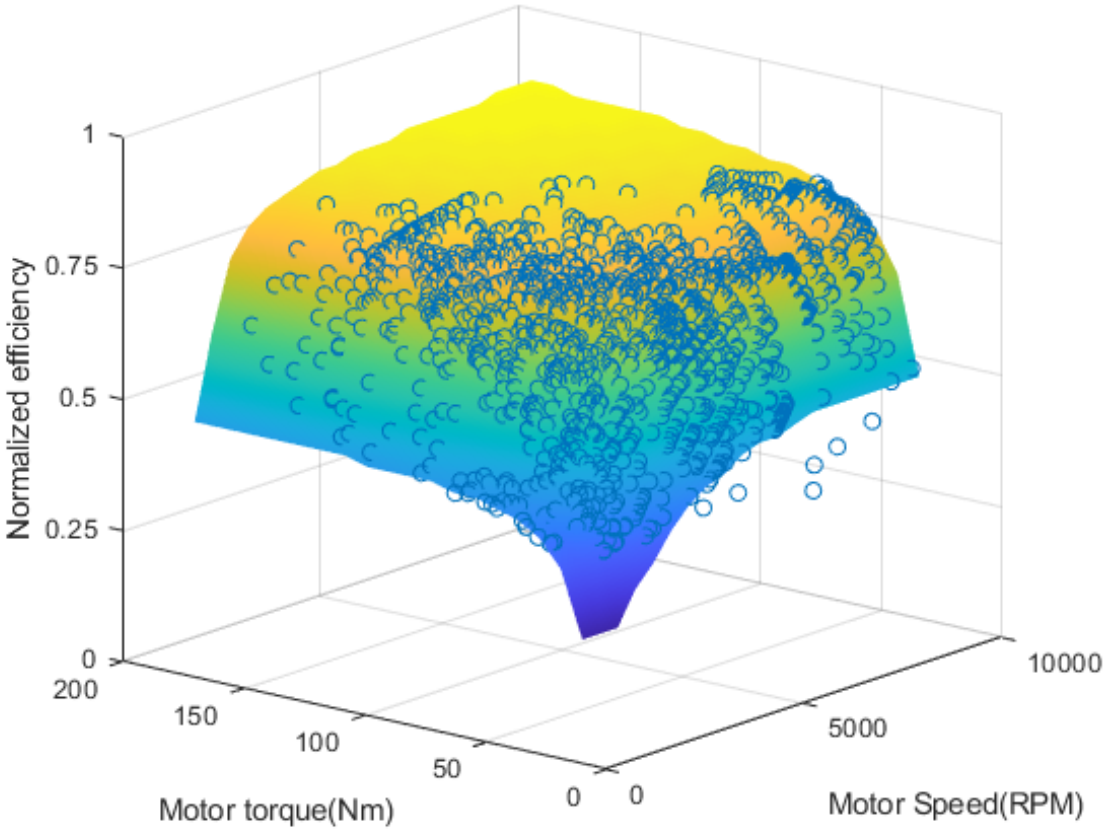

Figure 5.3: Operating points for WLTP in the Efficiency Map of Speed vs Torque vs Efficiency (Normalised)

The operating point at mean efficiency is considered for the WLTP driving cycle. The contribution from the machine elements at this point is shown in Figure 5.4. For the mean efficiency for WLTP cycle, the major contributors are gear mesh, churning and thrust washer losses. For real time driving scenarios, the breakdown of losses will be different. The thrust washer friction can be minimised by reducing the axial forces on it. The churning losses can be minimised by using a better lubricant with lower viscosity and/or by reducing the quantity of the lubricant. This would influence wear and temperature adversely. Further investigation is required to study these effects.

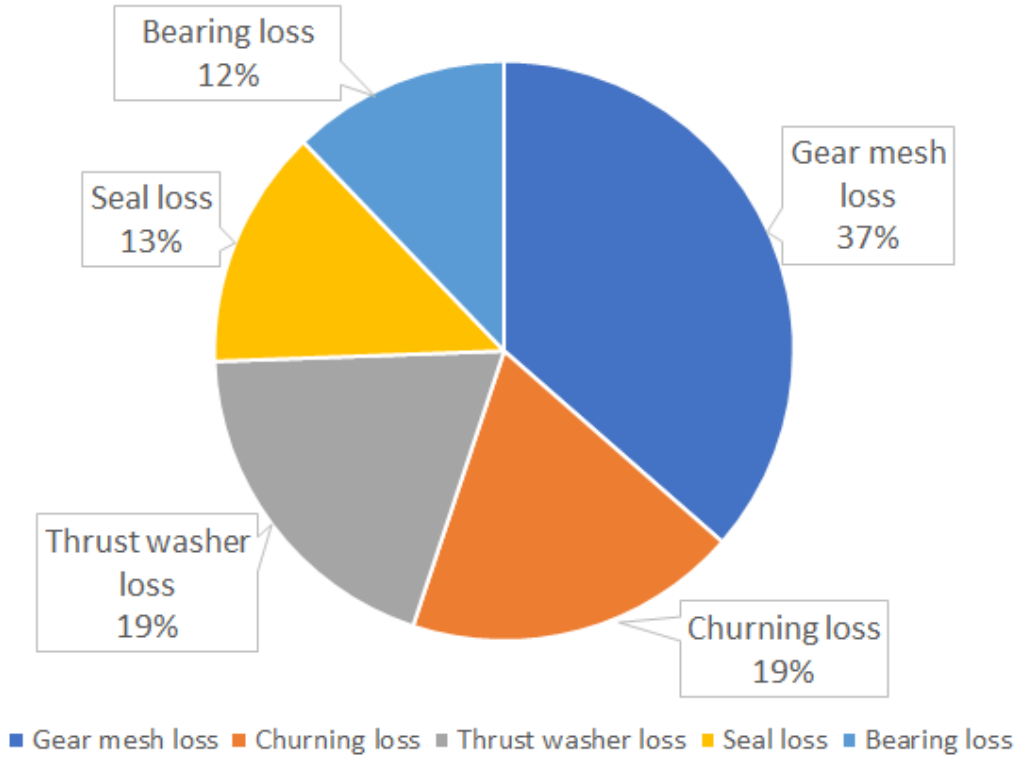

Figure 5.4: Mean efficiency in WLTP cycle

5.2.2 FTP Highway driving cycle

To analyse how the transmission would perform on a highway drive cycle, it is also simulated on the FTP Highway drive cycle to show the operating points on the efficiency map. This drive cycle is a part of the QSS toolbox in the Electric and Hybrid vehicles(TME095). Figure 5.5 shows the plot of speed vs time for the FTP Highway drive cycle. The operating points of the transmission are plotted by interpolating on the normalised efficiency map shown in Figure 5.6. The efficiency map shows a cluster of operating points dominating between 4000 to 8000 rpm as the vehicle speeds are high in FTP Highway drive cycle.

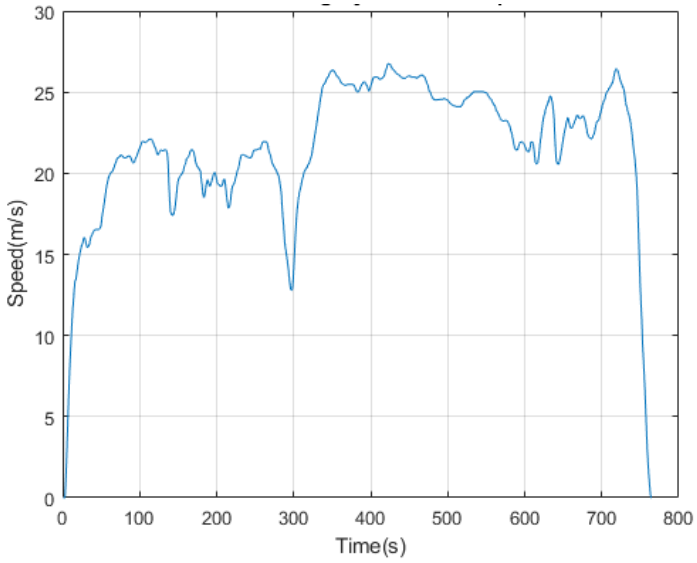

Figure 5.5: FTP Highway driving cycle speed vs time

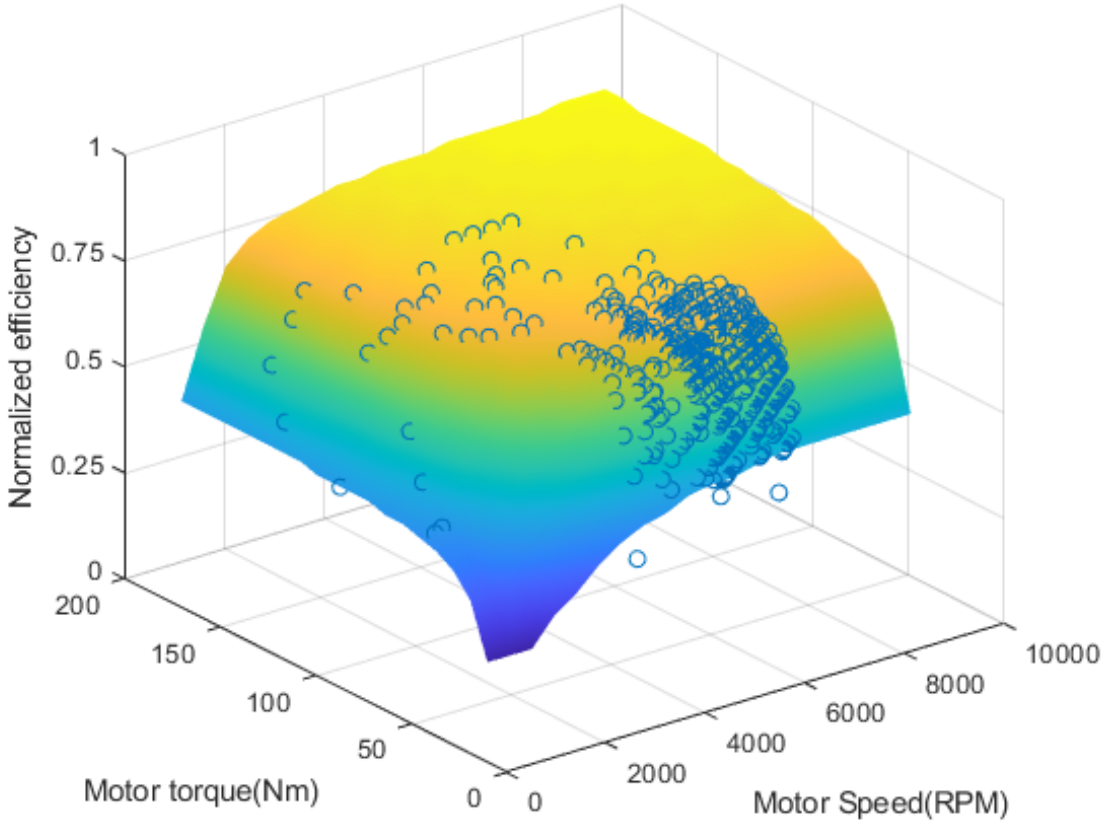

Figure 5.6: Operating points for FTP Highway in the Efficiency Map of Speed vs Torque vs Efficiency (Normalised)

The operating point at mean efficiency is considered for the FTP Highway driving cycle and the contribution from the machine elements at this point is shown in Figure 5.7. For the mean efficiency for FTP Highway drive cycle, the major contributors are gear mesh and churning losses. Churning and seal losses are comparatively higher because of the higher vehicle speeds. However, due to comparatively low torques the contribution of gear mesh losses is lower.

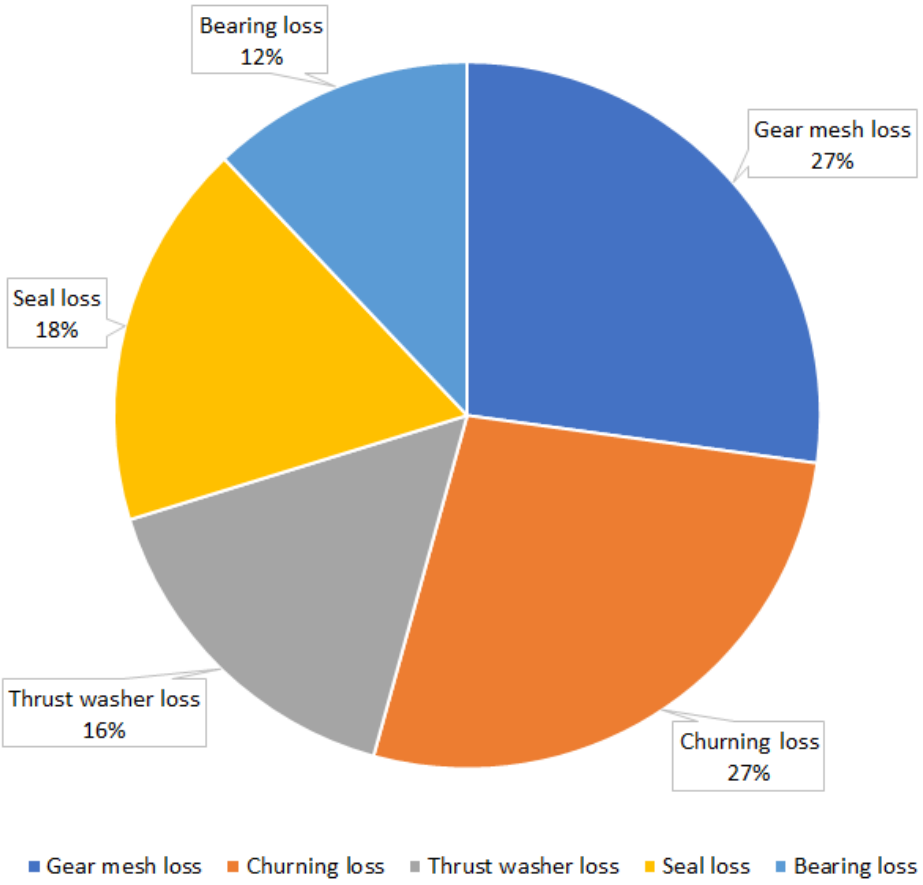

Figure 5.7: Mean efficiency in FTP Highway drive cycle

5.2.3 Gothenburg city driving cycle

In order to get a picture of how the transmission would perform in city driving conditions, it is simulated on the Gothenburg city drive cycle to show the operating points on the efficiency map. This drive cycle is a part of the QSS toolbox in the Electric and Hybrid vehicles(TME095). Figure 5.8 shows the plot of speed vs time for the Gothenburg city drive cycle. The operating points of the transmission are plotted by interpolating on the normalised efficiency map shown in Figure 5.9. The efficiency map shows a cluster of operating points dominating between 0 to 6000 rpm as the vehicle speeds are comparatively low in Gothenburg city drive cycle.

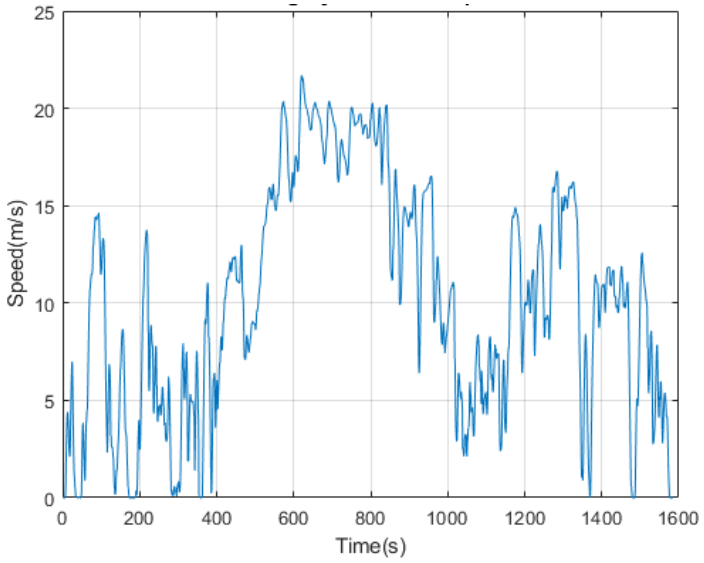

Figure 5.8: Gothenburg city driving cycle speed vs time

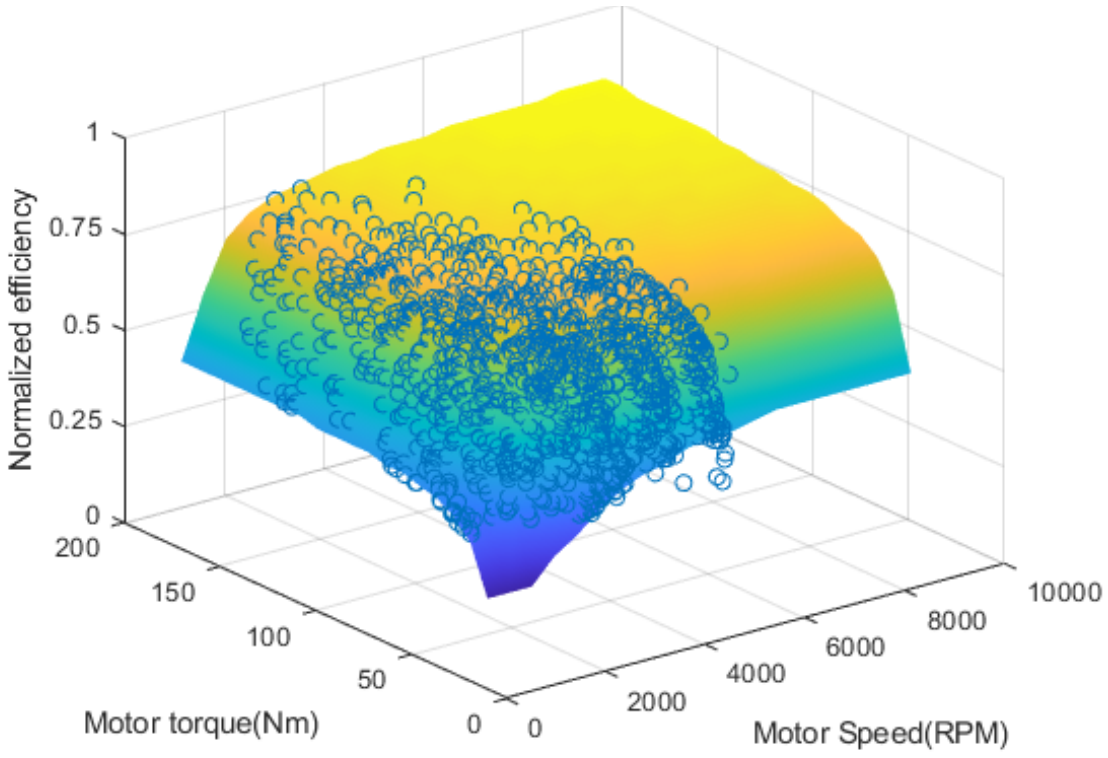

Figure 5.9: Operating points for Gothenburg city in the Efficiency Map of Speed vs Torque vs Efficiency (Normalised)

The operating point at mean efficiency is considered for the Gothenburg city driving cycle and the contribution from the machine elements at this point is shown in Figure 5.10. The Gothenburg city driving cycle has the least efficiency of the three driving cycles tested. The powerloss is comparatively higher because the vehicle operates at higher torques and lower speeds. Churning losses and seal losses are comparatively low due to low speeds. However, due to higher torques the contribution of gear mesh losses is higher.

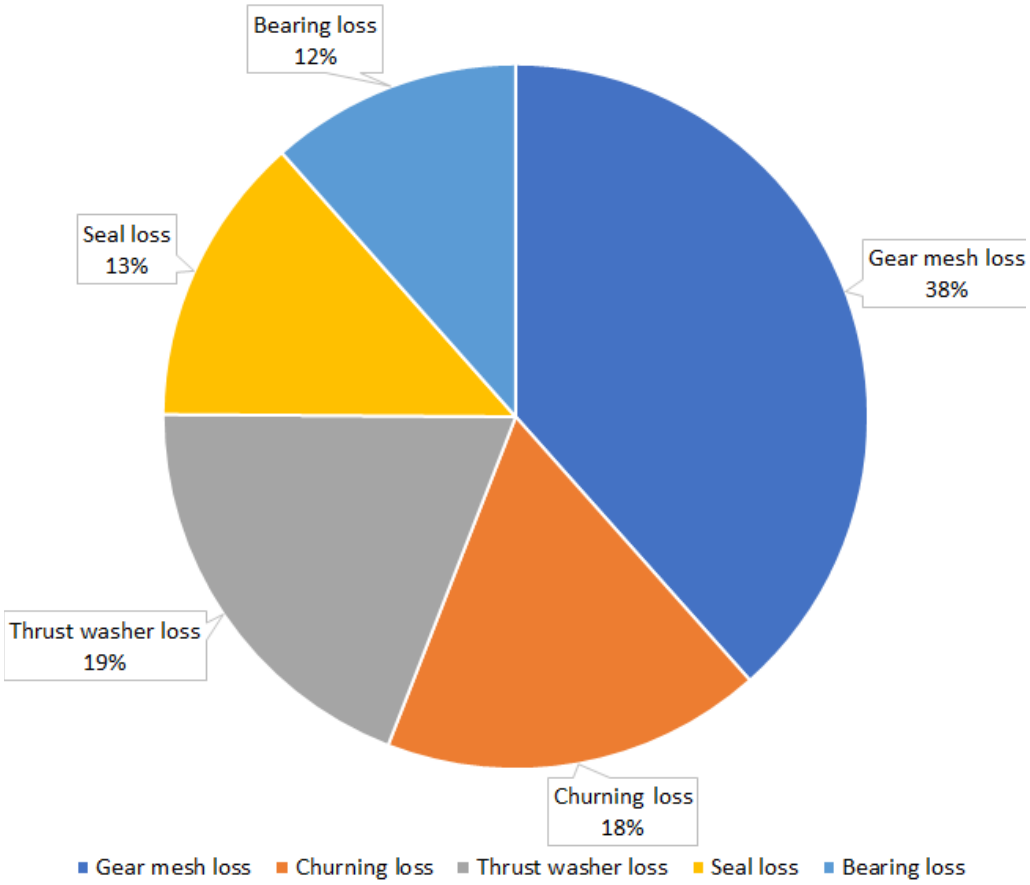

Figure 5.10: Mean efficiency in Gothenburg city drive cycle

Bibliography

[1] OS-15. *Measuring Radial Lip Seal Torque and Power consumption, Rubber Manufacturers Association*. 1986.

[2] N E Anderson and S H Loewenthal. "Effect of Geometry and Operating Conditions on Spur Gear System Power Loss". In: *Journal of Mechanical Design* 103.1 (Jan. 1981), pp. 151–159. ISSN: 0161-8458. DOI: 10.1115/1.3254854. URL: https://doi.org/10.1115/1.3254854.

[3] Neil E Anderson and Stuart H Loewenthal. *Efficiency of nonstandard and high contact ratio involute spur gears*. Tech. rep. 1986, pp. 119–126. URL: https://ntrs.nasa.gov/search.jsp?R=19840021154.

[4] Neil E Anderson and Stuart H Loewenthal. *Spur-Gear-System Efficiency at Part and Full Load*. Tech. rep. 1980. URL: https://ntrs.nasa.gov/search.jsp?R=19800009206.

[5] ANSI/AGMA 6023-A88 (R2000). *Design Manual for enclosed Epicyclic Gear Drives*. 1988.

[6] H.P. Otto B.R. Höhn K. Michaelis. "Flank load carrying capacity and power loss reduction by minimized lubrication". In: *Gear Technology* (2008), pp. 53–62.

[7] C. Changenet and Philippe Velex. "A model for the prediction of churning losses in geared transmissions - Preliminary results". In: *Journal of Mechanical Design, Transactions of the ASME* 129.1 (Jan. 2007), pp. 128–133. ISSN: 10500472. DOI: 10.1115/1.2403727.

[8] P H Dawson. "Windage Loss in Larger High-Speed Gears". In: *Proceedings of the Institution of Mechanical Engineers, Part A: Power and Process Engineering* 198.1 (Feb. 1984), pp. 51–59. ISSN: 0263-7138. DOI: 10.1243/PIME{_}PROC{_}1984{_}198{_}007{_}02. URL: https://doi.org/10.1243/PIME_PROC_1984_198_007_02.

[9] Dennis P. Townsend. *Dudley's Gear Handbook*. Second Ed. McGraw-Hill, Inc, 1992.

[10] Carlos M.C.G. Fernandes et al. "Gearbox power loss. Part I: Losses in rolling bearings". In: *Tribology International* 88 (Apr. 2015), pp. 298–308. ISSN: 0301679X. DOI: 10.1016/j.triboint.2014.11.017.

[11] Carlos M.C.G. Fernandes et al. "Gearbox power loss. Part II: Friction losses in gears". In: *Tribology International* 88 (Apr. 2015), pp. 309–316. ISSN: 0301679X. DOI: 10.1016/j.triboint.2014.12.004.

[12] *Gear Contact Friction*. URL: https://link.springer.com/referenceworkentry/10.1007/978-3-642-22647-2_68.

[13] "Gear Oil Test". In: (). URL: https://link.springer.com/referenceworkentry/10.1007%2F978-3-642-22647-2_70.

[14] Groschopp. *The Importance of Gearbox Efficiency Factors [Accessed on 2020-02-11]*. 2013. URL: https://www.groschopp.com/gearbox-efficiency-factors-2/.

[15] Kotzalas N. Michael Harris A. Tedric. *Rolling Bearing Analysis - Essential Concepts of Bearing Technology*. 5th. Boca Raton, FL: Taylor & Francis Group, 2007.

[16] Petra Heingartner and David Mba. "Determining power losses in the helical gear mesh; case study". In: *Proceedings of the ASME Design Engineering Technical Conference*. Vol. 4 B. 2003, pp. 965–970. DOI: 10.1115/detc2003/ptg-48118.

[17] Doleschel A Höhn B-R Michaelis K. "Evaluation of the frictional properties of transmission lubricants." In: *14th International Colloquium Tribology,Technische Universitaet Esslingen, vol 1* (2004).

[18] Michaelis Klaus Höhn Bernd-Robert and Hinterstoißer Michael. "Optimization of Gearbox Efficiency". 2009.

[19] *ISO/TR 14179-1, Gears - Thermal capacity - Part 1: Rating gear drives with thermal equilibrium at 95 C sump temperature*. Tech. rep. Geneva, Switzerland, 2001.

[20] *ISO/TR 14179-2, Gears - Thermal capacity - Part 2: Thermal load-carrying capacity*. Tech. rep. Geneva, Switzerland, 2001.

[21] Jing Liu, Zhanglin Yan, and Yimin Shao. "An investigation for the friction torque of a needle roller bearing with the roundness error". In: *Mechanism and Machine Theory* 121 (2018), pp. 259–272. ISSN: 0094114X. DOI: 10.1016/j.mechmachtheory.2017.10.028.

[22] Xiaobin Lu, M. M. Khonsari, and E. R.M. Gelinck. "The Stribeck curve: Experimental results and theoretical prediction". In: *Journal of Tribology* 128.4 (Oct. 2006), pp. 789–794. ISSN: 07424787. DOI: 10.1115/1.2345406.

[23] Satya Seetharaman M.S B.E. "An investigation of Load-Independent power losses of gear systems". PhD thesis. The Ohio State University, 2009.

[24] W Mauz. "Zahnradschmierung — Leerlaufverluste". In: FVA-Forsch (1985).

[25] Klaus Michaelis, Bernd Robert Höhn, and Michael Hinterstoißer. "Influence factors on gearbox power loss". In: *Industrial Lubrication and Tribology* 63.1 (2011), pp. 46–55. ISSN: 00368792. DOI: 10.1108/00368791111101830.

[26] Klaus Michaelis and Bernd-Robert Höhn. *DETC2009-86663 Lubricant influence on gear efficiency*. Tech. rep. 2009.

[27] H. Ohlendorf. "Verlustleistung und Erwärmung von Stirnrädern". PhD thesis. Technische Hochschule München, 1958.

[28] A. Palmgren. *Ball and Roller Bearing Engineering*. 3rd. Burbank, Philadelphia, 1959.

[29] "Rating the pitting resistance and bending strength of spur and helical involute gear teeth". In: *AGMA 218.01* (1982).

[30] *Simrit: Radialwellendichtringe, Katalog Nr.100*. 1976.

[31] SKF. *SKF General Catalogue*. Tech. rep. 2008.

[32] David Talbot, Ahmet Kahraman, and Satya Seetharaman. "A Helical Gear Pair Pocketing Power Loss Model". In: *Journal of Tribology* 136.2 (Feb. 2014). ISSN: 0742-4787. DOI: 10.1115/1.4026502. URL: https://doi.org/10.1115/1.4026502.

[33] A.S. Terekhov. "Hydraulic losses in gearboxes with oil immersion". In: *Vestnik Mashinostroeniya* 55.5 (1975), pp. 13–17.

A

Appendix 1

A.1 Helical Gear mesh powerloss

A.1.1 ISO 14179-1 model

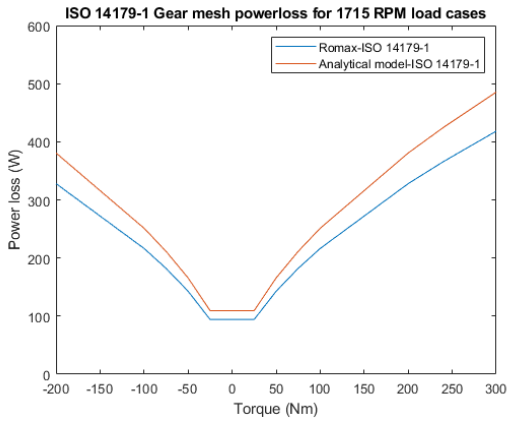

(a) Input speed 1715RPM (∼25km/h)

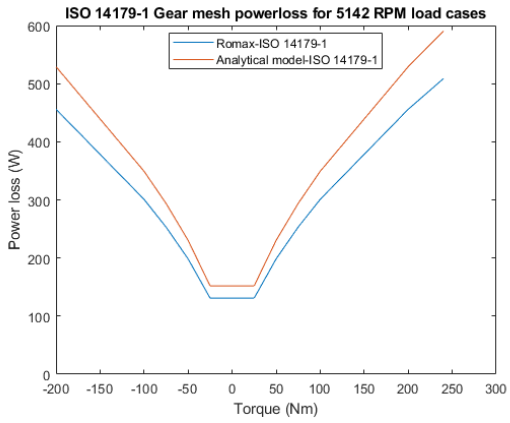

(b) Input speed 5142RPM (∼80km/h)

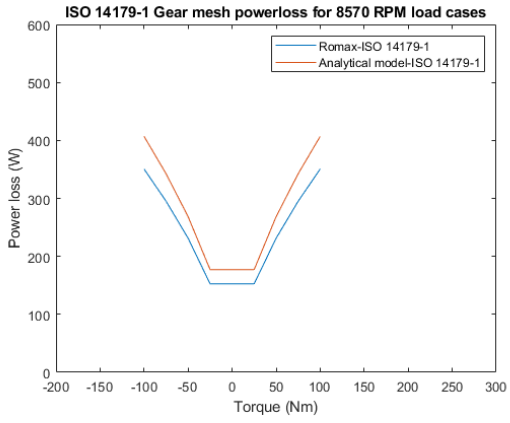

(c) Input speed 8570RPM (∼130km/h)

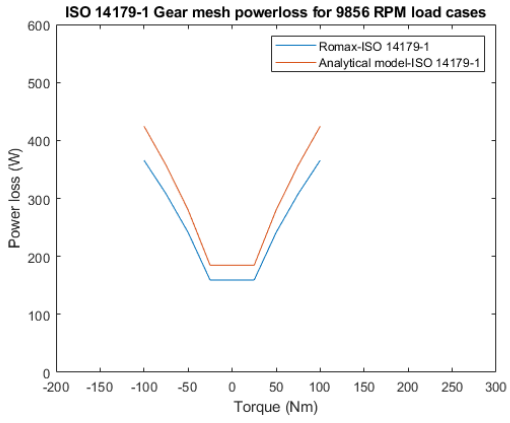

(d) Input speed 9856RPM (∼150km/h)

Figure A.1: ISO 14179-1 - ROMAX and analytical model powerloss results for helical gear mesh

A.1.2 ISO 14179-2/ FVA-345 model

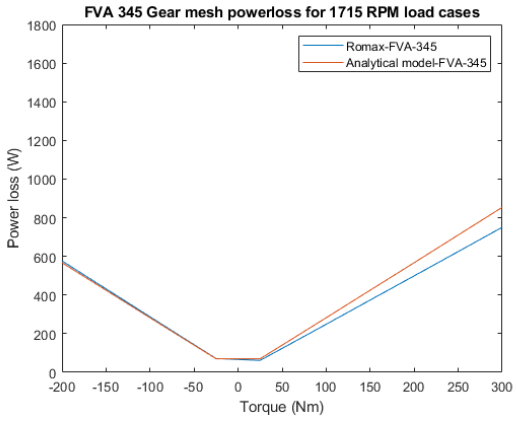

(a) Input speed 1715RPM (∼25km/h)

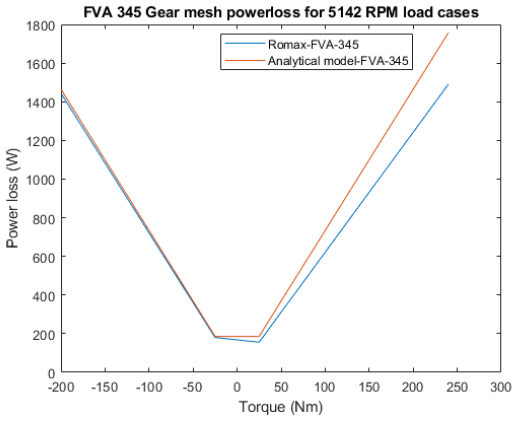

(b) Input speed 5142RPM (∼80km/h)

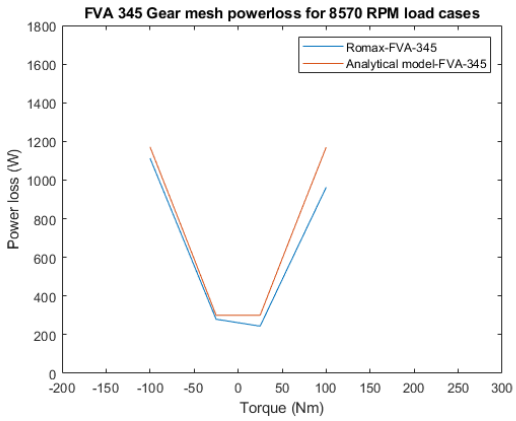

(c) Input speed 8570RPM (∼130km/h)

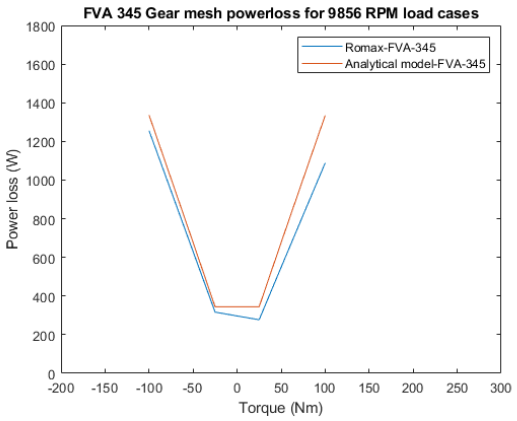

(d) Input speed 9856RPM (∼150km/h)

Figure A.2: ISO 14179-2/ FVA-345 - ROMAX and analytical model powerloss results for helical gear mesh

A.1.3 Micro-geometry model with variable friction coefficient

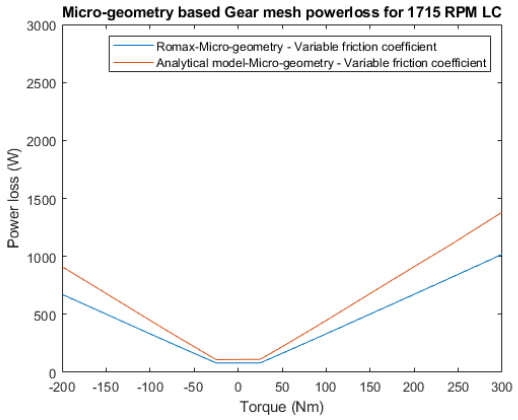

(a) Input speed 1715RPM (∼25km/h)

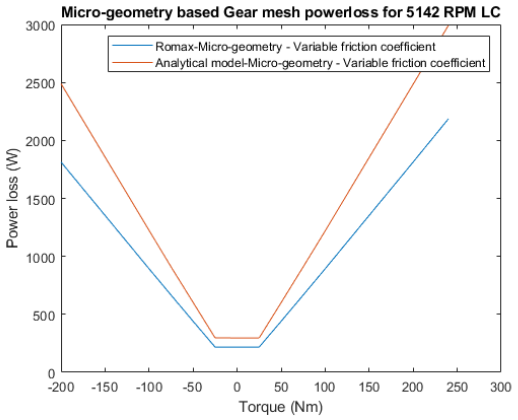

(b) Input speed 5142RPM (∼80km/h)

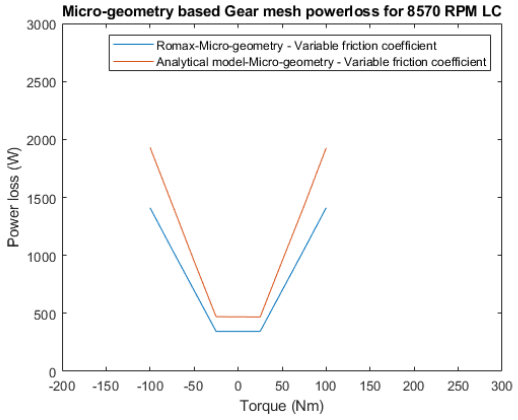

(c) Input speed 8570RPM (∼130km/h)

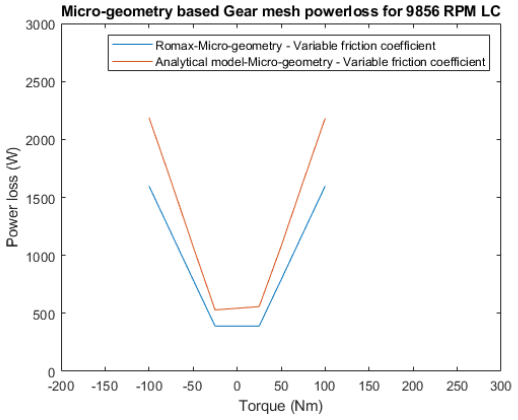

(d) Input speed 9856RPM (∼150km/h)

Figure A.3: Micro-geometry model with variable friction coefficient - ROMAX and analytical model powerloss results for helical gear mesh

A.2 MATLAB code of analytical models

A.2.1 Bearing losses

A.2.1.1 ISO 14179-1 model

```
% Bearing losses : ISO 14179 - 1 model


function [P_Bi] =
 ↪  Bearing_ISO_14179_1(d_i,d_o,C_0,F_a,F_x,F_y,n,f_2)

% d_i = Bearing bore diameter [mm]
% d_o = Bearing outside diamter [mm]
% C_0 = Basic static load rating [N] (from manufacturer's bearing
 ↪  tables)
% F_a = Axial load [N]
% F_x = X-componenet of Raidal load [N]
% F_y = Y-componenet of Raidal load [N]
% n = Bearing rotational speed [rpm]
% f_2 = Factor depending on bearing design and lubrication (0.003
 ↪  - Oil lurication in full complement single row bearings)

%Bearing Data
a = 1 ;          % Exponent
b = 1 ;          % Exponent

%Radial load [N]
F_r = sqrt((F_x^2) + (F_y^2))

ratio = F_a/F_r;
% This ratio should not exceed 0.5 for single - row full
 ↪  complement bearings

P_0 = (0.5*F_a) + (0.6*F_r)              % Equivalent static Bearing
 ↪  load [N]

if P_0< F_r
    P_0 = F_r
else
 P_0 = (0.5*F_a) + (0.6*F_r)
end

f_1 = (0.0009) * ((P_0/C_0)^0.55)        % Coefficient of Friction
 ↪  (0.0006 ..... 0.0009)
```

```
P_1 = (3*F_a) - (0.1*F_r)
if P_1 < F_r
    P_1 = F_r
else
    P_1 = (3*F_a) - (0.1*F_r)           % Bearing dynamic load [N]
end


d_m = (d_i+d_o)/2;                      % Bearing mean diameter
 ↪  [mm]

M_1 = (f_1*((P_1)^a)*((d_m)^b))/(1000)  % Bearing load dependent
 ↪  torque [Nm]

M_2 = (f_2*F_a*d_m)/1000                % Axial load dependent
 ↪  moment in cylindrical roller Bearing [Nm]

P_Bi = 1000*((M_1+M_2)*n)/9549;         % Power loss for the
 ↪  individual bearing [W]

end
```

A.2.1.2 Palmgren model

```
% Bearing losses : Deep groove ball bearings - Palmgren model

function [Power,M_t] = Palmgren(F_a,Z_1,d,D,n,F_x,F_y)
% F_a = Axial load [N]
% Z_1 = Number of bearing elements
% d = Bearing bore diameter [mm]
% D = Bearing outside diamter [mm]
% n = Bearing rotational speed [rpm]
% F_x = X-componenet of Raidal load [N]
% F_y = Y-componenet of Raidal load [N]

%Bearing Data
i=1;                    % Number of rows of rolling elements
alpha=0; %[degree]      % Contact angle [degree]
z= 0.0004;              % From Table 10.1 in the book by Harris A.
 ↪  et al.
y= 0.55;                % From Table 10.1 in the book by Harris A.
 ↪  et al.
X_s = 0.6;              % From Table 9.3 in the book by Harris A.
 ↪  et al.
Y_s = 0.5;              % From Table 9.3 in the book by Harris A.
 ↪  et al.
v_o= 18;                % Lubricant kinematica viscosity [cSt]
f_0 = 2;                % Factor depending on the type of bearing
 ↪  and method of lubrication.

% Bearing mean diameter [mm]
d_m = (d+D)/2;

%Radial load [N]
F_r = sqrt(((F_x)^2) + ((F_y)^2))


F_s = (X_s*F_r)+ (Y_s*F_a);                 % Static equivalent
 ↪  load [N]
Q_max = (5*F_r)/(i*Z_1*cosd(alpha));        % Maximum loaded
 ↪  rolling element load
C_s = 0.2*i*Z_1*Q_max* cosd(alpha);         % Basic static load
 ↪  rating

f_1 = z*(F_s/C_s)^y;                        % Palmgren frictional
 ↪  coefficient
%F_beta = (3*F_a) - (0.1*F_r)
F_beta = F_r;
```

```
M_1 = f_1*F_beta*d_m;                          % Load friction torque
 ↪  [Nm]
M_v = (10^(-7))*f_0*(v_o*n)^(2/3)*(d_m)^3     % Viscous friction
 ↪  torque [Nm]

M_t = M_1+M_v;                                % Total frictional torque
 ↪  [Nm]

Power = 2*pi* (n/60)*M_t*(10^(-3));           % Power loss for the
 ↪  bearing [W]
end
```

A.2.1.3 SKF model

A.2.1.3.1 FAG 61822-Y bearing

```
% Bearing losses : Deep groove ball bearings - FAG 61822-Y bearing
 ↪  - SKF model

function [M,P] = SKF_Big_bearing(d,D,n,F_a,F_x,F_y,H,v)
%Bearing B13 Data
% d = Bearing bore diameter [mm]
% D = Bearing outside diamter [mm]
% n = Bearing rotational speed [rpm]
% F_a = Axial load [N]
% F_x = X-componenet of Raidal load [N]
% F_y = Y-componenet of Raidal load [N]
% H = Oil level
% v= Lubricant kinematica viscosity [cSt]

K_rs = 3*10^(-8);          % Replenishment/starvation constant
K_Z = 3.1;                 % Bearing type related geometric constant

mu_bl = 0.12;              % Constant depending on movement:
mu_EHL = 0.1;              % Sliding friction coefficient in full-film
 ↪  conditions.
%mu_EHL = 0.05;
V_M = 0.00005;             % Drag loss factor
i_rw = 1;                  % Number of ball rows
C_0= 30500;                % Basic static load rating [N] (from
 ↪  manufacturer's bearing tables)

%Bearing series: Deep groove ball bearings: '618'
R_1 = 4.7*10^(-7);
R_2 = 1.7;
S_1 = 6.5*10^(-3);
S_2 = 0.78;

%Bearing mean diameter [mm]
d_m = (d+D)/2;

%Radial load [N]
F_r = sqrt((F_x^2) + (F_y^2))


%%
%Coefficient of inlet shear heating factor
phi_ish =  1/(1 + (1.84*10^(-9)*((n*d_m)^(1.28))*(v^(0.64))));
```

```
%Kinematic replenishment/starvation reduction factor
phi_rs = 1/(exp((K_rs*v*n*(d+D)*(sqrt(K_Z/2*(D-d))))));
%phi_rs_try = 1/(exp((K_rs*7.36*n*(d+D)*(sqrt(K_Z/2*(D-d))))))

alpha_f = 24.6*(F_a/C_0)^(0.24);

% Rolling frictional variable
G_rr = R_1*(d_m^(1.96))*(F_r+((R_2*F_a)/(sind (alpha_f))))^(0.54);
%G_rr = real(G_rr);

%Rolling frictional moment
M_rr = phi_ish * phi_rs * G_rr * ((v*n)^(0.6));

 %%
%Weighting factor for the sliding friction coefficient
phi_bl = 1/(2.718^((2.6*10^(-8))*((n*v)^(1.4))*d_m));

%Effect of lubrication on sliding friction
mu_sl = (phi_bl*mu_bl) + (1-phi_bl)*mu_EHL;

%Sliding frictional variable
G_sl = S_1*(d_m^(-0.145))*((F_r^5)+((S_2*(d_m^(1.5))*F_a^4)/(sind
↪  (alpha_f))))^(1/3);
% G_sl = real(G_sl);

%Sliding frictional moment
M_sl = G_sl*mu_sl;


%%
K_ball = (i_rw*K_Z*(d+D)*10^(-12))/((D-d));          % Rolling
↪  elements related constants

f_A = 0.05*(K_Z*(D+d))/(D-d);
t = 2*acos((0.6*d_m - H)/(0.6*d_m));
R_s = 0.36*(d_m^2)*(t-sin (t))*f_A;
f_t = sin (0.5*t);

%l_D = 5*(K_L*B}/d_m;

%C_w = (2.789*10^(-10)*l_D^3) - (2.786*10^(-4)*l_D^2)+ 0.0195*l_D
↪  + 0.6439;

% Frictional moment of drag losses for ball bearings
M_drag = (0.4*V_M*K_ball*(d_m^5)*n^2) +
↪  (1.093*10^(-7)*(n^2)*(d_m^3)*((n*(d_m^2)*f_t/v)^(-1.379))*R_s)
```

```
%%
%Total frictional moment [Nm]
M = M_rr + M_sl + M_drag

P = 2*pi*(n/60)*M*(10^(-3));     % Power loss for the individual
 ↪  bearing [W]
end
```

A.2.1.3.2 FAG 6009 bearing

```
% Bearing losses : Deep groove ball bearings - FAG 6009 bearing -
 ↪  SKF model

function [P,M] = SKF_small_bearing(d,D,n,F_a,F_x,F_y,H,v)
%Small Bearing -B14 Data
% d = Bearing bore diameter [mm]
% D = Bearing outside diamter [mm]
% n = Bearing rotational speed [rpm]
% F_a = Axial load [N]
% F_x = X-componenet of Raidal load [N]
% F_y = Y-componenet of Raidal load [N]
% H = Oil level
% v= Lubricant kinematica viscosity [cSt]

K_rs = 3*10^(-8);          % Replenishment/starvation constant
K_Z = 3.1;                 % Bearing type related geometric constant

mu_bl = 0.12;              % Constant depending on movement
mu_EHL = 0.1;              % Sliding friction coefficient in full-film
 ↪  conditions.
%mu_EHL = 0.05;
V_M = 0;                   % Drag loss factor
i_rw = 1;                  % Number of ball rows
C_0= 14400;                % Basic static load rating [N] (from
 ↪  manufacturer's bearing tables)

%Bearing series: Deep groove ball bearings: '60'
R_1 = 4.1*10^(-7);
R_2 = 1.7;
S_1 = 3.73*10^(-3);
S_2 = 14.6;

%Bearing mean diameter
```

```
d_m = (d+D)/2;

%Radial load [N]
F_r = sqrt(((F_x)^2) + ((F_y)^2))


%%
%Coefficient of inlet shear heating factor
phi_ish =  1/(1 + (1.84*10^(-9)*((n*d_m)^(1.28))*(v^(0.64))))

%Kinematic replenishment/starvation reduction factor
phi_rs = 1/(exp((K_rs*v*n*(d+D)*(sqrt(K_Z/2*(D-d))))))
%phi_rs_try = 1/(exp((K_rs*7.36*n*(d+D)*(sqrt(K_Z/2*(D-d))))))

alpha_f = 24.6*(F_a/C_0)^(0.24);

% Rolling frictional variable
G_rr = R_1*(d_m^(1.96))*(F_r+((R_2*F_a)/(sind (alpha_f))))^(0.54);
%G_rr = real(G_rr);

%Rolling frictional moment
M_rr = phi_ish * phi_rs * G_rr * ((v*n)^(0.6))

 %%
%Weighting factor for the sliding friction coefficient
phi_bl = 1/(2.718^((2.6*10^(-8))*((n*v)^(1.4))*d_m));

%Effect of lubrication on sliding friction
mu_sl = (phi_bl*mu_bl) + (1-phi_bl)*mu_EHL;

%Sliding frictional variable
G_sl = S_1*(d_m^(-0.145))*((F_r^5)+((S_2*(d_m^(1.5))*F_a^4)/(sind
↪  (alpha_f))))^(1/3);
% G_sl = real(G_sl);

%Sliding frictional moment
M_sl = G_sl*mu_sl


%%
K_ball = (i_rw*K_Z*(d+D)*10^(-12))/((D-d));          % Rolling
↪  elements related constants

f_A = 0.05*(K_Z*(D+d))/(D-d);
t = 2*acos((0.6*d_m - H)/(0.6*d_m));
R_s = 0.36*(d_m^2)*(t-sin (t))*f_A;
```

```
f_t = sin (0.5*t);

%l_D = 5*(K_L*B}/d_m;
%C_w = (2.789*10^(-10)*l_D^3) - (2.786*10^(-4)*l_D^2)+ 0.0195*l_D
 ↪  + 0.6439;

% Frictional moment of drag losses for ball bearings
M_drag = (0.4*V_M*K_ball*(d_m^5)*n^2) +
 ↪  (1.093*10^(-7)*(n^2)*(d_m^3)*((n*(d_m^2)*f_t/v)^(-1.379))*R_s)

%%
%Total frictional moment
M = M_rr + M_sl + M_drag;

P = 2*pi*(n/60)*M*(10^(-3));        % Power loss for the individual
 ↪  bearing [W]
end
```

A.2.1.4 Needle bearings - Palmgren model

```
% Bearing losses : Needle bearings - Palmgren model

function [F_r, Power] = Palmgren_Needle(D,d,v,n,F_x,F_y)
%Bearing Data
% D = Bearing outside diamter [mm]
% d = Bearing bore diameter [mm]
% v = Lubricant kinematica viscosity [cSt]
% n = Bearing rotational speed [rpm]
% F_x = X-componenet of Raidal load [N]
% F_y = Y-componenet of Raidal load [N]

f_0 = 6;          % Coefficient determined by the bearing type and
 ↪  lubricant conditions - 6 for Oil spray lubrication conditions
% zeta =0.0004 ;         % Dimensionless parameters
% tau = 0.55;           % Dimensionless parameters

% X_s = 0.6;
% Y_s = 0.5;

%Bearing mean diameter
d_m = (d+D)/2;

%Radial load [N]
F_r = sqrt(((F_x)^2) + ((F_y)^2));

% Static equivalent load [N]
%F_s = (X_s*F_r)+ (Y_s*F_a);
%F_s = X_s*F_r;
P = F_r;        % Applied load [N]

% Load independent frictional torque [Nm]
m = v*n ;
if m>= 2000
    M_0 = (10^(-7))*f_0*(v*n)^(2/3)*(d_m)^3
else
    M_0 = (160*10^(-7))*f_0*(d_m)^3
end


%%
% f_1 = zeta*(F_s/C_s)^(tau)
f_1 = 0.00055;       % table 10.3, pg: 187 in Harris book -
 ↪  Essential concepts of bearing technology
```

```
M_1 = f_1*P*d_m;     % Load dependent frictional torque [Nm]


%%
M_t = M_0 + M_1;         % Total frictional torque [Nm]

Power = 3*2*pi* (n/60)*M_t*(10^(-3)) ;          %Total power loss
↪  for 3 bearings (Either left or right set of bearings) [W]

end
```

A.2.2 Gear mesh losses

A.2.2.1 ISO 14179-1 model

```
% Gear mesh losses : ISO 14179 1 model

function [P_Mi] =
 ↪  ISO(b_w,T_1,n_1,beta_w,alpha_w,z_1,z_2,r_o1,r_o2,r_w1,r_w2,V)
% b_w = Face width in contact [mm]
% T_1 = Pinion Torque [Nm]
% n_1 = Pinion rotational speed [rpm]
% beta_w = Operating Helix angle [degree]
% alpha_w = Transverse operating pressure angles [degree]
% z_1 = Number of pinion teeth
% z_2 =  Number of gear teeth
% r_o1 = Pinion outside radius [mm]
% r_o2 = Gear outside radius [mm]
% r_w1 = Pinion operating pitch radius [mm]
% r_w2 = Gear operating pitch radius [mm]
% V = Tangential pitch line velocity [m/s]

v = 8.038 ;  %Kinematic oil viscosity at operating sump
 ↪  temperature [mm^2/s]

%Constants
C_1 = 3.239;
j = -0.223;
g = -0.40;
h = 0.70;


%Gear ratio
u = z_2/z_1;

%Load intensity
K = (1000.*T_1.*(z_1 + z_2))./(2.*b_w.*(r_w1.^2).*z_2)

%Mesh coefficient of friction
f_m = ((v^j).*(K.^g))./(C_1*(V.^h))

%Sliding ratio at the start of approach
H_s = (u+1).* (( ((r_o2.^2)/(r_w2.^2)) - (cosd(alpha_w)).^2 ).^(0.5)
 ↪  - sind(alpha_w))

%Sliding ratio at the end of recess
H_t = ((u+1)/u).* (((r_o1.^2)/(r_w1.^2) - (cosd(alpha_w)).^2).^(0.5)
 ↪  - sind(alpha_w))
```

```
%Mesh mechanical advantage
 M = ((2.*cosd(alpha_w)).*(H_s + H_t))./((H_s.^2) + (H_t.^2))

% Gear mesh losses
P_Mi =(1000.*f_m.*T_1.*n_1.*(cosd(beta_w)).^2)./(9549.*M); % Power
 ↪  loss in [W]

end
```

A.2.2.2 ISO 14179-2/FVA 345 method

```
function [mu_m,mu_mz] =
 ↪  mu_mz_FVA(F_t,phi,b,red_radius,v_pitch,h0,p_h,neta_oil,Ra)

% F_t = %Tangential tooth force [N]
% phi = Working normal pressure angle
% b = Working Face width [mm]
% red_radius = Radius of curvature at pitch point[mm]
% v_pitch = Velocity at pitch point [m/s]
% h0 = Min film thickness [micro meter]
% p_h = Contact pressure [N/mm^2]
% neta_oil = dynamic oil viscosity at oil temperature [mPas]
% Ra = Surface roughness of gear and pinion [micro meter]

% Constants for FVA
%EHD
mu_EHDR = 5.5e-2;    %Refrence value from test
p_R = 1000;          %[N/mm2]
v_REHD = 8.3;        %[m/s]

neta_R = 20;             %dynamic refrence oil viscosity at oil
 ↪  temperature [mPas]
%alpha_EHD = -(5e-2);    %Pressure(or load) exponent for fluid
 ↪  friction from test
alpha_EHD = -(9e-2);
beta_EHD = 4e-2;         %speed exponent for fluid friction from
 ↪  test
gamma_EHD = 0.37;        %viscosity exponent for fluid friction from
 ↪  test

%Solid
mu_fr = 8.77e-2; %solid friction coefficient, reference value from
 ↪  test
v_RF = 0.2;      %reference value of speed for solid friction [m/s]
alpha_F = 9e-3; %pressure exponent for solid friction from test
%alpha_F = -3e-2; %pressure exponent for solid friction from test
beta_F = -0.14;   %speed exponent for solid friction from test

%FVA coefficients
lambda = h0/Ra;
if lambda >= 2
    zeta = 1;
else if lambda < 2
        zeta = 1-(1-(lambda/2))^2
    end
```

```
end

%With coefficients
mu_f = mu_fr*((p_h/p_R)^(alpha_F))*((v_pitch/v_RF)^(beta_F));
mu_EHD =
 ↪  mu_EHDR*((p_h/p_R)^(alpha_EHD))*((v_pitch/v_REHD)^(beta_EHD))*((neta_oil/neta_R
mu_m = ((1-zeta)*mu_f) + (zeta*mu_EHD)

%Estimation method
X_L = 0.9; %Constant

F_bt = F_t/cosd(phi);
mu_mz = 0.048*((F_bt/b)/(v_pitch*red_radius))*neta_oil*Ra*X_L
end
```

```
% Ohlendorf factor for external gear mesh

function [H_v] = ohlendorf_s1(z_1,u,beta_b,E_alpha,E_1,E_2)
H_v = (pi*(u+1)/(z_1*u*cosd(beta_b)))*(1 - E_alpha + ((E_1)^2) +
 ↪  ((E_2)^2))
end
```

```
% Ohlendorf factor for internal gear mesh
function [H_v] = ohlendorf_s2(z_1,u,beta_b,E_alpha,E_1,E_2)
H_v = (pi*(u+1)/(z_1*cosd(beta_b)))*(1 - E_alpha + ((E_1)^2) +
 ↪  ((E_2)^2))
end
```

A.2.2.3 Micro-Geometry model with Variable friction coefficient

```
%Gear mesh losses : Micro-Geometry model with Variable friction
 ↪  coefficient

function [P_VZP] = Micro_geometry(n,T,H_v,mu_mz)
% n = Speed of driver[rpm]
% T = Nominal torque [Nm]
% H_v = Gear loss factor by Ohlendorf
% mu_mz = Mean coefficient of gear friction (from Romax)

% Transmitted power
P_a = 2*pi*n*T/60;  % Transmitted power [W] (Sun gear/ Large Planet
 ↪  gear)

P_VZP = P_a * mu_mz * H_v *3;   % Power loss  [W]

end
```

```
% Ohlendorf factor for external gear mesh

function [H_v] = ohlendorf_s1(z_1,u,beta_b,E_alpha,E_1,E_2)
H_v = (pi*(u+1)/(z_1*u*cosd(beta_b)))*(1 - E_alpha + ((E_1)^2) +
 ↪  ((E_2)^2))
end
```

```
% Ohlendorf factor for internal gear mesh
function [H_v] = ohlendorf_s2(z_1,u,beta_b,E_alpha,E_1,E_2)
H_v = (pi*(u+1)/(z_1*cosd(beta_b)))*(1 - E_alpha + ((E_1)^2) +
 ↪  ((E_2)^2))
end
```

A.2.3 Gear drag/Churning losses

A.2.3.1 ISO 14179-1 model

```
% Gear drag/Churning loss - ISO 14179 - 1 model

function [P_loss] = churn_ISO1(dp,z,f_g,n,D,a_g,F,beta)
% dp = Refrence pitch circle diameter [mm]
% z = Number of tooth
% f_g = Gear dip coefficient
% n = Rotational speed [RPM]
% D = Gear outer diameter [mm]
% a_g = Arrangement constant
% F = Gear face width [mm]
% beta = Helix angle [degree]

v = 18 ;    %Kinematic viscosity [cSt]

m_t = dp./z %Transverse module

%Roughness factor
R_f = 7.93 - (4.648/m_t)

% Smooth outside diameter
%P_GWi = (7.37*f_g*v*n^3*D^4.7*L)/(a_g*10^26);

% Smooth sides of disc
P_GW_side = (1.474*f_g*v*(n^3)*(D^(5.7)))/(a_g*(10^(26)))

% Tooth surfaces
P_GW_tooth =
 ↪  (7.37*f_g*v*(n^3)*(D^(4.7))*F*(R_f/sqrt(tand(beta))))/(a_g*(10^(26)))


P_loss = (P_GW_side + P_GW_tooth)*1000; %Total churning loss in W
end
```

A.2.3.2 ISO 14179-2 model

```
% Gear drag/Churning loss - ISO 14179 - 2 model

function [P_loss] =
 ↪  churn_ISO2(h_e0,h_e1,h_emax,h_c,AG,UM,b,b_0,n,v_t,v_t0)
% h_e0 = Reference value of immersion depth [mm]
% h_e1 = Tip circle immersion depth with oil level stationary [mm]
% h_emax = Maximum Tip circle immersion depth with oil level
 ↪  stationary [mm]
% h_c = Height of point of contact above the lowest point of the
 ↪  immersing gear [mm]
% AG = Enclosure area [mm^2]
% UM = Enclosure Circumference [mm]
% b = Tooth width [mm]
% b_0 = Reference value of tooth width [mm]
% n = Gear speed [rpm]
% v_t = Tangential speed [m/s]
% v_t0 = Reference Tangential speed [m/s]

l_h = (4*AG)/UM    % Hydraulic length [mm]

%C_1 = (0.063*((h_e1+h_e2)/h_e0)) + (0.0128*((b/b_0)^3));
C_1 = (0.063*((h_e1)/h_e0)) + (0.0128*((b/b_0)^3))

%C_2 = ((h_e1+h_e2)/(80*h_e0)) + 0.2;
C_2 = ((h_e1)/(80*h_e0)) + 0.2

% Splash oil factor
C_SP = (((4*h_emax)/(3*h_c))^(1.5))*(2*h_c/l_h)

T_H = C_SP*C_1*exp(C_2*v_t/v_t0)        % Total hydraulic loss
 ↪  torque [Nm]

P_loss =T_H*pi*n/30             %Total churning loss in WW
end
```

A.2.3.3 Terekhov model

A.2.3.3.1 Gears dipped in lubricant: The same function is applied for both large and small planet gears dipped in the lubricant.

```
% Gear drag/Churning loss - Terekhov model
% Sun gear - Large planet gear - in contact with lubricant

function [P_loss] =
 ↪  Terekhov_v2_large(N_s,R,b,h,V_g,V_o,sigma_V_g,l,l_0,R_o)
% N_s = Rotational speed [RPM]
% R =  Outer radius [m]
% b =  Gear width [m]
% h = Immersion depth of gear into oil [m]
% V_g = Immersed volume of the gear [m^3] - large planet
% V_o = Volume of oil poured into the gear [m^3]
% sigma_V_g = Total immersed volume of all the gears [m^3]
% l = Tooth depth [m]
% l_0 = Scale factor for length introduced for dimensional
 ↪  compensation
% R_o = Radius of the pitch circle [m]

g = 9.81 ;                % Gravity acceleration [m/s^2]
rho = 847;                % Lubricant density [kg/m^3]
v = 18*10^(-6);           % Kinematic viscosity of oil [m^2/s]

% Angular velocity of the gear [r/s]
omega = ((pi*N_s)/30);

Re = (omega*R^2)/v            % Reynolds number
% The fluid flow becomes turbulent at Re>= 2250

Fr = ((omega^2)*R)/g          % Froude number

% Range check
% Ratio of the depth of the immersion of the gear to its radius
HR = h/R

% Ratio of the breadth of the gear to its radius
BR = b/R

% Ratio of the immersed volume of the gear to the volume of the
 ↪  oil poured
% over it.
VV = V_g/V_o
SVV = sigma_V_g/V_o
```

```
C_m_1 = 0;
C_m_2 = 0;
C_m_3 = 0;
C_m_4 = 0;

if Re>36000
    Re = 36000;
end

if Fr>1400
    Fr = 1400;
end
if Re>=10 && Re<= 36000 && Fr>=1.6 && Fr<= 1400 && HR>=0.025 &&
 ↪  HR<= 1 && BR>=0.006 && BR<= 1 && VV>=0.1 && VV<= 0.25 &&
 ↪  SVV>=0.02 && SVV<= 0.5

% Moment of disc losses of each gear
% Zone 1_1 (Equation 1)
C_m_1 = 4.57 * (Re^(-0.6)) * (Fr^(-0.25)) * ((h/R)^(1.5)) *
 ↪  ((b/R)^(-0.4)) * ((V_g/V_o)^(-0.3)) * ((sigma_V_g/V_o)^(-0.2));

% Zone 1_2 (Equation 2)
C_m_2 = 2.63 * (Re^(-0.6)) * (Fr^(-0.25)) * ((h/R)^(1.5)) *
 ↪  ((b/R)^(-0.17)) * ((V_g/V_o)^(-0.53)) *
 ↪  ((sigma_V_g/V_o)^(-0.2));

% Zone 2 (Equation 3)
C_m_3 = 0.376 * (Re^(-0.3)) * (Fr^(-0.25)) * ((h/R)^(1.5)) *
 ↪  ((b/R)^(-0.124)) * ((V_g/V_o)^(-0.376)) *
 ↪  ((sigma_V_g/V_o)^(-0.2));

% Equation 6
C_m_4 = 0.506 * (Re^(-0.32)) * (Fr^(-0.25)) * ((h/R)^(2.1)) *
 ↪  ((b/R)^(-0.27)) * ((V_g/V_o)^(-0.8)) * ((sigma_V_g/V_o)^(-0.2));

end

% Moment of the disc losses in one gear
M_D = rho *(omega^2) * (R^4) * b * C_m_3


%Reynolds number
Re_2 = (omega*R_o*l)/v;
Re_2 = 2100;
% Froude number
Fr_2 = ((omega^2)*R_o^2)/(g*l);
```

```
Fr_2 = 3112;

if Re>2100
    Re = 2100;
end

if Fr>3112
    Fr = 3112;
end

% Range check
% Ratio of the tooth depth to the scale factor for length
 ↪  introduced for dimensional compensation
LL = (l/l_0)

% Ratio of the Gear width to the scale factor for length
 ↪  introduced for dimensional compensation
BL = (b/l_0)


C_m_oil_1 = 0;
C_m_oil_2 = 0;

if Re_2>=7 && Re_2<= 2100 && Fr_2>=22 && Fr_2<= 3112 && LL>=0.45 &&
 ↪  LL<= 1.8 && BL>=1 && BL<= 6
% Losses caused by yhe expulsion of the oil
% Zone 1
C_m_oil_1 = 616.6 * (Re_2^(-0.65)) * (Fr_2^(-0.46)) *
 ↪  ((l/l_0)^(-1.66)) * ((b/l_0)^(-0.46));

% Zone 2
C_m_oil_2 = 5623 * (Re_2^(-0.88)) * (Fr_2^(-0.78)) *
 ↪  ((l/l_0)^(-1.6)) * ((b/l_0)^(-0.36));

end

% Moment of the losses due to the oil expulsion
M_oe = rho *(omega^2) * (R_o^3) * b * l * C_m_oil_2

% Total moment
M = M_D +M_oe

P_loss = M*omega %Total churning loss in W

end
```

A.2.3.3.2 Gears dipped in air: The same function is applied for both large and small planet gears which are dipped in air.

```
% Gear drag/Churning loss - Terekhov model
% Sun gear - Large planet gear - in contact with air

function [P_loss] =
 ↪  Terekhov_v2_large_air(N_s,R,b,h,V_g,V_o,sigma_V_g,l,l_0,R_o)
% N_s = Rotational speed [RPM]
% R =  Outer radius [m]
% b =  Gear width [m]
% h = Immersion depth of gear into oil [m]
% V_g = Immersed volume of the gear [m^3] - large planet
% V_o = Volume of oil poured into the gear [m^3]
% sigma_V_g = Total immersed volume of all the gears [m^3]
% l = Tooth depth [m]
% l_0 = Scale factor for length introduced for dimensional
 ↪  compensation
% R_o = Radius of the pitch circle [m]

g = 9.81 ;                % Gravity acceleration [m/s^2]
rho = 1.2;                % Lubricant density [kg/m^3]
v = 19.86*10^(-6);        % Kinematic viscosity of oil [m^2/s]

% Angular velocity of the gear [r/s]
omega = ((pi*N_s)/30);

Re = (omega*R^2)/v            % Reynolds number
% The fluid flow becomes turbulent at Re>= 2250

Fr = ((omega^2)*R)/g          % Froude number

%Range check
% Ratio of the depth of the immersion of the gear ro its radius
HR = h/R

% Ratio of the breadth of the gear to its radius
BR = b/R

% Ratio of the immersed volume of the gear to the volume of the
 ↪  oil poured
% over it.
VV = V_g/V_o
SVV = sigma_V_g/V_o

C_m_1 = 0;
```

```
C_m_2 = 0;
C_m_3 = 0;
C_m_4 = 0;

if Re>36000
    Re = 36000;
end

if Fr>1400
    Fr = 1400;
end
if Re>=10 && Re<= 36000 && Fr>=1.6 && Fr<= 1400 && HR>=0.025 &&
 ↪  HR<= 1 && BR>=0.006 && BR<= 1 && VV>=0.1 && VV<= 0.25 &&
 ↪  SVV>=0.02 && SVV<= 0.5

% Moment of disc losses of each gear
% Zone 1_1 (Equation 1)
C_m_1 = 4.57 * (Re^(-0.6)) * (Fr^(-0.25)) * ((h/R)^(1.5)) *
 ↪  ((b/R)^(-0.4)) * ((V_g/V_o)^(-0.3)) * ((sigma_V_g/V_o)^(-0.2));

% Zone 1_2 (Equation 2)
C_m_2 = 2.63 * (Re^(-0.6)) * (Fr^(-0.25)) * ((h/R)^(1.5)) *
 ↪  ((b/R)^(-0.17)) * ((V_g/V_o)^(-0.53)) *
 ↪  ((sigma_V_g/V_o)^(-0.2));

% Zone 2 (Equation 3)
C_m_3 = 0.376 * (Re^(-0.3)) * (Fr^(-0.25)) * ((h/R)^(1.5)) *
 ↪  ((b/R)^(-0.124)) * ((V_g/V_o)^(-0.376)) *
 ↪  ((sigma_V_g/V_o)^(-0.2));

% Equation 6
C_m_4 = 0.506 * (Re^(-0.32)) * (Fr^(-0.25)) * ((h/R)^(2.1)) *
 ↪  ((b/R)^(-0.27)) * ((V_g/V_o)^(-0.8)) * ((sigma_V_g/V_o)^(-0.2));

end

% Moment of the disc losses in one gear
M_D = rho *(omega^2) * (R^4) * b * C_m_3


%Reynolds number
Re_2 = (omega*R_o*l)/v;
Re_2 = 2100;
% Froude number
Fr_2 = ((omega^2)*R_o^2)/(g*l);
Fr_2 = 3112;
```

```
if Re>2100
    Re = 2100;
end

if Fr>3112
    Fr = 3112;
end

% Range check
% Ratio of the tooth depth to the scale factor for length
↪  introduced for dimensional compensation
LL = (l/l_0)

% Ratio of the Gear width to the scale factor for length
↪  introduced for dimensional compensation
BL = (b/l_0)


C_m_oil_1 = 0;
C_m_oil_2 = 0;

if Re_2>=7 && Re_2<= 2100 && Fr_2>=22 && Fr_2<= 3112 && LL>=0.45 &&
↪  LL<= 1.8 && BL>=1 && BL<= 6
% Losses caused by yhe expulsion of the oil
% Zone 1
C_m_oil_1 = 616.6 * (Re_2^(-0.65)) * (Fr_2^(-0.46)) *
↪  ((l/l_0)^(-1.66)) * ((b/l_0)^(-0.46));

% Zone 2
C_m_oil_2 = 5623 * (Re_2^(-0.88)) * (Fr_2^(-0.78)) *
↪  ((l/l_0)^(-1.6)) * ((b/l_0)^(-0.36));

end

% Moment of the losses due to the oil expulsion
M_oe = rho *(omega^2) * (R_o^3) * b * l * C_m_oil_2

% Total moment
M = M_D +M_oe

P_loss = M*omega %Total churning loss in W

end
```

A.2.4 Seal losses

A.2.4.1 ISO 14179-1 model

```
% Left driveshaft seal and Rotor shaft seal- (Material - Viton)
% Seal losses : ISO 14179 - 1 model

function [T_s,P_Si] = Seal_ISO_14179_1(D_s,n)
% D_s = Shaft diameter [mm]
% n = Shaft speed [rpm]

% Oil seal Torque [Nm]
T_s = (3.737*10^(-3))*D_s;

% Power loss for each individual oil seal [W]
P_Si = (1000*T_s*n)/9549;

end
```

A.2.4.2 ISO 14179-2 model

```
% Left driveshaft seal and Rotor shaft seal
% Seal losses : ISO 14179 - 2 model

function [P_VD] = Seal_ISO_14179_2(D_s,n)
% D_s = Shaft diameter [mm]
% n = Shaft speed [rpm]

% Power loss for each individual radial shaft seal
P_VD = (7.69*10^(-6))*(D_s^2)*n;  % [W]

end
```